

# ***Microbubble generation and application in healthcare***

A thesis submitted in partial fulfilment of the requirements for the degree of

**Doctor of Philosophy**

***By***

***Mahroo Karimpoor***

***Department of Mechanical Engineering, University College London,  
Torrington Place, London, WC1E 7JE.***

***School of Pharmacy, Department of Pharmaceutics, University College  
London, 29/39 Brunswick Square, London, WC1N 1AX. UK***

**August 2018**

**United Kingdom**

# Declaration

I, Mahroo Karimpoor, confirm that the work presented in this thesis is my own. Where information has been derived from other sources, I confirm that this has been indicated in the thesis.

.....

***Mahroo Karimpoor***

## Abstract

The aim of this work is to investigate the application of microbubbles for targeted drug delivery and anticancer drug sensitivity investigations. Microbubbles were prepared using a microfluidic device to act as a carrier for drug delivery or building scaffolds for three-dimensional (3D) cell culture. The lifetime and bursting process of alginate microbubbles and the role of microbubbles for delivering drugs through oral administration were investigated. It was shown that the collection of microbubbles in calcium chloride solution or glycerol, along with the incorporation of gold nanoparticles into the shell of the microbubbles increased the lifetime of the microbubbles. To mimic the physiological condition, the stability of the generated microbubbles was examined under acidic pH and body temperature. Simulation of the oesophageal condition using porcine tissue showed the enhanced absorption of the drug using alginate microbubbles. This result supports the application of microbubbles for oral drug delivery to oesophageal mucosa.

The other application of microbubbles in regard to anticancer drugs in this work was to measure the sensitivity of myeloid leukaemia cells to various types of antileukaemia agents in a 3D culture. A porous calcium alginate foam-based scaffold was developed using microfluidic technology. The foam-based 3D culture supported the growth and proliferation of both normal haematopoietic and leukaemia cells. The myeloid differentiation in both leukaemia and normal haematopoietic cells was enhanced in the foam-based 3D culture, compared to the 2D culture. The sensitivity of the leukaemia cell

line models; K562 and HL60 and primary acute myeloid leukaemia (AML) cells to antileukemia agents; Imatinib and doxorubicin were reduced in the 3D compared to the 2D culture, which is similar to as was reported *in vitro* investigations. The result of this study proposes the application of calcium alginate foams as scaffold in 3D culture for antileukaemia sensitivity screens in drug discovery investigations.

# Publications

## Refereed Journal Papers

**Karimpoor M, Illangakoon E, Reid AG, Claudiani S, Edirisinghe M, Khorashad JS.** *Development of artificial bone marrow fiber scaffolds to study resistance to antileukemia agents. British Journal of Haematology 2017 Aug 2.*

**Karimpoor M, Yerba-Fernandez E, Parhizkar M, Orlu M, Craig D, Khorashad JS, Edirisinghe M.** *Alginate foam-based 3D culture to investigate drug sensitivity in primary leukaemia cells. Journal of Royal Society Interface. 2018 Apr; 15(141).*

**Karimpoor M, Orlu M, Craig DQM, Edirisinghe M.** *Preparation of Alginate Microbubbles using V-junction microfluidic device for drug delivery (in preparation).*

## Conference Presentations

*Mahroo Karimpoor. Microbubbles stability in targeted drug delivery: Application in gastrointestinal systems. PhD UCL Conference, London, UK, 2015.*

*Mahroo Karimpoor. Microfluidics techniques for stabilizing microbubbles. PhD UCL Conference, London, UK, 2016.*

*Mahroo Karimpoor. Application of microbubbles for drug delivery. UK Pharmsci, Glasgow, UK, 2016.*

*Mahroo Karimpoor. Stabilizing microbubbles for drug delivery purposes. The International PharmTech Conference, Leicester, UK, 2016.*

*Karimpoor M, Illangakoon E, Reid AG, Claudiani S, Edirisinghe M, Khorashad JS. Development of a 3-dimensional culture using various scaffolds to mimic bone marrow microenvironment in order to study the mechanism of resistance to anti-leukaemia agents. European Hematology Association, Madrid, Spain, 2017.*

*Ficol C, Karimpoor M, Chiapini C, Claudiani S, Khorashad JS. Identification of signaling pathways in patients with acute myeloid leukaemia using pooled shRNA library. Leuka, September 2017.*

*Karimpoor M, Yebra-Fernandez E, Parhizkar M, Orlu M, Craig D, Edirisinghe M, Khorashad JS. Development of foam-based 3-dimensional culture to investigate drug sensitivity in primary leukaemia cells. Blood 2017 130:3824; American Society of Hematology, Atlanta, December 2017.*

## **Participating in Symposia**

*Particle Engineering Workshop by Electrohydrodynamic Atomisation (EHDA) Network /Engineering and Physical Sciences Research Council (EPSRC) in University of Portsmouth, UK. 25th April, 2017.*

## Acknowledgements

First of all, I would like to thank Professor Mohan Edirisinghe for his unending support during my PhD project. His mentorship has been invaluable throughout; I could not have reached this stage without his help. I will never be able to thank him enough for always being there for me.

I would like to thank my second supervisor Professor Duncan Craig for his guidance and encouragement throughout the project. In addition to having a busy schedule as Head of UCL School of Pharmacy (SoP), he made time to ensure my stay at UCL was pleasant throughout.

I would like also to thank Dr. Jamshid Sorouri Khorashad for helping me with biological experiments related to this work, for giving directions and reviewing my work during this project.

I am also grateful for the advice and guidance from Dr. Mine Orlu, along with her kindness and support during this study.

For many parts of this thesis I received help from Dr. Maryam Parhizkar. Daily discussion on the research aims of my projects with her was enlightening, while improving and expanding the ongoing work.

The staff of UCL Mechanical Engineering and School of Pharmacy supported me in this work in diverse ways. All my colleagues, both in Engineering and School of Pharmacy offered valuable guidance throughout my study in the difficult moments. Thank you to these and many more.

Last but not least, a big thank to my sisters Dr. Mahta Karimpoor and Kiana Karimpoor for their support during this journey. Your love and support have been wonderful and I am most grateful.

I cannot imagine to be able to have this achievement without these important people. Thank you all.

# **DEDICATION**

*To*

*My Father;*

*Majid Karimpoor*

*for his sacrifices and supports throughout my life  
and mostly during the time of this research*

*And to my Mother;*

*Minou Olfati*

*Her love and sacrifices for our family and many  
others are exceptional and worthy of praise.*

# Nomenclature

Symbol	Definition	Units
$Q_g$	Gas flow rate	ml/min
$P_g$	Gas pressure	kPa
$\mu_l$	Liquid viscosity	mPa s
$\mu_g$	Gas viscosity	mPa s
$\rho_l$	Liquid density	kg/m <sup>3</sup>
$P_{lg}$	Gas outlet pressure downstream of junction	kPa
$u_l$	Liquid velocity	m/s
$u_g$	Gas flow velocity	m/s
$\sigma_l$	Liquid surface tension	mN/m
$D_{ch}$	Microchannel diameter	$\mu\text{m}$
$D_b$	Bubble diameter	$\mu\text{m}$
$M$	Molecular weight	g/mol
$T$	Temperature	K or ( $^{\circ}\text{C}$ )
$t$	Time	s
$\mu\text{m}$	Micro molar	$\mu\text{M}$
$Q_l$	Liquid flow rate	ml/min
$V$	Volume	m <sup>3</sup>
$F_G$	Gravity force	N/kg

## Glossary of abbreviations

AML	Acute myeloid leukaemia
BC	Blast crisis of chronic myeloid leukaemia
BM	Bone Marrow
CML	Chronic myeloid leukaemia
CMR	Complete molecular response
DAS	Dasatinib
DNA	Deoxyribonucleic acid
EHDA	Electrohydrodynamic atomisation
FBS	Foetal bovine serum
FDA	Food and drug administration
G-CSF	Granulocyte colony-stimulating factor
GM-CSF	Granulocyte macrophage colony-stimulating factor
HIFU	High intensity focused ultrasound
HSC	Haematopoietic stem cell
IM	Imatinib
KD	Kinase domain
LSC	Leukaemia stem cells
MEMS	Microelectromechanical systems
MNC	Mononuclear cells
MRI	Magnetic resonance imaging

PBS	Phosphate buffered saline
PCR	Polymerase chain reaction
PEG	Polyethylene glycol
pH	Logarithmic scale used to specify the acidity
PMMA	Poly (methyl methacrylate)
PMN	Polymorphonuclear leukocyte
RNA	Ribonucleic acid
SEM	Scanning electron microscopy
TKI	Tyrosine kinase inhibitor
WBC	White blood cell
2D	2-dimensional
3D	3-dimensional
MB	Microbubbles

# Table of Contents

DECLARATION .....	2
ABSTRACT .....	3
PUBLICATIONS.....	5
REFEREED JOURNAL PAPERS .....	5
CONFERENCE PRESENTATIONS.....	6
PARTICIPATING IN SYMPOSIA .....	7
ACKNOWLEDGEMENTS.....	8
DEDICATION .....	10
NOMENCLATURE.....	11
LIST OF TABLES .....	20
LIST OF FIGURES .....	21
<b>CHAPTER 1</b> .....	<b>25</b>
INTRODUCTION AND BACKGROUND .....	25
1.1 INTRODUCTION.....	25
1.2 OBJECTIVES OF THE RESEARCH .....	31
1.2.1 PREPARATION OF MICROBUBBLES VIA V-JUNCTION.....	31
1.2.1.1 Characterising the microbubbles and improving their stability.....	32
1.2.1.2 Mucoadhesive study.....	32
1.2.2 PRODUCTION OF CALCIUM ALGINATE FOAM SCAFFOLD USING MICROFLUIDIC METHOD .....	33

1.2.2.1 Calcium alginate foam scaffold generation.....	33
1.2.2.2 Drug sensitivity test.....	33
1.3 THE THESIS STRUCTURES.....	33
<b>CHAPTER 2.....</b>	<b>36</b>
LITERATURE REVIEW .....	36
2.1 INTRODUCTION.....	36
2.2 THE APPLICATIONS OF MICROBUBBLES .....	37
2.2.1 ULTRASOUND CONTRAST AGENT .....	37
2.2.2 MICROBUBBLES IN TARGETED DRUG DELIVERY .....	38
2.2.2.1 Oesophageal structure and its diseases.....	41
2.2.2.2 Oral drug delivery .....	43
2.2.2.3 Approaches to gastro retentive drug delivery system .....	46
2.2.2.3.1 Bioadhesive or mucoadhesive systems .....	47
2.2.2.3.2 Nanoparticles and mucoadhesion for drug delivery .....	47
2.2.2.4 Floating drug delivery system.....	48
2.2.3 SCAFFOLDS FROM MICROBUBBLES FOR TISSUE ENGINEERING .....	48
2.2.4 THE ROLE OF MICROBUBBLES IN FOOD ENGINEERING .....	50
2.2.5 MICROBUBBLES APPLICATION IN WATER AND WASTEWATER TREATMENT ..	51
2.3 METHODS FOR MICROBUBBLES FABRICATION .....	51
2.3.1 SONICATION.....	52
2.3.2 COAXIAL ELECTROHYDRODYNAMIC ATOMISATION (CEHDA) .....	53
2.3.3 MICROFLUIDICS SETUP .....	54
2.3.3.1 Co-flowing devices.....	55
2.3.3.2 Flow focusing devices .....	56
2.3.3.3 Cross flowing (T-junction) devices .....	57
2.4 MICROBUBBLE SIZE AND STABILITY.....	57
2.5 BIOMATERIALS .....	58
2.5.1 BIOCOMPATIBLE POLYMERS .....	59
2.5.2 NATURAL POLYMERS .....	60
2.5.3 SCAFFOLD FABRICATION METHODS .....	64
2.5.3.1 Particle leaching technique .....	65

2.5.3.2 Emulsion freeze drying technique .....	65
2.5.3.3 Foaming via pressure quenching .....	66
2.6 ACUTE MYELOID LEUKAEMIA .....	66
2.7 CHRONIC MYELOID LEUKAEMIA.....	69
2.8 PRINCIPLES OF CELL CULTURE.....	72
2.8.1 COMMONLY APPLIED CELL CULTURES FOR STUDYING HAEMATOPOIETIC STEM CELLS .....	77
2.8.2 DIFFERENT TYPES OF 3D CULTURE FOR STUDYING VARIOUS PHENOTYPES OF HSC/LSC.....	79
2.8.3 SCAFFOLDS FROM MICROBUBBLES FOR TISSUE ENGINEERING .....	81
2.8.4 SCAFFOLD-BASED 3D CULTURES AS AN <i>IN VITRO</i> MODEL FOR BM .....	82
2.8.5 THE SIGNIFICANCE OF A BM-LIKE CULTURE FOR STUDYING AML .....	85
2.9 FLOWCYTOMETRY .....	86
<b>CHAPTER 3.....</b>	<b>88</b>
EXPERIMENTAL DETAILS.....	88
METHODS AND MATERIALS .....	88
3.1 INTRODUCTION.....	88
3.2 MATERIALS FOR EVALUATION OF BUBBLE FORMATION .....	88
3.2.1 SODIUM ALGINATE .....	88
3.2.2 SURFACTANTS .....	90
3.2.3 PHOSPHOLIPID .....	91
3.2.4 PHOSPHATE BUFFERED SALINE (PBS) .....	91
3.2.5 GLYCEROL.....	91
3.2.6 ETHANOL .....	92
3.2.7 CALCIUM CHLORIDE .....	92
3.2.8 GOLD NANOPARTICLE .....	92
3.3 MATERIAL AND SOLUTION PREPARATION FOR MICROBUBBLE PRODUCTION ..	93
3.4 CHARACTERISATION OF THE SOLUTIONS.....	93
3.4.1 SURFACE TENSION .....	93
3.4.2 VISCOSITY .....	94
3.4.3 ELECTRICAL CONDUCTIVITY AND PH.....	95

3.5	CHARACTERISATION METHODS .....	95
3.5.1	OPTICAL MICROSCOPY .....	95
3.5.2	CONFOCAL LASER SCANNING MICROSCOPY .....	96
3.5.3	FLUORESCENCE MICROSCOPY .....	96
3.5.4	SCANNING ELECTRON MICROSCOPY (SEM).....	97
3.5.5	HOT-STAGE MICROSCOPY .....	98
3.6	MICROFLUIDIC EXPERIMENTAL SETUP.....	98
3.6.1	V-JUNCTION DEVICE .....	99
3.7	APPARATUS DESIGN .....	100
3.8	MEMBRANES FOR MUCOADHESIVE STUDY.....	101
3.9	REQUIREMENTS OF THE CELL CULTURES .....	102
3.9.1	MEDIUM .....	102
3.9.2	SERUM-CONTAINING MEDIA.....	103
3.9.3	SERUM-FREE MEDIA .....	103
3.9.3.1	Source of media.....	104
3.9.4	CELL CULTURE PLATES .....	104
3.9.5	ENVIRONMENT FOR CELL CULTURE.....	105
3.10	BASIC LABORATORY DESIGN AND EQUIPMENT.....	105
3.10.1	LAMINAR FLOW CABINETS .....	105
3.10.2	CENTRIFUGES .....	106
3.10.3	INCUBATORS .....	106
3.10.4	COUNTING CELLS .....	106
3.10.5	STORAGE AND OTHER FACILITIES .....	107
3.10.6	SOLUTION PREPARATION FOR SCAFFOLD PRODUCTION .....	107
3.10.7	SCAFFOLD PREPARATION.....	108
3.11	THE METHOD FOR DRYING FOAM-BASED SCAFFOLD.....	109
3.11.1	PREPARATION OF NORMAL HAEMATOPOIETIC AND AML CELLS .....	109
3.11.2	CELL LINES .....	111
3.11.3	STERILISATION OF THE FOAM-BASED SCAFFOLD.....	112
3.11.4	CELL CULTURE .....	113
3.11.5	MEASURING THE LOWEST INHIBITORY DOSE OF DOXORUBICIN OR IMATINIB ON HL60 OR K562.....	114
3.11.6	CO-CULTURE OF HS-5 WITH HL60 OR K562 CELLS.....	115
3.11.7	DIFFERENTIATION OF THE CELLS USING FLOWCYTOMETRY.....	118

3.11.8	MTS ASSAY .....	120
3.11.9	STATISTICAL ANALYSIS .....	122
3.12	UV-VIS SPECTROSCOPY.....	123
<b>CHAPTER 4</b>	.....	<b>125</b>
CREATING MICROBUBBLES USING MICROFLUIDIC TECHNOLOGY		
FOR POTENTIAL AND THERAPEUTIC USE IN HEALTHCARE .....		
4.1	INTRODUCTION.....	125
4.1.1	CHARACTERISATION OF ALGINATE SOLUTION .....	127
4.1.2	MICROBUBBLE PREPARATION USING MICROFLUIDIC V-JUNCTION .....	128
4.1.3	MICROBUBBLE SIZE .....	130
4.1.3.1	Effect of gas pressure on size of the microbubble .....	130
4.1.3.2	Effect of liquid flow rate on size of microbubble .....	131
4.1.3.3	The impact of surfactant type on the size of the microbubble.....	132
4.1.3.4	The effect of the capillary size on the microbubble size.....	133
4.1.4	PREPARATION OF MICROBUBBLES FOR DRUG DELIVERY .....	135
4.1.5	MONODISPERSITY AND POLYDISPERSITY .....	137
4.1.6	MICROBUBBLES STABILITY .....	137
4.1.6.1	Modifying alginate suspension: the effect of gold nanoparticles on the stability of alginate microbubbles .....	138
4.1.6.2	Modifying collection media .....	140
4.1.6.3	Collection of alginate microbubbles in glycerol.....	141
4.1.7	COLLECTION OF ALGINATE BUBBLES IN GASTRIC CONDITION .....	143
4.1.7.1	Introduction to effect of temperature .....	145
4.1.7.2	Effect of temperature on microbubble stability .....	146
4.2	MUCOADHESIVE STUDY .....	149
4.2.1	INTRODUCTION TO MUCOADHESIVE TEST .....	149
4.2.2	MICROBUBBLE PREPARATION FOR THE MUCOADHESIVE TEST .....	151
4.2.3	INCORPORATION OF RHODAMINE B.....	152
4.2.4	<i>IN SITU</i> STUDIES .....	154
4.2.5	CONFOCAL IMAGING STUDIES.....	156
4.2.6	CALIBRATION CURVE AND CALCULATION FOR UV ANALYSIS .....	157

4.2.6.1 UV analysis of dye content within the animal tissue sample.....	158
4.3 DISCUSSION .....	160
<b>CHAPTER 5.....</b>	<b>168</b>
DRUG RESISTANCE INVESTIGATIONS IN LEUKAEMIA USING MICROBUBBLES .....	168
5.1 INTRODUCTION.....	168
5.2 THE AIMS OF THIS CHAPTER .....	173
5.3 CHARACTERISATION OF MATERIALS AND SOLUTIONS.....	174
5.4 FOAM-BASED SCAFFOLD.....	175
5.5 BIOACTIVITY AND BIOCOMPATIBILITY OF SCAFFOLD .....	177
5.6 THE LOWEST INHIBITORY DOSE OF IMATINIB AND DOXORUBICIN .....	179
5.7 DIFFERENTIATION OF THE PRIMARY HAEMATOPOIETIC CELLS AND ACUTE MYELOID LEUKAEMIA CELLS.....	181
5.8 RESISTANCE OF THE CML AND AML CELLS TO INHIBITORY EFFECT OF THE DRUGS .....	189
5.9 DISCUSSION .....	192
<b>CHAPTER 6.....</b>	<b>196</b>
CONCLUSIONS AND FUTURE WORK .....	196
6.1 CONCLUSION .....	196
6.2 FUTURE WORK.....	199
6.2.1 FURTHER IMPROVEMENT OF MICROBUBBLES AS A METHOD OF DRUG DELIVERY .....	200
6.2.2 FURTHER MODIFICATION OF THE ALGINATE SCAFFOLDS.....	200
6.2.3 EXPLORING THE MECHANISMS THROUGH WHICH THE ALGINATE SCAFFOLD EXERTS ITS BIOLOGICAL IMPACT ON THE CELLS .....	200
REFERENCES .....	203
APPENDIX.....	225

## List of Tables

Table 1: Characterisation of alginate microbubbles solution.....	127
Table 2: Dye measurement in actual animal tissue.....	159
Table 3: Dye measurement in artificial tissue membrane. ....	160
Table 4: The percentage of myeloid markers on normal and two AML samples in 2D and 3D cultures. ....	187

## List of Figures

Figure 1: Thesis structure.....	31
Figure 2: Microbubbles in healthcare.....	37
Figure 3: Contrast agent Microbubble.....	39
Figure 4: A bubble with antibodies attached to its surface.....	40
Figure 5: Microbubbles in targeted drug delivery.....	41
Figure 6: Oesophagus structure and position in the body.....	43
Figure 7: Floating dosage form.....	45
Figure 8: Gastroesophageal junction.....	46
Figure 9: Coaxial electrohydrodynamic atomisation setup.....	54
Figure 10: Microfluidic bubbles generating geometries.....	55
Figure 11: Alginate acid.....	64
Figure 12: Schematic illustration of the normal and leukaemic human haematopoietic hierarchies.....	68
Figure 13: Targeting LSC is essential for preventing relapse following therapy.....	69
Figure 14: Mode of action of tyrosine kinases inhibitors imatinib.....	71
Figure 15: Mechanism of multiple drug resistance.....	72
Figure 16: Adherent and suspension cells in culture.....	76
Figure 17: Human embryonic cells.....	77
Figure 18: Rotating wall vessel bioreactor.....	80
Figure 19: Packed bed bioreactor setup.....	80
Figure 20: The BM haematopoietic niche.....	84
Figure 21: Schematic diagram of the working principle of flowcytometry....	87
Figure 22: Molecular structure of sodium alginate.....	90

Figure 23: Schematic illustration of a) tensiometer, and b) 3D of the plate's interaction with liquid sample. ....	94
Figure 24: Microfluidic setup. ....	99
Figure 25: Microfluidic V-junction device. ....	100
Figure 26: Apparatus for bioadhesive studies. ....	101
Figure 27: Alginate bubbles sample produced via V-junction. ....	109
Figure 28: Cell separation by Ficoll. ....	111
Figure 29: Optical microscopic images of the K562, HL60 and HS-5 cell lines. ....	112
Figure 30: The process for developing a 3D culture. ....	117
Figure 31: Removing the cells from the 3D culture. ....	118
Figure 32: The principle of MTS assay. ....	122
Figure 33: Different zones in the electromagnetic spectrum with a magnified visible range (Jeitziner, 2014). ....	124
Figure 34: Optical microscope image of alginate bubbles. ....	129
Figure 35: SEM image of alginate particles from burst bubbles. ....	130
Figure 36: Alginate bubbles with the different gas pressure. ....	131
Figure 37: Effect of liquid flow rate. ....	132
Figure 38: Time study graph. ....	133
Figure 39: Microfluidic V-junction, bubble preparation process and collection. ....	134
Figure 40: The effect of capillary size on the bubble size. ....	135
Figure 41: Alginate microbubble bursting process. ....	136
Figure 42: Monodispersity versus polydispersity. ....	137
Figure 43: Microbubbles coated with nanoparticles. ....	139
Figure 44: Optical microscope images from alginate bubbles. ....	139
Figure 45: Cross-linking process. ....	140

Figure 46: Cross-linking shell of the bubbles.....	141
Figure 47: Alginate microbubbles collected in glycerol. ....	142
Figure 48: Microbubbles in glycerol. ....	143
Figure 49: Collection of alginate microbubbles in hydrochloric acid. ....	144
Figure 50: The lifetime of the microbubbles collected in gastric condition. ....	144
Figure 51: Hot-stage microscopy. ....	147
Figure 52: Effect of temperature. ....	148
Figure 53: Fluorescent dye encapsulation. ....	152
Figure 54: Fluorescent microscopy imaging study. ....	153
Figure 55: Tissue preparation. ....	154
Figure 56: Bioadhesive test study. ....	155
Figure 57: Confocal imaging study.....	156
Figure 58: Calibration curve of rhodamine B in SBF solution. ....	157
Figure 59: Alginate microbubbles attached to mucosa. ....	167
Figure 60: Chapter 5 structure. ....	173
Figure 61: Optical micrograph of the alginate microbubbles generated by a microfluidic device. ....	175
Figure 62: Scaffold production process. ....	176
Figure 63: SEM image of the foam-based scaffold. ....	178
Figure 64: Optical microscope images from cells growing in the foam scaffold. ....	179
Figure 65: MTS assay to measure lowest inhibitory dose of imatinib. ....	180
Figure 66: The inhibitory effect of doxorubicin at various doses on (a) HL60 and (b) HS-5 cells. ....	181
Figure 67: The proliferation of primary AML cells in foam-based scaffold (3D) compared to 2D. ....	182
Figure 68: Myeloid differentiation in 2D and 3D culture in normal donor cells. .....	183

Figure 69: Myeloid differentiation in 2D and 3D culture in AML cells (patient 1). .....	184
Figure 70: Myeloid differentiation in 2D and 3D culture in AML cells (patient 2). .....	185
Figure 71: The statistical differences for the myeloid markers between 2D and 3D cultures.....	187
Figure 72: Reduced level of CD34 markers during differentiation in 3D compare to 2D in AML cells (patient 3).....	188
Figure 73: The inhibitory effect of imatinib and doxorubicin on leukaemia cell line and primary cells in the presence or absence of foam scaffold. ....	191

# Chapter 1

## Introduction and background

### 1.1 Introduction

Microbubbles have in recent years played an important role in a wide range of biomedical applications such as therapeutics and medical imaging. For therapeutic purposes the microbubbles are employed in pharmaceutical applications as vehicles for various drugs and gene delivery. In medical imaging, microbubbles are used for diagnostic purposes to enhance the acoustic contrast and improve the quality of ultrasonic images (Farook, Stride, & Edirisinghe, 2009).

Microbubbles have the potential to be used in a wide variety of industries. They are currently applied in aquaculture and hydroponic cultivation, food preservation and quality control, as well as water and wastewater treatment. Depending on for which applications the microbubbles are needed, various properties of the microbubbles such as stability, size, monodispersity or surface properties are taken into consideration (Owen et al., 2017).

Targeted drug delivery via microbubble methodology is widely used for therapeutic applications. For example, for intravascular ultrasound therapeutic approaches the application of microbubbles can improve drug penetration into the targeted tissue. Bubbles which are used for medical imaging and other therapeutic applications are tiny and can safely pass through the blood vessels without any risk of blockage (Parhizkar, Stride, &

Edirisinghe, 2014).

The development of bubbles as drug delivery vehicles is achieved by incorporating small amounts of drug in the shell of the bubbles. Drug that is dissolved in the bubbles can be targeted to a specific organ, using ligands or antibodies which are concentrated on the bubble's shell. Alternatively, they can be guided to the tumour by applying ultrasound, and then the ultrasound waves can break the bubbles and release the drug. This approach localises the release of drug to the region of interest and minimises any harmful side effect which might happen as a result of drug concentration in non-target areas (Carugo et al., 2015). In cancer treatment the exact location of microbubbles (loaded with the magnetic nanoparticles) can be detected by measuring the intensity of ultrasound pressure waves and analysing the pattern. Microbubbles can concentrate in the tumour area by having antibodies on their surface which are specific for the tumour tissue. In fact, the microbubbles reflect pressure waves with different intensities compared to the body tissues, thus allowing the bubbles to burst on demand and release the drug content at the correct treatment site (Owen et al., 2014). The delivery of drug to specific cancer sites allows for enhanced treatment of cancerous cells while minimising some of the negative side effects related to nonspecific targeting. In the current study, the potential use of microbubbles to improve oesophagus drug delivery and stability, as well as analysing the bubbles under gastric system, have been investigated.

In the second part of this study, microfluidic microbubbles were used to produce a three-dimensional (3D) foam scaffold. Leukaemia is a group

of cancers that usually begin in the bone marrow and result in abnormally high numbers of white blood cells (Wang and Dick, 2005).

One of the main methods for the treatment of AML is to kill as many leukaemia cells in the body as possible and reduce the risk of relapsing. The bone marrow (BM) niche is a specialised microenvironment where stem cells reside. The niche is believed to regulate stem cell quiescence, self-renewal and differentiation (Schofield, 1978). There are several components that regulate the function of the niches (Fraser et al., 1990; Haylock et al., 1992; Plaks, Kong, & Werb, 2015). These factors include cellular components such as osteoblasts, osteoclasts, endothelial cells, mesenchymal progenitors, and molecules such as stromal derived factor1 (SDF-1), stem cell factor, osteopontin, thrombopoietin (TPO) and N-cadherin (Di Maggio et al., 2011).

Traditionally monolayer cell culture has been used for studying haematopoietic stem cells (HSC), but it is not capable of producing a niche-like structure and therefore they have not been suitable models for this purpose (Tan et al., 2010). Considering the deficiencies of current two-dimensional (2D) cultures (Fang & Eglén, 2017), recent efforts have focused on developing 3D cultures which can mimic the BM microenvironment by accommodating the essential components of the BM. The cultures with only cellular and cytokine components, without having the 3D structure, have been able to support the expansion of the more differentiated haematopoietic precursor CD34<sup>+</sup> cells without establishing a support for long-term HSC self-renewal (Haylock et al., 1992). Lack of 3D structure and molecular matrix components are potential causes of their unsustainability for long-term HSC culture (Braccini et al., 2005). Molecules present in the 3D structure, including

segment-1(CS-1) and Arg-Gly-Asp (RGD) motifs which mimic the fibronectin domains of the extracellular matrix (ECM), have a significant impact on making the culture more similar to BM niches and contributing to the expansion of CD34<sup>+</sup> cells (Jiang et al., 2006). The development of an *ex vivo* 3D culture mimicking the BM microenvironment in providing niche-like structures for the HSC to reside and proliferate, provides an opportunity to study haematological malignancies. The acute myeloid leukaemia (AML) cells have a subpopulation called leukaemia stem cells (LSC). LSCs have the capacity to initiate the disease, continue producing leukaemia cells and perform self-renewal. The main challenge to studying AML cells for therapeutic target discovery screens has been the difficulty in the growth and maintenance of these cells in an *in vitro* culture (Griessinger et al., 2014). The majority of AML cells usually undergo spontaneous apoptosis and only a subpopulation of the cells proliferate during *in vitro* culture (Bendall et al., 1994). The proliferation and survival of the AML cells increase in the presence of haematopoietic growth factors, being cultured with stromal cells and residing in a 3D environment (Bendall et al., 1994; Stolze et al., 1995; Griessinger et al., 2014). It has also been shown that AML cells have reduced sensitivity to chemotherapeutic agents in 3D cultures (Aljitawi et al., 2014). Insufficient information on molecular interaction between the AML LSCs and their microenvironment is one of the main reasons for the failure of current therapeutic approaches (Tabe & Konopleva, 2015). The new approaches should be focused on selectively inhibiting LSCs by disrupting the interaction between them and their niche environment, but at the same time preserving the normal haematopoiesis. Long-term detection of the low-level BCR-ABL1 oncogene by sensitive polymerase chain reaction (PCR) techniques, in

chronic myeloid leukaemia (CML) patients who achieve major molecular response to tyrosine kinase inhibitors (TKI), is believed to be due to the survival of LSC in the BM niches, in spite of inhibiting BCR-ABL1 kinase activity (Bhatia et al., 2003). A 3D culture mimicking a BM microenvironment is expected to provide a model through which the mechanism of LSC maintenance is explored. This would facilitate the investigations towards developing drugs which can target the survival pathways activated by such interactions. Various 3D cultures have been developed so far for studying leukaemia cells. The auteur of this thesis has already reported the development of a PMMA-HA fibre-based scaffold to investigate the influence of 3D culture on reduced sensitivity of leukaemia cells to the tested antileukaemia agents (Karimpoor et al., 2017). The PMMA-HA scaffold provided a 3D structure which simulates some characteristics of the bone by having hydroxyapatite (HA) in its structure. However, it lacked the spongy structure of the BM. In this work to develop a scaffold with pores similar to bone lacuna, a foam-based scaffold with spongy structure was developed using alginate biomaterial. Microbubble technology was applied to produce the foam with the expected size of the pores (Parhizkar et al., 2014). This foam-based 3D culture supported the growth of normal haematopoietic and also leukaemia cells, and similar to *in vivo* condition, it promoted cell differentiation. This system reduced the sensitivity of the leukaemia cells to antileukaemia agents. Due to simulating the physiological condition, the 3D cell culture with the foam-based scaffold can be used for drug sensitivity investigation of the leukaemia cells.

## **Aim of the study**

The aim of this study was to investigate the feasibility of alginate microbubbles for drug delivery and drug discovery investigations. Microbubbles obtained from this project were used as materials for the design of an oral drug delivery system. It began with the fabrication of bubbles using a microfluidic device, followed by measuring the stability of alginate bubbles in the various gastric conditions. Once microbubbles were obtained, characterisation studies were performed. It was found in this study that adding solid particles to the bubble coating and using the right collection media improved the structure of the microbubbles for effective drug delivery.

In the second part of this work, calcium alginate microbubbles were used to develop a foam scaffold for antileukaemia drug sensitivity investigations. To accurately predict the sensitivity of the leukaemia cells in an *in vitro* assay, a culturing system containing the essential components of the BM was required. In this work a porous calcium alginate foam-based scaffold was developed in combination with human bone marrow-derived stromal cells to provide a BM-like microenvironment for drug screening purposes. This culturing system simulates *in vivo* condition in regard to haematopoietic cell differentiation. It also enhances resistance to antileukaemia drugs.

## 1.2 Objectives of the research

An overview of the thesis is presented in figure 1. This includes preparation of microbubbles for drug delivery to the oesophagus and development of scaffolds for drug sensitivity investigation.

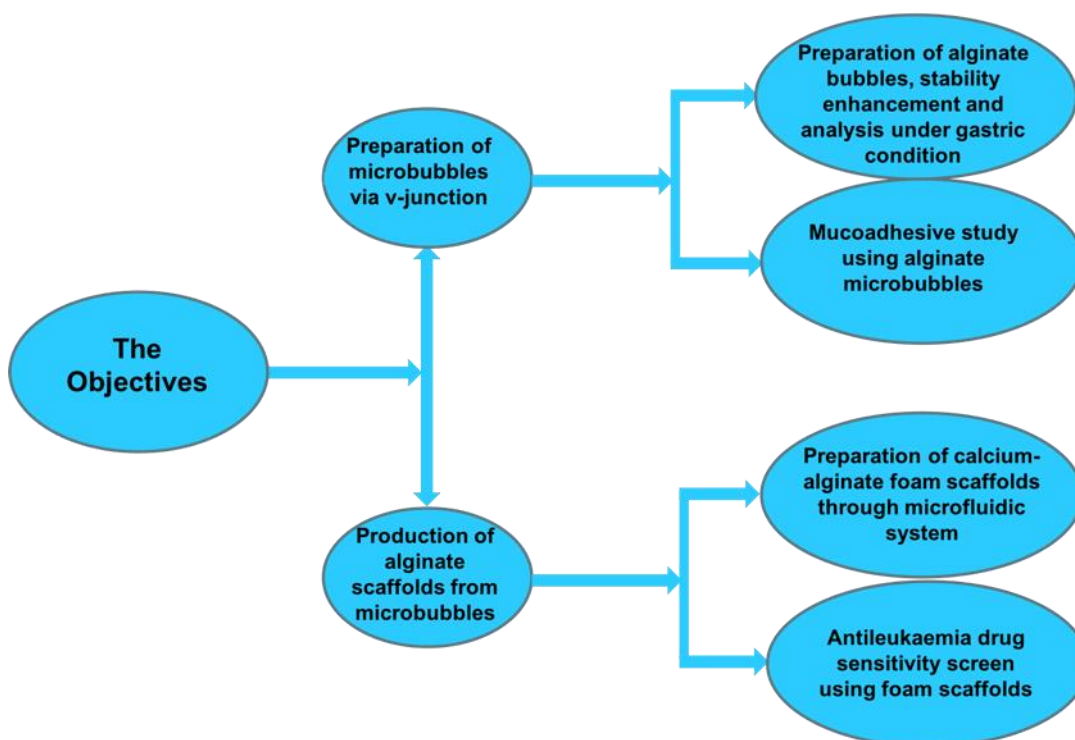


**Figure 1: Thesis structure.**

*The flowchart sets out the key objectives of this study. The detail of each objective is discussed below.*

### 1.2.1 Preparation of microbubbles via v-junction

The first objective of the study was to produce bubbles in a simple capillary embedded V-junction device. This section of the work demonstrated that a

microfluidic device could successfully produce microbubbles with control over size and size distribution under ambient conditions.

#### **1.2.1.1 Characterising the microbubbles and improving their stability**

Following microbubble production for drug delivery, the size of the microbubbles was characterised. It was shown that the size and size distribution of the microbubbles could be controlled through the range of operating parameters such as solution and gas flow rates, channel diameter, and the different properties of the solution such as surface tension and the viscosity during the process of production. The optimisation of the microbubbles is explained in detail in this work. The optimisation process included improving the stability of the microbubbles through coating their shell with gold nanoparticles and modifying the collection media to increase their lifetime. The stability of the microbubbles was examined under gastric condition. It was intended in this work to produce a model to predict the influence of various conditions such as acidity and body temperature on the lifetime of the bubbles.

#### **1.2.1.2 Mucoadhesive study**

To complete the first part of the study, a mucoadhesive test was designed using porcine tissue and fluorescent dye. The purpose was to validate the benefit of using alginate microbubbles for improving drug delivery in the oesophageal area.

## **1.2.2 Production of calcium alginate foam scaffold using microfluidic method**

This section explains how calcium alginate was used for the preparation of the scaffold foam using microfluidic setup. The impact of calcium alginate foam-based 3D culture on the differentiation of normal haematopoietic stem/progenitor cells and AML cells was investigated, followed by drug sensitivity screening of the leukaemia cells in this 3D culture.

### **1.2.2.1 Calcium alginate foam scaffold generation**

This section indicates how alginate microbubbles were prepared via microfluidic method and cross-linked to produce foam scaffold for drug sensitivity study purposes.

### **1.2.2.2 Drug sensitivity test**

This part of the project is focused on the role of microenvironment in increasing the resistance of leukaemia cells to antileukaemia agents. We applied microfluidic microbubble technology to develop a 3D culture mimicking BM structure, in order to investigate the leukaemia cells' response to various antileukaemia agents.

## **1.3 The thesis structures**

The thesis dissertation describes the way in which the research proceeded

by surveying literature, assembling the experimental setup, selecting materials and methods, and conducting experiments. This thesis describes how these experiments exploited the potentially available V-junction microfluidic device as being a viable technique to prepare microbubbles primarily for medical and drug discovery applications. The organisation of this thesis is given in this section.

**Chapter 1** provides background information about the research project, including an overview about the basics of microbubble formation in V-junction microfluidics and the stability of bubbles, followed by information regarding 3D cell culture for drug sensitivity testing. An overview of the thesis is summarised in this chapter, providing a brief background to various themes explored in this work, and an outline of the aim, objectives, organisation and scope of this thesis.

**Chapter 2** describes the literature review of theories, concepts and other researches relevant to themes explored in this work. Since the goal of the research is to produce microbubbles through V-junction microfluidics and optimisation of the microbubbles with nanoparticles, and also the methodology for production of foam scaffolds from microbubbles, an extensive collection of literature has been searched to understand the principles of microfluidics and 3D cell culture, the procedures and their uses, as well as the materials and the methods used for the preparation of microbubbles and scaffolds. This part covers the literature review of theories, concepts and other studies relevant to themes explored in the thesis.

**Chapter 3** presents the applied materials, the experimental setups, the experiments and details of the procedures which were carried out and the protocols which were followed throughout the study.

**Chapter 4** is split into two sections; **section 4.1** explains how the bubbles' stability was evaluated and the alginate bubbles were chosen for assessing the impact of gastric condition on microbubble stability. In **section 4.2**; the bioadhesive property of microbubbles for drug delivery was investigated.

**Chapter 5** represents the role of microbubbles in the production of foam-based scaffolds. This chapter has two sections. **Section 5.1** focuses on the production of calcium alginate foams for building scaffolds from the microbubbles. **Section 5.2** has a detailed description of the main techniques for culturing cell line models and leukaemia cells from patients. This section describes the application of porous scaffolds for the development of 3D culture and how this 3D culture was used for studying myeloid differentiation of the normal and leukaemia cells as well as antileukaemia drug sensitivity.

**Chapter 6** is divided into two main sections. **Section 6.1** includes the conclusions of all the results from this work. **Section 6.2** has recommendations for future work, including the approaches for further developing microbubbles to generate 3D cultures which are capable of mimicking BM microenvironment more closely, and exploring the mechanisms through which 3D cultures increase drug resistance.

# Chapter 2

## Literature review

### 2.1 Introduction

This chapter is a review of the literature in the field of microfluidic microbubble technology, and its application in biomedical engineering and biological investigation of drug resistance in leukaemia. It focuses on reviewing the techniques used for the production of microbubbles and how these microbubbles have been used for healthcare applications. Other applications of microbubbles in cosmetics, wastewater treatment and the food industry are briefly discussed. As one of the aims of this thesis is to use microbubbles for drug discoveries in leukaemia, this work also reviews the biological methodologies for measuring drug sensitivities in primary leukaemia cells and leukaemia cell line models. This starts with the development of 3D cultures where leukaemia cells are grown and treated with antileukaemia drugs. In this thesis various types of 3D culture and different types of the scaffold which have been used for development of these 3D cultures are reviewed. It is followed by reviewing the methods for cell separation, cell proliferation assays and the flowcytometry method for assessing differentiation of the cells. Developing a structure mimicking BM for drug investigation is one of the aims of this study. As an introduction to this aim, the structure of the BM and its essential components which might be required for development of a 3D culture are reviewed.

## 2.2 The applications of microbubbles

As mentioned earlier, microbubbles are used in many industries. In the following section, further details are presented for some of the common biomedical applications of microbubbles. Figure 2 shows the basic structure of various types of microbubbles which are commonly used in healthcare.

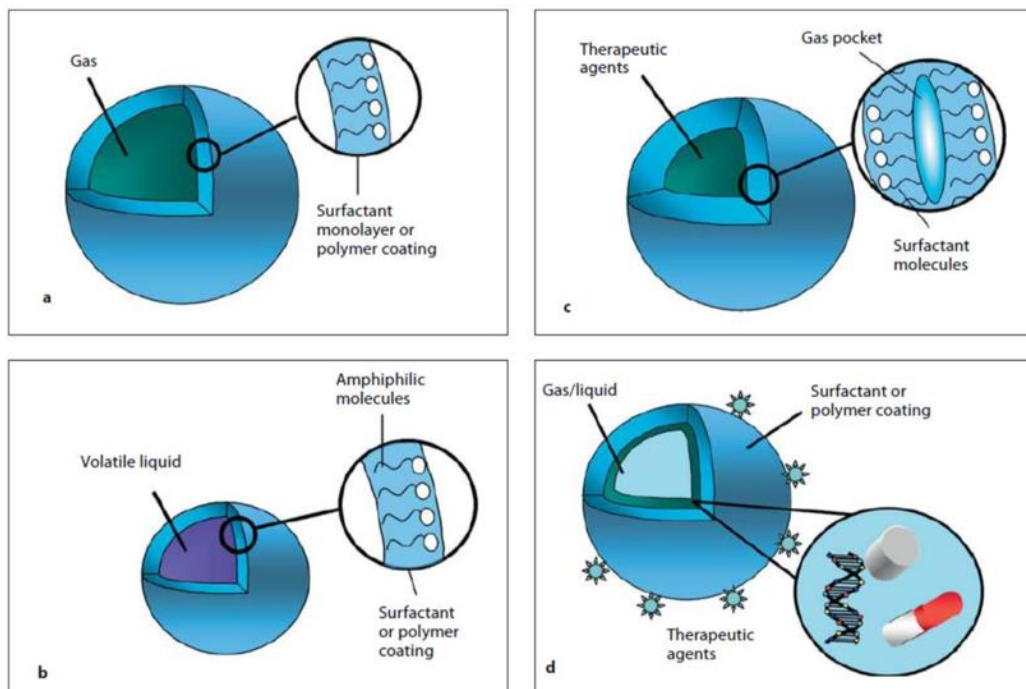


**Figure 2: Microbubbles in healthcare.**

*Different types of microbubble agent used for ultrasound imaging and therapy. a) Coated microbubble. b) Phase shift emulsion. c) Echogenic liposome. d) Multilayered microbubble. This figure is adopted from the work by Stride & Edirisinghe (Stride & Edirisinghe, 2009).*

### 2.2.1 Ultrasound contrast agent

Ultrasound imaging is a popular medical diagnostic technique. This popularity is attributed to a superior safety record, as ultrasound imaging does not use

any ionizing radiation, which makes it safer compared to other methods. Ultrasound imaging is also attractive due to its low cost and easy accessibility compared to other imaging techniques, such as computed tomography (CT) scan, positron emission tomography (PET) and magnetic resonance imaging (MRI) (Kang & Yeh, 2012). Microbubbles can be used as contrast agents, for improving the power of the imaging techniques to enhance the image qualities, and the detection of more accurate details (Cui et al., 2005). Figure 3 explains the principle for the microbubble application as a contrast agent in ultrasonography. The applied ultrasound acoustic wave causes bubble oscillation, leading to bubble collapse. This produces pressure waves that travel through the body and are finally detected by sensors. Microbubble contrast agents have the following properties (Ahmad, Stride, & Edirisinghe, 2012): they are micron-sized bubbles filled with a non-toxic low-soluble gas such as Perfluorobutane ( $C_4F_{10}$ ) and coated with a surfactant polymer or lipid shell to increase their lifetime (as an example in chapter 4, alginate microbubbles prepared with nitrogen gas in the core and PEG as a surfactant in the shell). The stability of these bubbles is determined by the material used to generate them and the surfactant used in the solution. These parameters directly affect the lifetime of the generated bubbles.

### **2.2.2 Microbubbles in targeted drug delivery**

A drug delivery system refers to the methods which are used to transport a pharmaceutical product to the targeted organ using a carrier. An effective drug delivery system will deliver a drug to the target tissue in the body at the right time.

There are various forms of drug delivery system and different methods to improve the delivery system, such as oral delivery which can be improved by controlled-release systems. The most common methods of drug delivery system include the oral (through the mouth), topical (skin), transmucosal (through nasal, buccal, sublingual, vaginal, ocular rectal), parental (injection into system circulation) and inhalation routes.

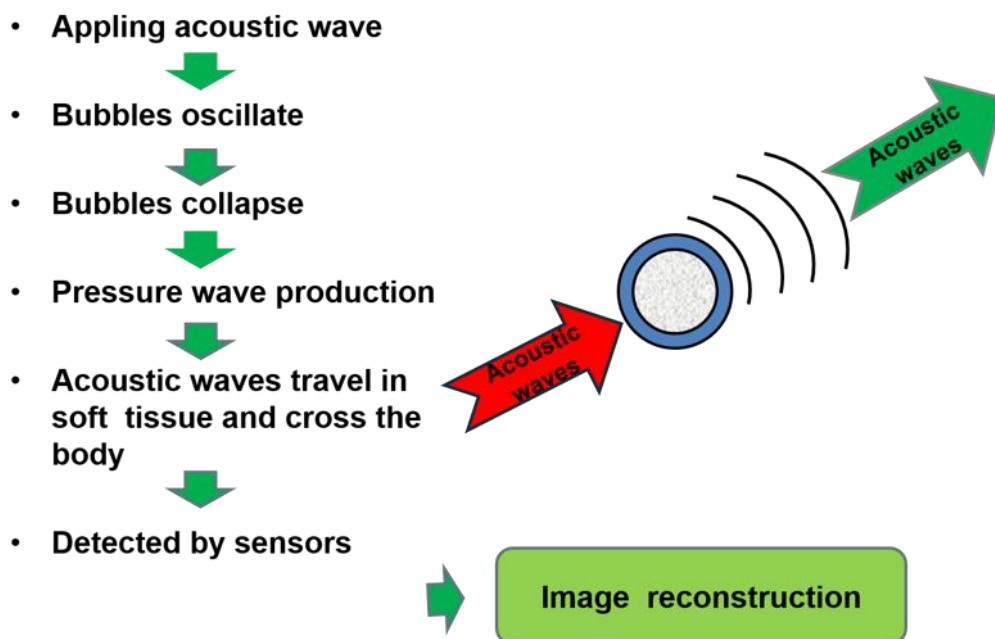


**Figure 3: Contrast agent Microbubble.**

*Extraction of microbubbles through acoustic waves to reconstruct and enhance the image.*

Microbubbles have been used as contrast agents in the field of diagnostic imaging. The application of microbubbles has led to the enhanced quality of images. The recent studies have concentrated on the application of microbubbles in the targeted delivery of drugs to various tissues in the body

(Owen et al., 2014). A popular approach for targeted delivery is the use of ligands and antibodies attached to the outer layer of the gas-filled bubbles (Figure 4). This allows the contrast agents to reach the region of interest.

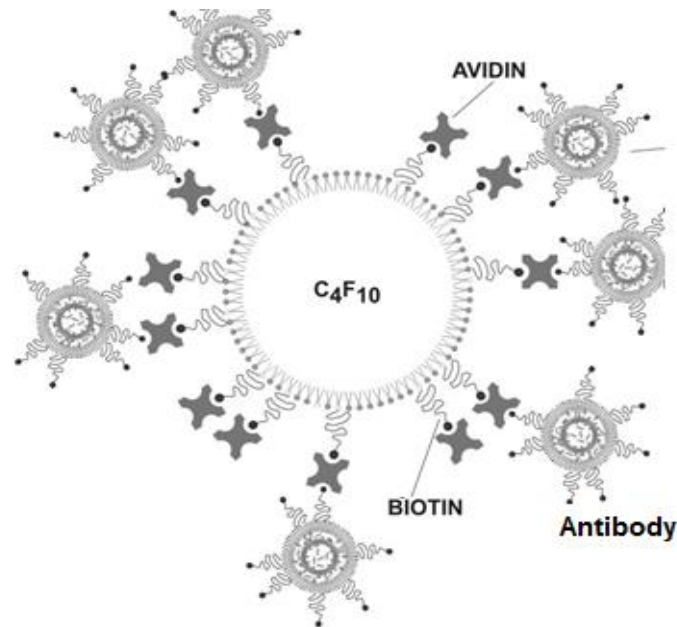


**Figure 4: A bubble with antibodies attached to its surface.**

*Ligands include molecules such as antibodies or nanoparticles that can be attached to the surface of the bubbles and used for target delivery. This figure was adopted from Lentacker et al. 2009 (Lentacker, De Smedt and Sanders, 2009).*

For targeted drug delivery, microbubbles are used as a vehicle filled with therapeutic agents. They are then drawn to the delivery site using low-intensity ultrasound and are subsequently destroyed via a high-intensity wave in order to release their content locally (Figure 5). This approach prevents the side effects associated with systemic administration, such as toxic chemotherapy. Using this method the applied drug is localised to the target region, and as a result the harmful side effects are substantially reduced (Carugo et al., 2015).

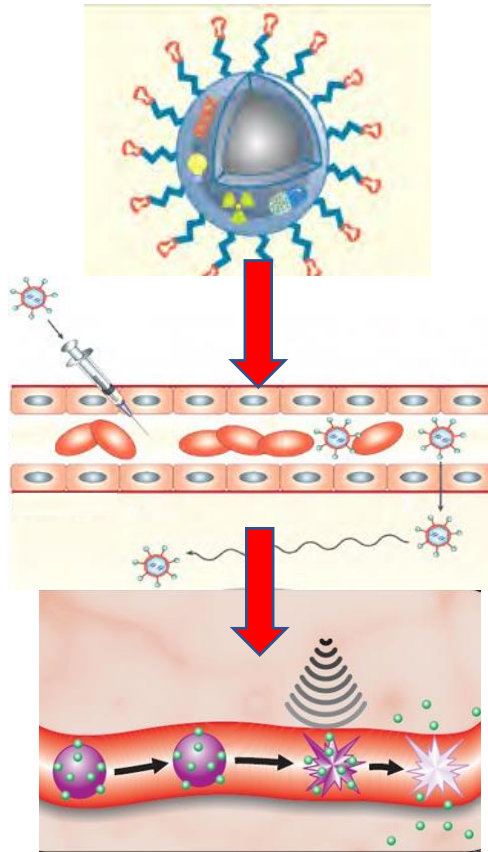


**Figure 5: Microbubbles in targeted drug delivery.**

*Diagram shows a microbubble with the ligands on its surface. High intensity ultrasound waves, shown as grey curvy lines, are applied to bubbles in the blood vessels, leading to the release of the payload drugs from the surface of the microbubbles (<https://thefutureofthings.com/3805-ultrasound-activated-microbubbles-fight-cancer/>, 01 August 2018, 11.05am).*

### **2.2.2.1 Oesophageal structure and its diseases**

A summary of the oesophagus structure and its diseases is described here because the main focus of chapter 4 is on the development of microbubbles for drug delivery to the oesophagus.

The oesophagus is located behind the trachea and heart and in front of the spinal column; it passes through the muscular chest diaphragm before

entering the stomach. Both ends of the oesophagus are closed off by muscular constrictions known as sphincters. At the upper end is the upper oesophageal sphincter, and at the lower end is the oesophageal sphincter, as shown in figure 6.

The control and action of different components within the oesophageal tube enable the passage of food, which is the main function of the oesophagus. The lower oesophageal sphincter is a 3–5 cm long muscle which remains closed, except during swallowing, vomiting and belching. This part is influenced by three factors: smooth muscle sphincter, autonomic and enteric innervation, and the presence of gastrointestinal hormones and peptides. The relative difference in pressure prevents reflux of the stomach contents into the oesophagus (Mittal & Goyal, 2006).

Oesophageal blockage leads to an inability of the organ to transport food from the mouth to the stomach. One of the most common disorders is gastro-oesophageal reflux. Gastro-oesophageal reflux disease (GORD) is a common condition, where acid from the stomach leaks up into the oesophagus. It usually occurs as a result of the ring of muscle at the bottom of the oesophagus becoming weak. Gastro-oesophageal reflux can cause oesophageal damage because of the effect of acidic contents of the stomach on the oesophageal mucosa (Kikendall et al., 1983).

There are various techniques for the treatment of GORD or its complications. The medications which increase the motility of the oesophagus, such as cisapride, or the ones which reduce the acidity of the stomach, such as omeprazole, are applied for the treatment of GORD (Toussaint et al., 1991;

Welage & Berardi, 2000). The other significant disease affecting the oesophagus is cancer, which is the uncontrolled proliferation of the oesophagus epithelial cells. The most common symptom of oesophageal cancer is difficulty in swallowing. There are two types of oesophageal cancer based on the type of malignancy: squamous cell carcinoma and adenocarcinoma. GORD and Barrett oesophagus may increase the risk of oesophageal adenocarcinoma. Heavy alcohol drinking and smoking increases the risk of oesophageal squamous cell carcinoma (Mohamed Abdulkadir Hassan Kadle, 2015).

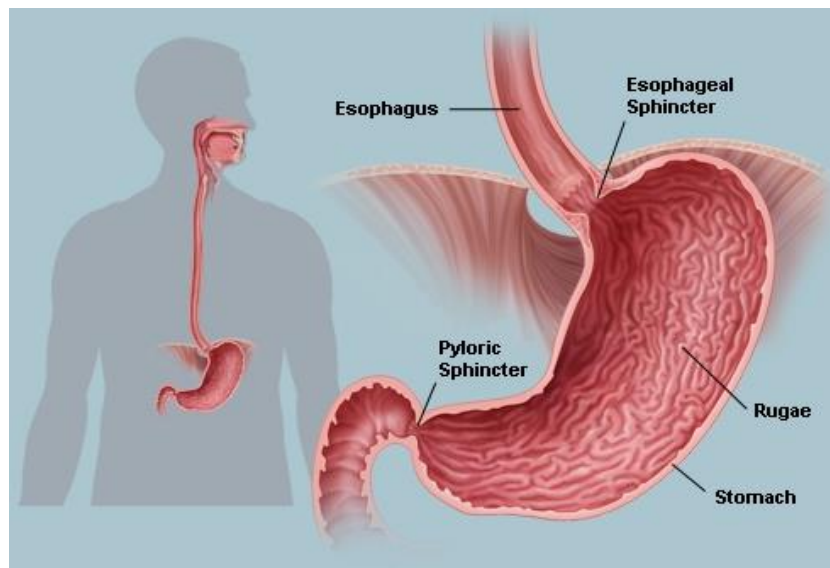


**Figure 6: Oesophagus structure and position in the body.**

*This figure is taken from the human body sections of defenderauto (<http://defenderauto.info/pyloric-sphincter/>, 03 August 2018, 10.24am).*

#### **2.2.2.2 Oral drug delivery**

There are several methods of drug administration such as oral, injections, sublingual, buccal, rectal, vaginal, ocular, otic and nasal routes. Oral drug delivery is the preferred administration route due to its perceived ease of

administration. The oral routes provide maximum active surface area for the administration of different drugs.

There are some issues associated with oral drug delivery method such as incomplete release, the requirement for repetitive dosing, as well as unpredictable absorption, which have led to the concept of the oral control release system. A control drug release system works using many different mechanisms to control drug release.

One of the factors influencing oral drug delivery methods is the gastric retention time (GRT). This is important for drug delivery to the gastroesophageal region, as following taking drugs orally, increased gastric retention time will increase the chance of the drug's contact with the gastroesophageal region and improved efficacy of the drug. In contrast, short GRT results in reduced release of the drug. A gastro retentive dosage form (GRDF) can overcome the problems associated with short GRT (Nayak, Maji, & Das, 2010). A GRDF system is defined as a system which is retained in the stomach for a long enough time interval against all the physiological barriers, releasing the active component in a controlled manner (Pawar et al., 2011). This method improves bioavailability, therapeutic efficacy and may allow a reduction in the dose, due to the steady therapeutic levels of the drug (Baumgartner et al., 2000). An example of such a system is the floating dosage form, as shown in figure 7.

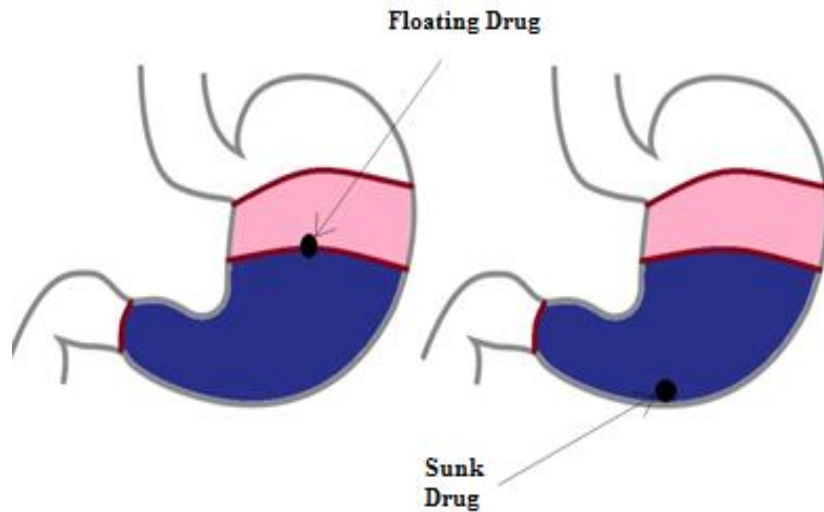


**Figure 7: Floating dosage form.**

*This figure shows the difference between the status of the floating drug and sunk drug in the stomach. The lower-density drugs remain in the stomach for a longer period and this provides a longer time for the release of the drug, while the drugs with higher density have a higher possibility of leaving the stomach due to sinking in the stomach and being closer to the exit.*

One aim of this study, as discussed in chapter 4, is the development of a method for the oral delivering of drugs to the oesophageal regions. The connected section of the oesophagus to the stomach (gastroesophageal region) (Figure 8) has the highest significance in regard to drug delivery. The special geometry and angle position of this region has made drug delivery to this region a challenge, especially in patients with oesophageal dysplasia (Kappelle & Vleggaar, 2016). In this study the application of microbubbles for delivering drugs to the oesophagus was investigated.

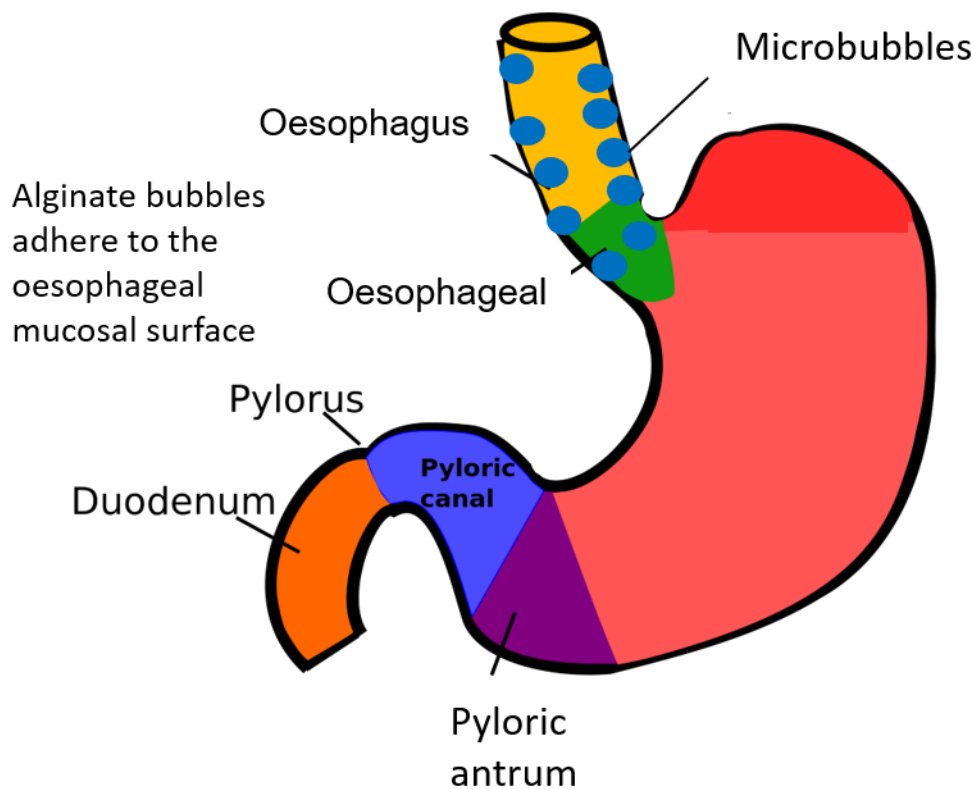


**Figure 8: Gastroesophageal junction.**

*This figure illustrates the oesophageal region (sphincter) in green. The lower oesophageal sphincter is located partly in the abdomen and partly in the hiatal canal. The lower oesophageal sphincter is a 3-5 cm long muscle section that is continuous with the circular muscle of the inner oesophageal tube (Mahadevan, 2017). Except during swallowing, vomiting and belching, this part remains closed. As this region is involved in a variety of oesophageal disorders, such as gastroesophageal reflux and malignant transformations, delivery of drugs to this region of the oesophagus is of significant importance. This figure is a modification from the Houston Sleeve Surgeon website (<https://houstonsleevesurgeon.com/the-gastric-fundus-and-lap-band-removal/>, 05 August 2018, 11.21am).*

### **2.2.2.3 Approaches to gastro retentive drug delivery system**

Several techniques can be used in order to achieve a successful gastro retentive drug delivery system (GRDDS). The following are the main currently

used techniques (Pooja Mathur, Kamal Saroha, Navneet Syan, 2010).

#### **2.2.2.3.1 Bioadhesive or mucoadhesive systems**

These methods are used to increase drug absorption in the lumen area of the body covered by mucosal layer, such as gastrointestinal system. This method applies bioadhesive polymers, which stick to the epithelial surface of the gastro intestinal tract (GIT). The mechanism through which bioadhesion-mediated drug delivery is achieved is the formation of hydrogen and electrostatic bonding at the mucus-polymer boundary (Pooja Mathur, Kamal Saroha, Navneet Syan, 2010).

The definition of mucoadhesion is the interaction between two surfaces, while one of the surfaces is made of biological materials such as mucosa membrane. The interaction between the two surfaces is usually as a result of interfacial forces which hold this contact for a long time (Smart, 2005). Mucoadhesion has been increasingly used in recent years for more effective drug delivery as it improves the therapeutic efficacy of the drugs, and in particular, it has improved tumour targeting in cancer therapy by facilitating the delivery of various biological agents, such as peptides or antibodies, through a variety of administration routes (Andrews, Lavery, & Jones, 2009; Mansuri et al., 2016).

#### **2.2.2.3.2 Nanoparticles and mucoadhesion for drug delivery**

Encapsulation of active drug into microbubbles has been possible through nanotechnology. Improvement of drug delivery can be achieved by the

addition of nanoparticles and choosing appropriate nanoparticle material which can help to improve targeting and increase bioavailability of the administered drug, to introduce further modification which gives the drug more suitable mucoadhesive properties. Microbubbles have been introduced to drug delivery application due to their large surface area, and low weight. These qualities can improve the adhesiveness of the system. Their ability in loading drug and providing high adsorption efficiency makes them suitable carriers for trans-mucosal drug delivery (Malik et al., 2015).

#### **2.2.2.4 Floating drug delivery system**

Floating systems, as initially described by Davis in 1968, are defined by their lower bulk density than that of the gastric fluid, thus remaining buoyant in the stomach for an extended period.

Different floating systems have been created to improve the retention of the oral dosage within the gastric system. These are low-density systems with sufficient buoyancy to float on top of the gastric content and persist in the stomach for longer, allowing the drug to be released slowly and at the desired rate (Talukder & Fassihi, 2004).

#### **2.2.3 Scaffolds from microbubbles for tissue engineering**

Cell culture in three dimensions has recently become the popular approach in regenerative medicine and for investigation of cell–cell interactions, mechanisms of stem cell differentiation and drug sensitivity studies. Various materials are available to develop scaffolds for 3D culture.

In clinical medicine, in addition to the role of microbubble technology in drug delivery, microbubbles have the potential to be used for drug discoveries. It was shown before (Ahmad, Stride, & Edirisinghe, 2012) that microbubble technology could be used for building tissue-like structures suitable for various biological applications. However, the microbubble scaffold has not been used so far for drug investigations. Microbubble scaffolds mimic the spongy structure, having the potential to be used for drug discoveries for leukaemia.

Currently, microbubbles have been used as pore generators in the biomedical field (Wang et al., 2009). It has been shown that a sponge-type, multiple-layer alginate scaffold could be made by collecting bubbles over a period of time (Haynesworth, Reuben, & Caplan, 1998; Cutroneo, 2003; Dhandayuthapani et al., 2011).

The scaffolds produced by biomaterial processing act as extracellular matrices (ECM) and can be produced from natural or synthetic polymers, or a combination of both (Carletti et al., 2011; Pereira et al., 2013). To mimic the function of the natural ECM available in the human body, scaffolds must balance mechanical function with the transport of bioactive agents (Hollister, 2005; Chan & Leong, 2008). While a denser scaffold offers a better function and mechanical strength, a more porous scaffold provides greater diffusion of gas/liquid components and provides cell growth (Carletti et al., 2011). Porous and spongy structures with interconnections and large pores are ideal templates for the development of scaffolds for cell culture. To satisfy these requirements they must have high porosity, high surface area and uniform 3D shape (Vats et al., 2003). Different methods are still under investigation for

constructing artificial organs. Recently, alginate-based 3D cell culture systems like foam scaffold structure have been developed. Foam alginate scaffold has the advantage of having the ability to change the physical characteristics of the hydrogel by changing the amount or type of gelling ions or alginate and can evolve into an ideal environment in which cells can proliferate or differentiate.

The modification of alginate can be achieved by the attachment of peptides that mimic extracellular matrix proteins (such as calcium chloride), thereby allowing immobilised cells to seemingly interact with the alginate hydrogel (3D Cell Culture in Alginate Hydrogels).

In addition to the application of the microbubbles in ultrasound-guided delivery of contrast agents in medical imaging, and also in targeted drug delivery, there are other applications for microbubbles in food engineering, and the water and waste treatment industries.

#### **2.2.4 The role of microbubbles in food engineering**

Bubbles can be used in the manufacturing of many food products such as cakes, ice creams and soft drinks. The application of microbubbles in the food industry has many advantages such as lowering the cost and forming novel structures (Campbell & Mougeot, 1999). Microbubbles can be used to modify the texture, appearance and shelf life of food. Furthermore, microbubbles have the ability to be coated with nutritional ingredients or drugs that could help to improve the nutrition or act as a medicinal aid in food (Shen, Longo, & Powell, 2008).

### **2.2.5 Microbubbles application in water and wastewater treatment**

Bubbles are used in the treatment and filtering of water and wastewaters for the removal of volatile contaminants or particulate materials from the aqueous phase (Ahmed & Jameson, 1985; Ketkar, Mallikarjunan, & Venkatachalam, 1991; Chu et al., 2007). Because of the large surface area and relatively slow rise velocities, microbubbles are used in microflotation for wastewater treatment (Cassell, Kaufman, & Matuevic, 1975; Rodrigues & Rubio, 2007). When microbubbles rise in wastewater, they make contact with organic contaminants and other low-density particles in the water, and then carry them to the surface. This forms a collective layer for separation in the purification processes. In electroflotation, which is a similar method applied in the mineral industry, fine particles are separated from solutions using microbubbles (Jiménez et al., 2010). The generated hydrogen and oxygen gases from water electrolysis is usually used to float particles to the surface of water in a simple process like electroflotation (Chen, 2004).

### **2.3 Methods for microbubbles fabrication**

The generation of microbubbles in biomedical applications is generally carried out using three different methods: sonication, coaxial electrohydrodynamic, and T-junction. These methods are explained briefly here.

### 2.3.1 Sonication

Through sonication, high intensity ultrasound waves are applied to suspend microbubbles in a liquid containing either a surfactant or a polymer solution, suitable for forming a stabilising coating layer around the surface of the microbubbles (Suslick et al., 1999).

To start the suspension process, gas is distributed in liquid containing surfactant or appropriate material to cover the bubble's surface. In most cases this task is accomplished via a high-shear mixer or a sonicator.

There are multiple ways to achieve sonication. For example, gas and a surfactant solution held within a vial are sonicated through a very thin membrane while applying a focused ultrasound beam or an ultrasound probe. Alternatively, the same process can be achieved within the confines of a syringe with the addition of a low-power ultrasound pulsed assembly, attached to the body of the syringe (Prajapati & Agrawal, 2012).

Although sonification is one of the most commonly used methods of producing microbubbles, there are clear disadvantages to this method. Given the broad range of microbubbles produced, there is a need for further filtration of bubbles with sizes greater than 10  $\mu\text{m}$  (Klibanov, 1999). This is to allow for intravenous uses and the removal of excess surfactant. Despite this process, the resulting size distribution of the bubbles is still relatively wide, indicating the presence of a spectrum of resonance frequencies (Stride & Edirisinghe, 2009). Production of microbubbles with different sizes can be one of the disadvantages of the sonication method in the field of drug delivery. The

variable size distribution is dependent on the frequency, pulse and power of the ultrasound waves used. Additionally, a varying range of properties are observed from individual microbubble coatings, resulting in a noticeable change to their dynamic and acoustic response (Wang, Moser, & Wheatley, 1996).

### **2.3.2 Coaxial electrohydrodynamic atomisation (CEHDA)**

Another method of microbubble production is electrohydrodynamic atomisation. During this process, liquid is pushed through a capillary tract at a maintained flow rate. The liquid is sustained at several kilovolts in relation to a ground electrode placed a few centimetres away. This process allows for the liquid at the outlet of the capillary to form various shapes under the influence of the surrounding electric field (Tang & Gomez, 1994).

One such method is coaxial electrohydrodynamic atomisation (CEHDA) (Farook, Stride, & Edirisinghe, 2009; Stride & Edirisinghe, 2009). During this process, a concurrent coaxial flow of liquid medium, lipid agent and gas (i.e. air) are placed under the effects of a nearby electric field (Ahmad et al., 2009), which allows for the lipid to form an outer layer around air, forming the desired microbubbles. Figure 9 illustrates a CEHDA setup, where two needles are concentrically placed and supplied with fluids from separate syringe pumps (Loscertales et al., 2002).

Bubble size and consistency correlates with both the supplied voltage and the flow rate through the needles (Farook, Stride, & Edirisinghe, 2007). Even though the above process produces the desired microbubbles with a diameter

range of 1–10  $\mu\text{m}$  (suitable for medical applications), maintaining uniformity of the bubbles continues to be a challenge.

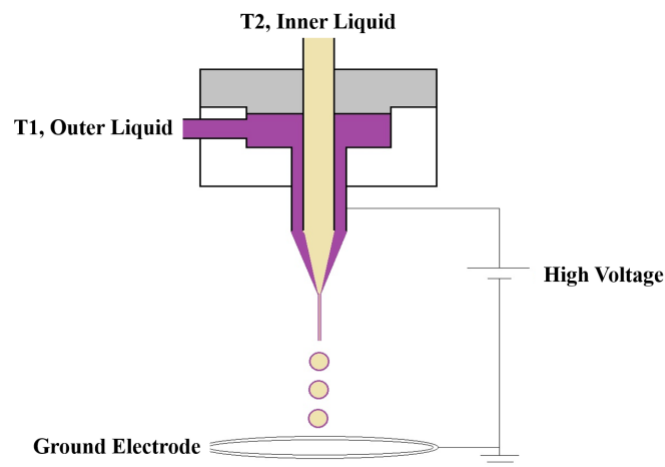


**Figure 9: Coaxial electrohydrodynamic atomisation setup.**

*In order to form the required microbubbles, the inner needle is filled with gas and the outer needle is supplied with a medium of a liquid solution. A voltage variance of several kilovolts is produced between the needles and an earthed electrode, which is positioned directly below and in close proximity to the end of the needles (Stride & Edirisinghe, 2009).*

### 2.3.3 Microfluidics setup

Microfluidic devices have recently been used to produce microbubble suspension in monodisperse liquid droplets, through the process of control and manipulation of liquids with the length scale in the order of a micrometre (Zhao & Middelberg, 2011). Microbubbles are formed through an orifice where a column of gas is mixed with a fluid flow. Consequently, at a specific distance from the orifice, the gas-liquid mixture becomes unstable and bubbles are formed via a “pinch off” process (Stride & Edirisinghe, 2009). Bubble size and regularity depend on the physical properties of the liquid, gas

and flow rates, as well as the dimensions and profile of the orifice and channels. Microfluidic devices enable the formation of monodisperse microbubbles since they can be fabricated with internal dimensions at the micrometre scale. New methods have been used to build microfluidic structures to produce monodisperse microbubbles using gas, fluid streams and microdroplets with two immiscible fluid streams (Zhang & Wang, 2009).

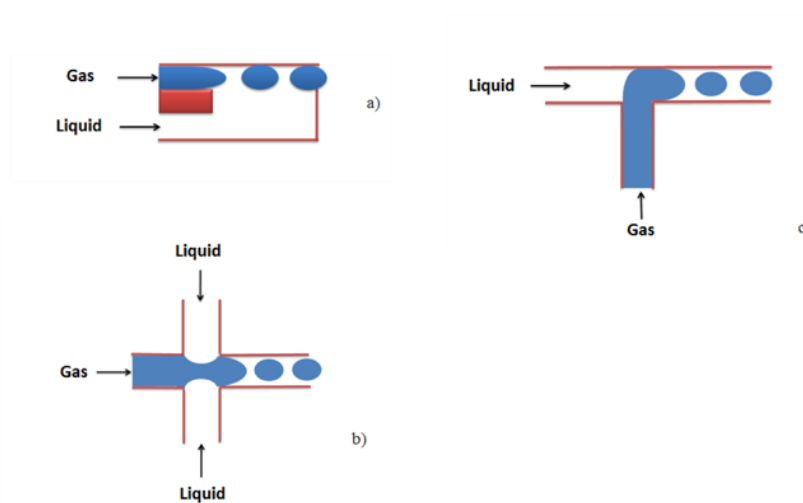


**Figure 10: Microfluidic bubbles generating geometries.**

*Illustrations of the three main microfluidic geometries used for bubble formation. (a) co-flowing, (b) flow focusing geometry, and (c) cross flowing streams in a T-shaped junction. This figure has been modified from Zhang and Wang (Zhang and Wang, 2009).*

### 2.3.3.1 Co-flowing devices

One of the techniques to generate monodisperse bubbles is the co-flowing microfluidic system (Figure 10a). The formation of the microbubbles in this device happens when the dispersed phase (gas for microbubbles and liquid for droplets) is given into the co-flowing continuous phase using a capillary (Zhang and Wang, 2009). A gas column enters the mixing channel, which

causes a bubble to start forming and move downstream. The velocity of the liquid flow pushes the bubble surface against the channel wall, and this leads to microbubble formation (Martinez, 2009).

### **2.3.3.2 Flow focusing devices**

Flow focusing (Figure 10b) is another method for generating spherical monodisperse microbubbles (H.A. Stone, A.D. Stroock, 2004; Yobas et al., 2006). In this device the continuous phase flows through two side channels and the dispersed phase is given through a middle channel. The squeeze of the dispersed phase leads to it breaking up into microbubbles at a mixing channel where the two phases meet. The dispersed phase is detained in the central region of the main channel, which results in the production of the spherical bubbles in the flow-focusing device. There are two modes of flow in this system: dripping and jetting (Zhou, Yue and Feng, 2006). Jetting and dripping occur at high and low flow rates, respectively. The flow focusing generators have either axisymmetric or asymmetric geometry. Axisymmetric flow focusing devices are made by inserting capillaries inside square channels, forming a coaxial arrangement. This leads the liquid channel to surround the gas channel, and along with the gas channel merge into a single stream (Martinez, 2009). By etching channels on a rigid substrate, such as glass or PDMS rectangular blocks, asymmetric devices are manufactured (Garstecki, Gañán-Calvo and Whitesides, 2005). The geometry of asymmetric devices is composed of a central channel that merges with two side channels into an exit opening in which the bubble breakup takes place.

### **2.3.3.3 Cross flowing (T-junction) devices**

The most commonly used method for generation of microbubbles is the T-junction geometry. Using this device, the two phases are injected vertically into the main flow channel (Figure 10c) (Garstecki et al., 2006; Van Der Graaf et al., 2006). The formation of the bubbles using T-junction geometry is remarkably different from that in the flow-focusing devices. In the T-junction method the dispersed phase (either gas or liquid) moves into the main fluid channel. This leads to the formation and expansion of a bubble until it obstructs the channel. Following the obstruction, the fluid pressure gradient distorts the bubble. Following the touching between the bubbles in the upstream and downstream side of the inlet channel, the bubble breakup occurs. The flows in T-junction geometries are in either cross-flowing or perpendicular channel mode. Low-cost maintenance and generating monodispersed microbubbles can be the advantages of this system.

## **2.4 Microbubble size and stability**

Microbubble size has a significant role in drug delivery, depending on the application. An appropriate size is vital in order to achieve accurate diagnosis or dosage release. Factors such as liquid and gas flow rates, as well as viscosity and capillary size, are influential parameters in determining the size of microbubbles (Zhang et al., 2012).

Another important factor in the microbubble drug delivery field is the stability of the bubbles. Microbubbles in biomedical applications are air-filled

microspheres and as a result can easily burst under the effects of pressure. Increasing microbubble stability leads to improved efficiency of drug dosage. Therefore, in using microbubbles in the healthcare field, attempts are made at enhancing the stability of microbubbles via different techniques (Owen et al., 2014). Gold nanoparticles have been used in the current study to stabilize microbubbles. It was shown previously through theoretical modelling as well as experimental investigations that incorporating solid nanoparticles into the solution results in increased stability and life span of the microbubbles (Mohamedi et al., 2012). Previous work shown that using gold nanoparticle suspension to coat the microbubbles was successful (Mahalingam, Meinders and Edirisinghe, 2014).

## **2.5 Biomaterials**

Biomaterials refer to specific groups of materials with medical/therapeutic applications. Biomaterials are natural or synthetic materials used in medical fields to improve quality of life by either replacing tissue/organ or assisting their function (Patel and Gohil, 2012).

A designed biomaterial product should function in the physiological environment without having a harmful effect on the organs. To fulfil this purpose, a biomaterial product should be non-toxic. In general, a non-toxic material has no carcinogenic, pyrogenic, allergenic or inflammatory effect in the body. A biomaterial product should not give off anything from its mass unless it is specifically engineered to do so. Some biomaterial products are designed to release a necessary amount of mass that is considered toxic, such as designed products for cancer therapy. Natural biomaterials are

derived from animals, microbials, or plants. One advantage of natural biomaterials is their similarity to the physiological structures. Natural materials, glass, metals or polymers have been used to make tissues which have been damaged by disease or injury. Recently, with the advent of molecular biology, it has been possible to design materials that have a specific biological function.

Novel biomaterials, which might be bioderived, bioinspired or biomimetic, or biocompatible self-healing materials, are used in a wide range of physiologically compatible structures such as coatings, membranes, gels, drug delivery carriers or cell culture scaffolds. The innovations in biomaterials include the development of products such as novelty metals, lightweight alloys, biodegradable metals, ceramic or polymeric materials, which have improved performance in regard to tissue integration or reduced device-related complications (Hendriks, 2011).

### **2.5.1 Biocompatible polymers**

Developments in the synthesis of new types of polymer have been very important for innovations leading to the introduction of advanced methods for drug delivery. The new polymers which are used for drug delivery have made the longer release of drugs possible. This has been achieved through a better control of the rate at which the pharmacological agents should be released (Liechty et al., 2010). Because of these developments, biocompatible polymers have started to be used extensively, as they have been shown to improve patients' tolerance by reducing the side effects. Compared to intravenous or intramuscular injections, when the drug dose suddenly rises

and also drops in the systemic circulation, the long and continuous release of the drug prevents such sudden fluctuations. Drug delivery using polymers also makes it possible to deliver a pharmaceutical agent to a particular site in the body or to a particular cell type (James et al., 2014). One of the factors influencing the pharmacokinetics of the drugs inside the body is the degradation of drugs by various factors, such as digestive enzyme of acidic condition of the stomach. Biocompatible polymers improve their efficacy by protecting drugs (Gombotz & Pettit, 1995). A particular polymer (such as a surface polymer) is chosen for its drug delivery properties and its physical and chemical structure, which are important in regard to its binding to the drug. Protection in a particular environmental condition should also be considered, such as stability against acidic condition of the stomach (Huang et al., 2003; Hu et al., 2014). Molecular weight, solubility and also adhesion of the polymers influence the controlled drug delivery system and determine the site of action (Pillai & Panchagnula, 2001). Amongst the widely used biocompatible polymers which have been approved by Food and Drug Administration (FDA), polyvinylpyrrolidones, Eudragit L100-55, Eudragit S100, poly( $\epsilon$ -caprolactone) and ethyl cellulose can be mentioned.

### **2.5.2 Natural polymers**

Natural polymers are known as the oldest class of polymers, as they are produced in nature by various living organisms (Mano et al., 2007). Their abundance in nature makes these polymers a relatively inexpensive class of biomaterials, used in numerous applications, particularly in the biomedical field.

Natural polymers are believed to have great prospects in the area of drug delivery, with an extensive range of properties and chemical structures, while retaining biodegradability, low toxicity and good structural stability (Sharma, Limaye, & Kale, 2012). Because of their biological similarity to the environment, these polymers have superior capabilities in activating specific cellular interaction with their neighbouring tissue (Gomes & Reis, 2004). Their breakup *in vivo* takes place through hydrolysis and enzymatic degradation (Gomes & Reis, 2004).

Natural polymers are also characterised by having reactive sites in their chemical structure, giving them extra importance in the pharmaceutical field. This property allows for cross-linking, ligand conjugation and other important modifications (Dang & Leong, 2006). Even without these modifications, natural polymers still provide numerous useful biological functions, such as polysaccharides, which have a major role in intercellular communications (Malafaya, Silva, & Reis, 2007).

However, despite their significant features, natural polymers suffer from limitations, such as their rapid degradation and inferior mechanical stability. To overcome these limitations, various techniques have been established to enhance the mechanical properties of these polymers. Their rapid degradation can also be improved through the active packaging of the polymer or natural fibre reinforcement (Jana et al., 2011). Due to extensive research and focus on enhancing their properties, the adoption of natural polymers has improved considerably, and they are used extensively in numerous biomedical applications, functioning as emulsifying agents, drug stabilisers, gene delivery vehicles and 3D culture scaffolds.

Natural polymers have been shown to be usually non-toxic, even when used in high concentrations and on a regular basis (Dang & Leong, 2006). This permits their extensive and long-term use without additional toxicity, in contrast to synthetic polymers. This feature is considered particularly beneficial for the development of treatments in cancer cases, which tend to incorporate higher dosages and longer durations of use. In this respect, one of the most popular natural polymers is alginate, widely used in drug delivery applications. It was selected as a model polymer for hydrophilic nanoparticle development and will be discussed further in the next section.

Alginate is a useful and thus popular polymer in the field of drug delivery; it is used as a suspending agent, tablet binder, or as stabiliser for emulsions (Kulkarni, Butte, & Rathod, 2012). Alginate drug delivery systems are recognised for their ability to improve the transport of drugs through extremely organised biological barriers, such as the ocular, intestinal and nasal routes (Goycoolea et al., 2009). For cancer treatments (Park et al., 2012) alginate has been suggested as an effective encapsulating material for efficient local delivery of drugs to target specific cancerous tissue.

The relatively easy gelation process of the alginate allows the use of this polymer in the encapsulation of different biological materials such as protein, DNA and even cells, without affecting their function. This is largely due to the inert and aqueous setting provided within alginate systems (Gombotz & Wee, 1998).

Alginate systems biodegrade under typical physiological conditions, which is a key feature of these drug delivery systems (Gombotz & Wee, 1998).

Alginate nanoparticles were found to significantly improve the bioavailability of encapsulated drugs, compared to those in the free form. This is in spite of the challenges faced in the fabrication of nanoscales (Kulkarni, Butte, & Rathod, 2012). Alginate belongs to the polysaccharides family of polymers. These are a class of natural polymers, comprising of simple sugar monomers, which are characterised by noteworthy properties, such as biocompatibility, biodegradability and non-toxicity (Malafaya, Silva, & Reis, 2007). These properties have enabled alginate to obtain substantial attention, within the category of polysaccharides. Alginate is commonly found in the shape of structural components of brown algae and certain soil bacteria, as a block of co-polymers made up of guluronic and mannuronic acids. These can be found in various block lengths and sequential arrangements where the ratio between the aforementioned acids and their sequential arrangement varies with the source of the alginate (see Figure 11) (Nair & Laurencin, 2007).

The molecular weight and the ratio between the guluronic acid and the mannuronic acid determine the gelling properties of alginate particles (Østberg, Vesterhus, & Graffner, 1993). The process of extracting alginate from algae, in the form of alginic acid, is usually accomplished through the reaction of a base solution with an acid (Nair & Laurencin, 2007).

It is possible to prepare alginates with a range of molecular weights, allowing for the development of alginate systems with a wide range of properties. In a purified state, alginates can be produced in different salt forms, such as sodium, potassium and calcium (Rinaudo, 2008). The key properties of an alginate which drive its biomedical suitability, such as biocompatibility, biodegradability and bioadhesiveness, are frequently attributed to the

hydrophilic nature of the polymer (El-Sherbiny and Yacoub, 2013). Alginate is known for its mucoadhesive properties due to its anionic nature, which allows alginate to selectively adhere to mucosal membranes. This is considered a beneficial feature in developing drug delivery systems for transmucosal applications. Additionally, alginate-based materials are known to be pH-sensitive, meaning that this property can be used to control the release of the encapsulated biomolecules from the delivery vehicle, subject to the pH of the targeted tissue (Malafaya, Silva, & Reis, 2007). Furthermore, alginate properties can be modified for specific uses within different applications. One of the main characteristics of the alginate gels is their high gel porosity and this is controlled via coating techniques, in order to provide a faster diffusion process of the encapsulated materials.

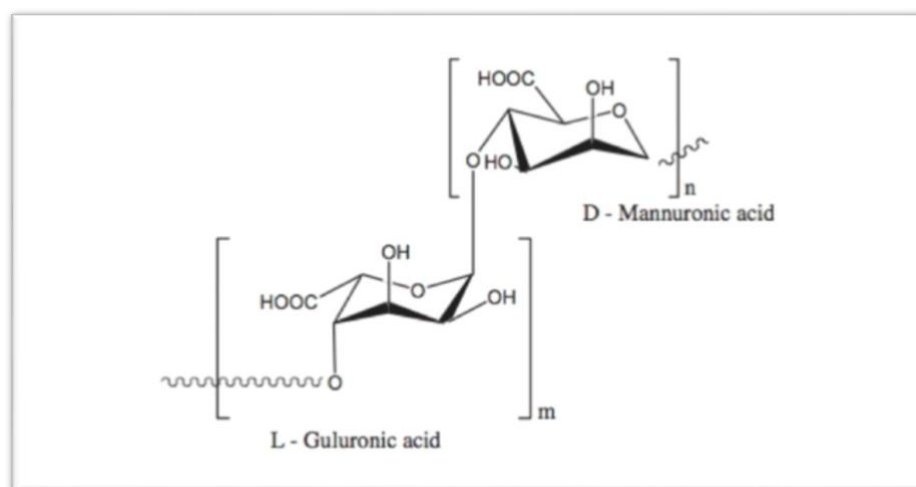


**Figure 11: Alginate acid.**

*The structure of alginate acid* (Nair & Laurencin, 2007).

### 2.5.3 Scaffold fabrication methods

Various fabrication techniques are used in scaffold production for healthcare

applications. Particle leaching (Mikos et al., 1994), polymer casting and phase separation (Liu et al., 2011), solvent casting, emulsion freeze-drying, electrospraying (Sullivan & Jayasinghe, 2007), electrospinning (Li et al., 2005) and foaming (Ekemen et al., 2011) are amongst the widely used techniques which are described here. Scaffolds generated by these methods have pores with a wide size and shape distribution, leading to a sufficient transport of nutrition, migration and attachment of cells (Lee, Silva, & Mooney, 2011).

#### **2.5.3.1 Particle leaching technique**

Generally, in this method, particles such as salt, sugar-leaching incorporates or specifically prepared spheres, are dissolved in a polymer sample and additionally washed out, after processing the polymer sample into the final form, creating additional porosity in the scaffold structure (Mikos et al., 1994). The benefit of this method is the generation of large pores with high control over the pore morphology. However, this method is not recommended for soluble protein scaffolds because of the risk posed by remaining material deposit that is harmful to the tissue after processing.

#### **2.5.3.2 Emulsion freeze drying technique**

An emulsion is formed by the homogenisation of water and a polymer-solvent system. The emulsion is then cooled down, resulting in solidification of the polymer and the formation of a polymeric porous structure. Further solvent and water content are removed through freeze-drying (Ma & Zhang, 1999).

Enabling the incorporation of proteins during the fabrication and production of relatively thick scaffolds with large pores are the hallmarks of this method. One of the limitations for this method is that the permeability of the pores in the obtained morphology is very poor, which leads to a limitation of cell growth and the transport of nutrients through the scaffold.

### **2.5.3.3 Foaming via pressure quenching**

In the foaming process, a soluble inert gas such as N<sub>2</sub> or CO<sub>2</sub> is used as a blowing agent, to obtain porosity in polymers by using the pressure quenching method. The superiority of this method over the others is due to the lack of solvents, removing the risk of there being remaining residue. One of the weaknesses of this method is that the pores are not infiltrated. Additional post-processing steps such as plasma treatment or pulsed ultrasound can help to obtain porous morphologies.

## **2.6 Acute myeloid leukaemia**

AML is a haematopoietic malignancy. It is characterised by the accumulation of cells which have stopped differentiation to more mature blood cells. An arrest in normal differentiation of the stem cells results in an accumulation of the cells which are immature, called blasts. An increased number of blast cells is associated with a decreased number of mature blood cells such as red blood cells (erythrocytes), white blood cells or platelets; this condition is called multilineage cytopenia. The reduction in the number of the normal blood cells will lead to infection, anaemia or bleeding disorders, which are

responsible for the morbidity and mortality in AML patients (Figure 12). Chemotherapeutic agents which are commonly used for treating the majority of AML patients, such as anthracycline and cytarabine, have not been able to prolong the survival of the patients within the last three decades. For the AML patients younger than 60 years, the five-year overall survival rates have ranged from 30% to 40% (Longo, 2015). The median overall survival for this category of patients has been nearly one year. The main reason for relapse in AML patients following an early response to treatment is believed to be due to the role of LSCs. LSCs in AML patients form a minor fraction of the leukaemia cell population and have the ability to reproduce themselves and the more differentiated leukaemia cells. The characterisation of the LSCs is based on the ability of the cells to settle in the BM of immunodeficient mice and to produce leukaemia cells when grafted into mice. When LSCs are transplanted into mice, they are capable of self-renewing, and also partially differentiating into non-LSC bulk blasts, that resemble the original disease but are unable to self-renew in serial transplantation (Dick, 2005). Because of the role of LSCs in the maintenance of leukaemia, even under current treatments, in order to eradicate the disease and achieve long-term remissions, a therapeutic approach should aim at eliminating the LSC population (Figure 13). The majority of AML samples (~75%) are positive for the expression of CD34 marker on their surface, and nearly all studies of AML LSCs have focused on this subgroup. CD34 is a cellular surface marker for identification of the normal haematopoietic stem and progenitor cells. This means that during the proliferation and differentiation of the normal stem cells to progenitor cells, this marker is present on the surface of the cells. CD34 disappears when the cells exit the progenitor stage following further

maturation. As AML results from maturation arrest of the stem or progenitor cells, the consequently developed AML cells are positive for CD34 marker.

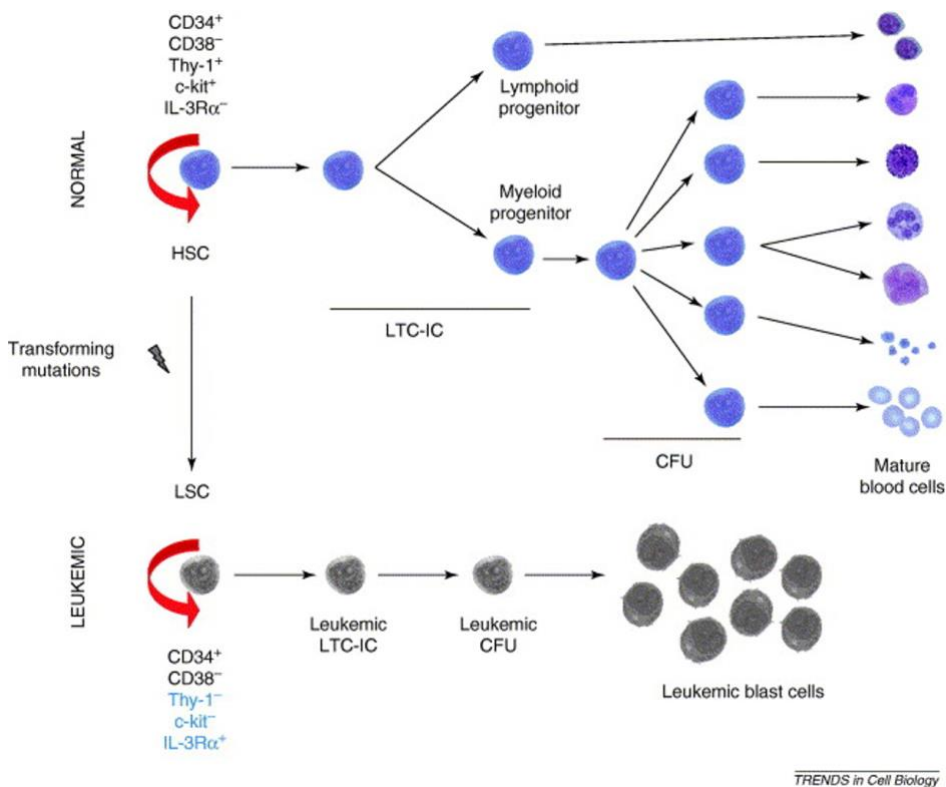


**Figure 12: Schematic illustration of the normal and leukaemic human haematopoietic hierarchies.**

*Human haematopoietic cells are organised in a hierarchy. The HSCs are a small fraction of the haematopoietic cells and maintain the blood cell population by self-renewal. In addition to self-production, HSCs give rise to more lineage-restricted, differentiated progenitors which have less self-renewal capacity (long-term culture-initiating cells (LTC-ICs); colony-forming units (CFUs)). These more committed cells produce mature blood cells with various functions. Aberrations in self-renewal and differentiation (caused by acquired mutations) generate LSCs, which are the source of sustained growth of the leukaemic cells. The altered pattern of growth and differentiation in LSCs is demonstrated by aberrant expression of some cell surface markers (indicated in blue) (Wang & Dick, 2005).*

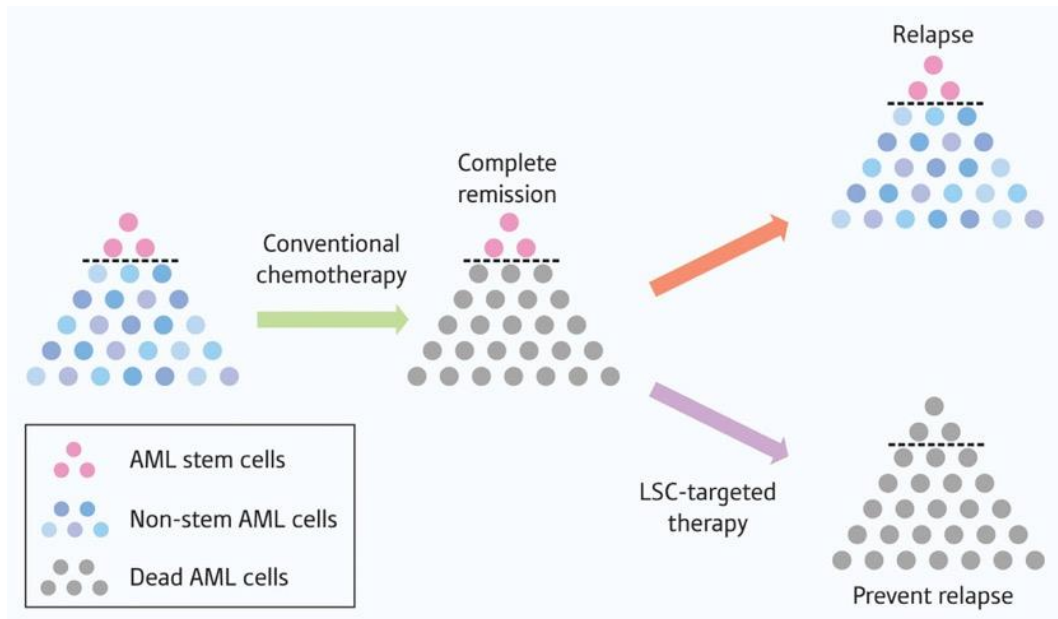


**Figure 13: Targeting LSC is essential for preventing relapse following therapy.**

*Chemotherapy results in killing the bulk of the AML cells, which is presented as an improvement in clinical condition of the patients and the return of the blood cell counts to normal level. For the majority of the AML patients this does not last long as the leukaemia returns, and patients present with relapse. The relapse is believed to be due to the activity of the LSCs, which are not eradicated by conventional chemotherapeutic agents. Eradication of the LSCs is currently believed to be the approach which can lead to a cure in AML patients (Ishikawa et al., 2007).*

## 2.7 Chronic myeloid leukaemia

Chronic myeloid leukaemia (CML) is a pluripotent haematopoietic stem cell malignancy, characterised by a balanced reciprocal translocation that involves chromosomes 9 and 22. This is termed a Philadelphia chromosome (Ph), and carries a *BCR-ABL1* fusion gene which is a constitutively active tyrosine kinase. The protein produced from this fusion gene encourages leukaemia cells to divide in an uncontrolled manner. This fusion is the

fundamental cause of the chronic phase of CML (Goldman & Melo, 2003). CML is mainly prevalent in adults, with incidence rates increasing with age, as almost half of the cases (48%) are diagnosed in those over 65 in the UK. As soon as it was known that *BCR-ABL1* function is responsible for the biological alterations and clinical presentations in CML, the *BCR-ABL1* kinase activity became the most attractive target for treatment (Figure 14). Due to the introduction of imatinib, a tyrosine kinase inhibitor (TKI), as the standard treatment for CML in 2001, the survival rate has greatly improved (Kantarjian et al., 2012). Despite the impressive outcomes of imatinib therapy, this treatment cannot be used in all cases. Resistance to imatinib can be split into BCR-ABL1-dependent and BCR-ABL1-independent mechanisms. The BCR-ABL1-dependent mechanism of resistance is mainly due to BCR-ABL1 tyrosine kinase domain mutations. The most frequently known BCR-ABL1-independent mechanism of resistance includes overexpression of efflux transporters, leading to low intracellular levels of imatinib, and downregulation of influx transporters which inhibits effective shuttling of imatinib in the cell or activation of compensatory pathways (Balabanov, Braig, & Brümmendorf, 2014) (Figure 15). The activation of a compensatory mechanism can be due to external stimulating signals from the BM microenvironment. Currently the main challenge in clinical management of CML patients is the continuous detection of low-level leukaemia cells using sensitive molecular techniques such as quantitative polymerase chain reaction following TKI therapy. The majority of CML patients who are treated with TKIs achieve a good response. However, they need continuous therapy, as the disease returns in up to 60% of the patients who stop treatment in the absence of detectable disease, leading to a re-starting of the treatment. This is of clinical and economical

significance. TKIs therapy is associated with various clinical side effects and therefore the concept of taking such medications for the rest of one's life makes the TKIs therapy compliance very difficult. Also, this has a heavy economic burden on the healthcare system. To identify the mechanisms through which the microenvironment causes resistance in CML cells against eradication is an important line of research.

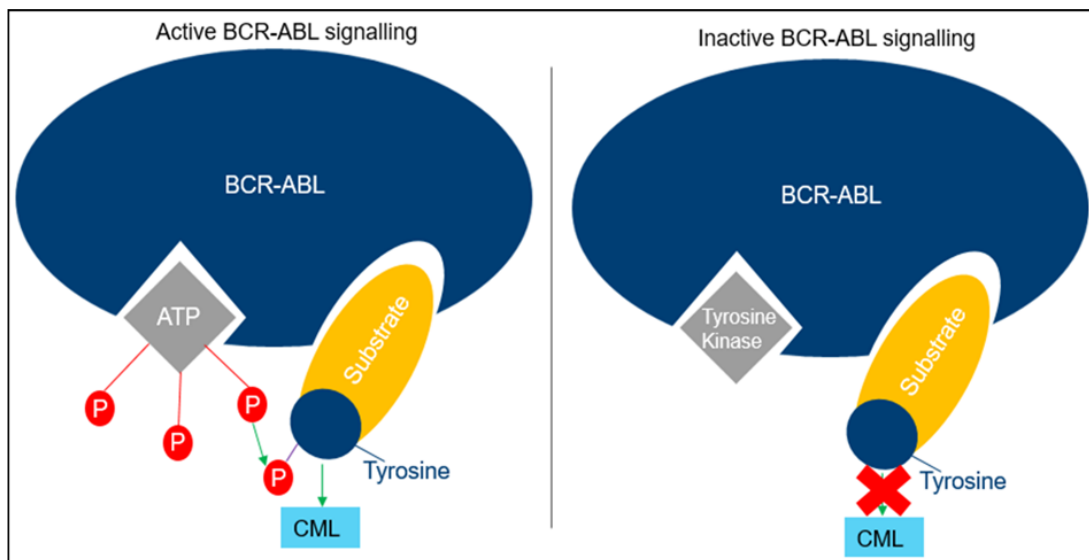


**Figure 14: Mode of action of tyrosine kinases inhibitors imatinib.**

*This figure shows the ATP binding to the active site of the tyrosine kinase of BCR-ABL, causing phosphorylation of selected tyrosine residues on its substrates, leading to activation of the downstream pathways that cause CML (Left). Tyrosine kinase inhibitors such as imatinib were designed to compete with ATP for incorporation to the kinase domain. By doing so, the substrate remains unphosphorylated and the pathways that promote CML are not activated. This figure has been adopted from (Levitzki and Gazit, 1995).*

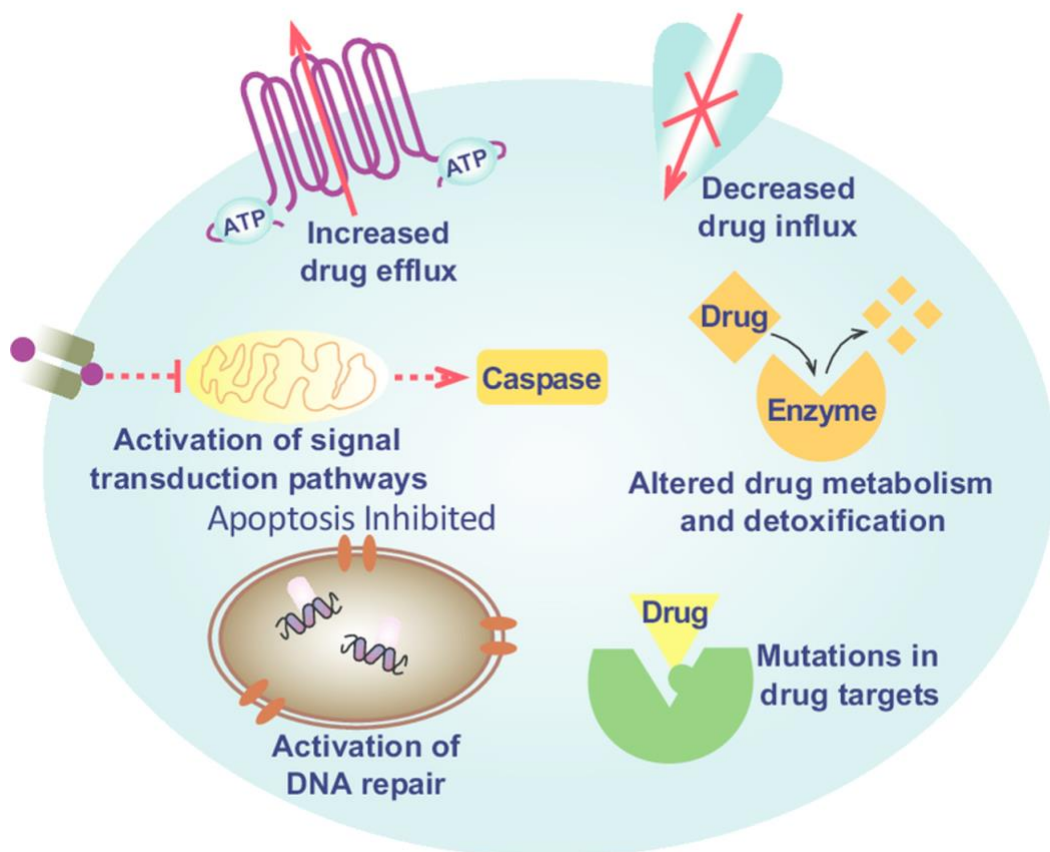


**Figure 15: Mechanism of multiple drug resistance.**

*The mechanism of resistance to anticancer drugs can be grouped into at least seven major categories: decreased drug influx, increased drug efflux via ATP driven extrusion pumps, altered drug metabolism and detoxification, secondary mutations in drug targets, activation of downstream or parallel signal transduction pathways, activation of DNA repair, and apoptosis inhibition. The image was modified and adapted from Yin et al. (2013).*

## 2.8 Principles of cell culture

Cells isolated from animal tissues can be grown in culture for research purposes. “Cell culture” refers to maintaining the disaggregated cells *in vitro*, while “organ culture” refers to a culture condition when cells are in the form of a non-disaggregated tissue. The term “tissue culture” is applied for both

forms of culture. Cell culture is an important method for biomedical investigations and is widely used for academic, clinical diagnostic and industrial aims. It has many applications, ranging from the discovery of new molecules and their function to high-throughput testing of anticancer drugs. The culture of cancerous cells from human tumours is routine. The cancerous cells are separated from the tumours through various methods, depending on the type of tumour. However, most experiments involving human research are based on using cell lines. Cell lines are cancer models which have originated from tumours, and are often cultured many times in media containing serum and other additives to promote their growth (Glaysher & Cree, 2011).

Animal cells go through extensive proliferation and differentiation in the early stages of development, while gradually differentiating into various tissues and organs. In an adult, the vast majority of cells are in a non-dividing state; although they are metabolically active and have their physiological functions, most are not actively proliferating.

Most normal adult cells only divide in response to stress and when there is a need to replace old or damaged cells. Only cells of specific tissues such as skin or epithelial cells in the gastrointestinal system have the capacity of dividing regularly. More than 200 different types of cells exist in the body and many of them cannot grow in culture following their removal from the original organ (Le et al., 2016).

A complex mixture of substances, such as minerals, amino acids, sugars, vitamins, and growth factors such as insulin or various cytokines, is required

for a suitable environment in which to support the growth and maintenance of cells.

Except for blood cells, nearly all the cells in the body do not grow as separate or free-floating. Because of the inability of most of the cells to grow in an anchorage-independent condition following removal from the tissue environment, the cells need a surface to which they can bind. If the released cells cannot find such a surface for attaching, they will not be able to divide and will shortly die (Le et al., 2016).

Following attachment of the released cells to the new surface, they start growing onto empty surfaces. This continues until a layer of cells covers the surface of the culture environment and forms a monolayer of cells. When a layer of cells covers the whole surface area, they do not divide any longer because the contact from the neighbouring cells releases inhibitory signals. This state is referred to as contact inhibition. If further expansion of these cells is required, they have to be removed and placed on a new surface where there is space to grow.

An enzyme such as trypsin is usually used for digestion of the proteins that mediate attachment of the cells to the surface, resulting in the release of the cells into solution. This cycle of cell attachment to surface, proliferation and detachment can be done several times. For normal cells the number of the cell-doubling is controlled by an internal cellular clock, which sends the final stop message when the number of cell divisions reaches a certain limit, called Hayflick (Hayflick, 1965; Shay & Wright, 2000). Most of the fresh cells from tissue are capable of doubling up to 40–60 times before they stop proliferation (becoming senescent). The contact inhibition is a hallmark of cells taken from

normal tissues. The cancerous cells taken from tumours have the capacity to overcome contact inhibition and to continue proliferation (Todaro & Green, 1963; Stride & Edirisinghe, 2008; Wells, 2005).

Cell lines are the immortal cells that proliferate and avoid the Hayflick limit. The cell lines are immortal in culture and can be cultured forever. This phenotype is different from the cells isolated from non-malignant tissues that usually die in cell culture (Schofield, 1978).

In many tissues of the human body there are a small number of cells called stem cells that can differentiate and form mature cells. The stem cells are the source of providing the new cells required for repair, maintenance, or tissue regeneration. In adults the stem cells have more limitation for forming various types of cells, as they can typically differentiate only to cells of their own lineage (Schofield, 1978).

As was mentioned earlier, the majority of the separated cells from tissues need a surface for attachment; however, some such as blood cells are capable of growing in suspension (Figure 16). Although culturing cells is straightforward in the lab using Petri dishes or flat flasks, it can be a challenge when a large scale of cell production is required. When large-scale production of certain proteins for therapeutic purposes is required, the cells that produce such proteins are engineered using molecular genetics techniques to enable them to grow in suspension.

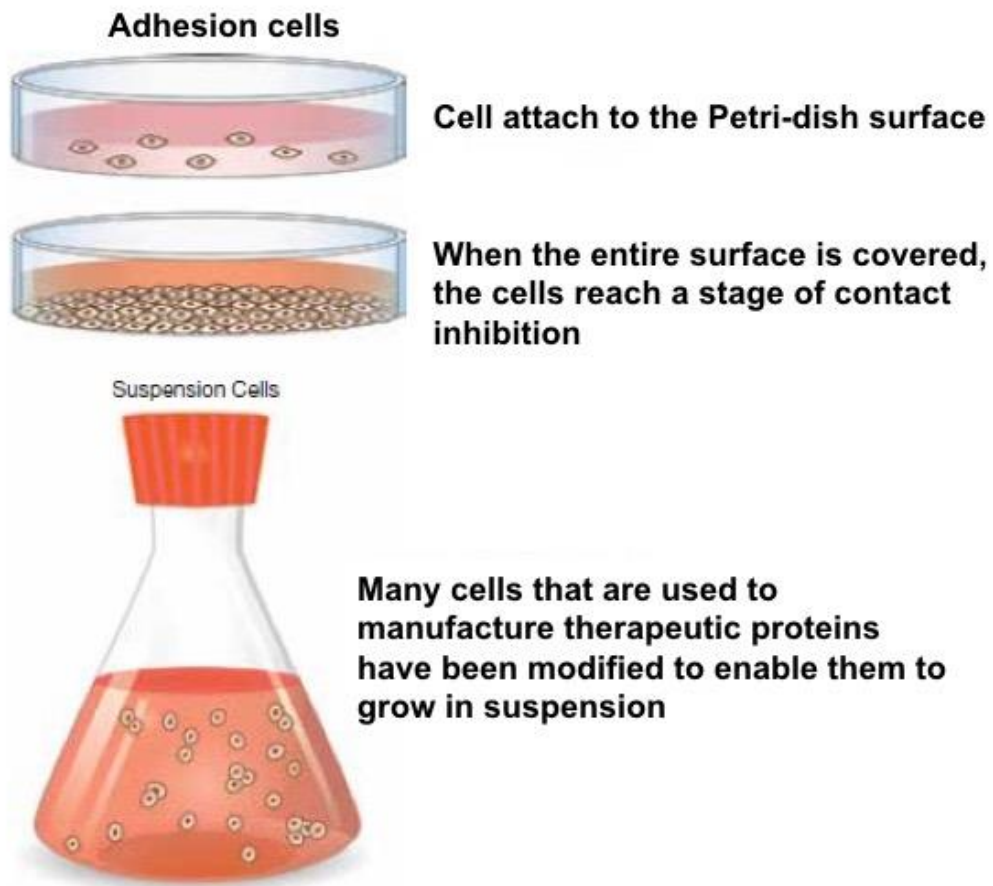


**Figure 16: Adherent and suspension cells in culture.**

*Most cells isolated from tissues are anchorage-dependent and require a surface for adhesion. Cells that are used to manufacture therapeutic proteins are modified to eliminate their need for surface attachment. This figure was taken from the paper by Le et al. (Le et al., 2016).*

Because the cells in suspension can grow without the limitations that adherent cells have, conversion of the cell lines to the cells which can grow in suspension is very valuable in the pharmaceutical industry. This conversion is through removing the cells from the surface and forcing them to grow in suspension. One method of growing the cells which are anchorage-dependent in a suspension culture is to employ small beads called microcarriers. These microcarriers provide a surface for cell adherence and

proliferation, while they provide the opportunity for the bead-and-cell complexes to be suspended (Figure 17).



**Figure 17: Human embryonic cells.**

*Human embryonic stem cells can be grown on beads, called microcarriers. Microbeads provide a surface, for the attachment of the cells and their growth. In this figure, the microcarriers are completely covered by the stem cells. The image was modified and taken from the published paper by Le et al. (Le et al., 2016).*

### **2.8.1 Commonly applied cell cultures for studying haematopoietic stem cells**

A suitable cell culturing system is required to characterise the various behaviours of HSCs or LSCs, such as proliferation, differentiation, self-renewal capacity and drug sensitivities. 2D cultures have been used for many years as the standard method for studying various cell types. Despite being widely used, 2D cultures have had deficiencies which has led to the

development of 3D cultures. These deficiencies have been mainly due to significant structural differences between the 2D culture and the *in vivo* BM microenvironment. The other deficiencies of 2D culture relate to its limited application in drug discovery studies, and the low value of the data gathered from 2D cultures in estimating the sensitivity of leukaemia or HSC to new discovered agents. This seems to be due to the absence of other components of the BM in the commonly used 2D cultures (Frantz, Stewart, & Weaver, 2010). The lack of the third dimension in 2D cultures results in a fraction of the cell membranes of the neighbouring cells being in touch with others, but a large part of each membrane is exposed to the culture medium (Ryan et al., 2016). To understand the proliferative behaviour of the LSC or HSC, or their response to treatment, it is important to investigate the whole process while cells are interacting with other cells and macromolecules, such as in the *in vivo* environment. In addition to the lack of the third dimension, the other missing factor in 2D cultures compared to the *in vivo* BM microenvironment is the ECM, which has an essential role for normal and aberrated cellular homeostasis (Frantz, Stewart, & Weaver, 2010; Gilkes, Semenza, & Wirtz, 2014). Regarding the deficiencies of the 2D cultures, various types of 3D cultures have been recently developed as an alternative method of culturing HSCs or LSCs. In addition to the influence of 3D cultures on proliferation, they have been shown to have an impact on the differentiation of the HSC, as it has been shown that HSCs keep their differentiation ability in 3D cultures but lose it in 2D cultures (Baker & Chen, 2012; Venugopalan et al., 2014). The 3D system has provided an opportunity to investigate how cells sense mechanical forces and their response to these forces (Meng et al., 2014). They have been shown to have advantages for the growth of HSC and cells

like chondrocytes, preserving the characteristics of these cells during the culture and also determining the phenotype of the cells they support. For example, chondrocytes when grown in 2D culture lose their morphology and become similar to fibroblasts, and even the matrix protein they synthesise changes. However, when these fibroblast-like cells are put in 3D culture they change their morphology and return to rounded chondrocytes (Lawrence & Madihally, 2008).

### **2.8.2 Different types of 3D culture for studying various phenotypes of HSC/LSC**

3D cultures can be categorised in various ways, depending on which aspect of their structure is used for classification. The general classification of the 3D cultures categorises them into 1) plate or culture dish, 2) spinner flask, 3) rotation wall vessel (RWV), and 4) perfusion bioreactor system. 1) The most commonly used system for culturing cells is plates or dishes, because of their low cost and ease of use. The main challenge for using them is for the culture of HSC or LSC as the growth of these types of cells in the plate or dish is reduced compared to the *in vivo* setting. 2 & 3) Spinner flasks and RWVs were developed to promote the culturing condition of the HSC or LSC, by improving the convection of the medium in the system and consequently increasing the quality and efficiency of the culture. RWVs are further developed, compared to spinner flasks, as they have two horizontal concentric cylinders with gas exchange happening through semipermeable membrane (Figure 18). In a perfusion bioreactor system, there is continuous perfusion of the medium to keep the balance of the environment (Figure 19).

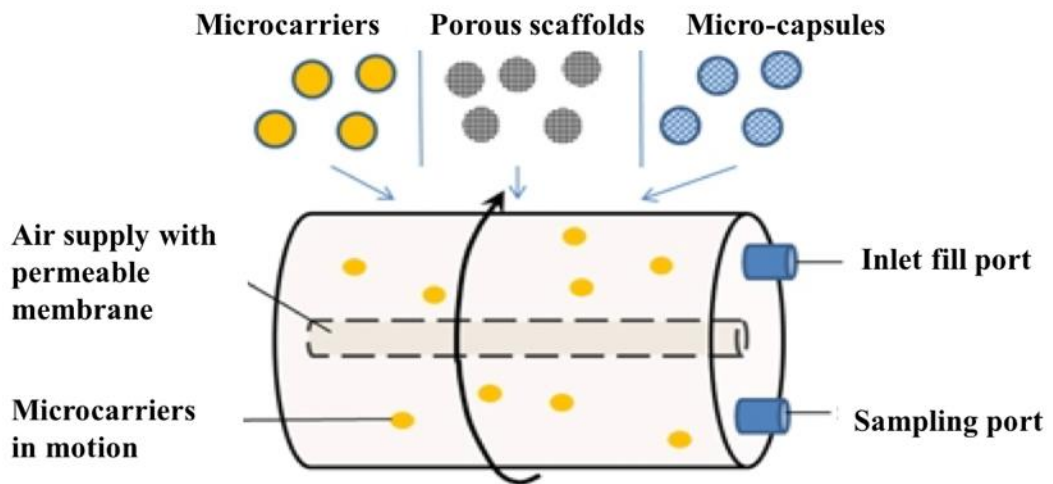


**Figure 18: Rotating wall vessel bioreactor.**

*Rotating wall vessel bioreactor schematic with any of the three 3D culture types rotating around the horizontal axis is shown. This figure was taken from the published paper by Kumar and Starly (Kumar & Starly, 2015).*

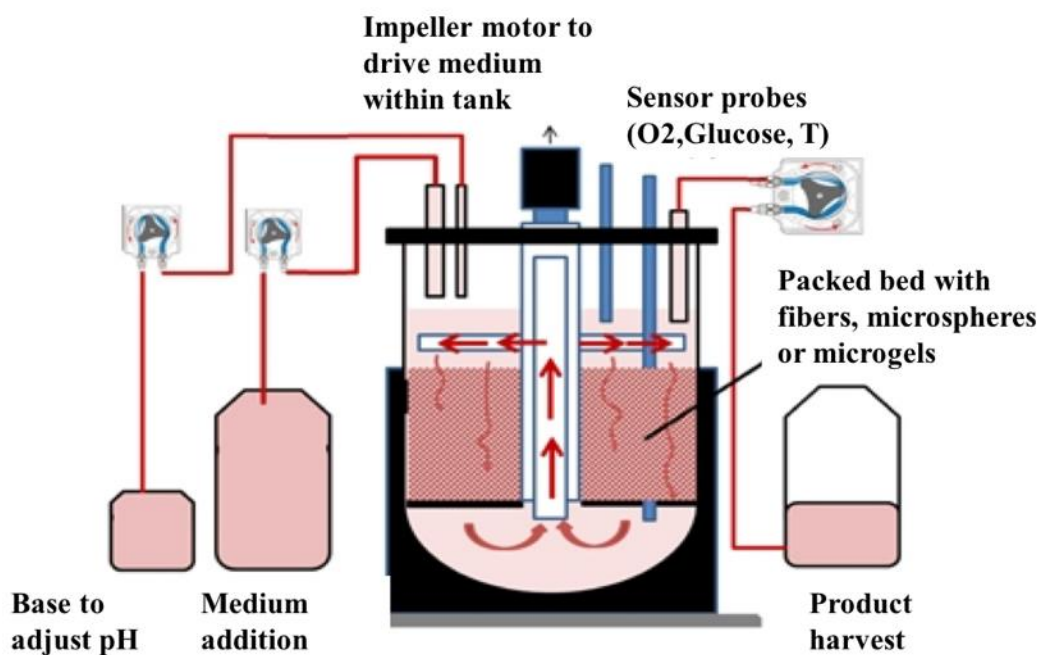


**Figure 19: Packed bed bioreactor setup.**

*Packed bed bioreactor setup. The co-controller station regulates oxygen and carbon dioxide through sensor probes. This figure was taken from the published paper by Kumar and Starly (Kumar & Starly, 2015).*

### **2.8.3 Scaffolds from microbubbles for tissue engineering**

Scaffolds play an important role in tissue engineering, for example, by acting as porous biodegradable structures containing various bio-products (cells, genes, drugs and proteins) (Haynesworth, Reuben, & Caplan, 1998; Cutroneo, 2003; Dhandayuthapani et al., 2011). They can serve as a replacement for ECM and can be produced from natural or synthetic material, or a combination of both (Carletti et al., 2011; Pereira et al., 2013). In order for scaffolds to mimic the function of the natural human ECMs, they must balance mechanical function with transport of bioactive agents (Hollister, 2005; Chan & Leong, 2008). While a denser scaffold offers a better function and mechanical strength, a more porous scaffold provides greater diffusion of gas/liquid components and provides cell growth (Carletti et al., 2011). Scaffolds are developed for tissue engineering to promote the growth of cells migrating from the surrounding tissue into the porous structure of the scaffold. As the primary function of the scaffolds is to support the growing tissue, they are required to allow cell migration, attachment and proliferation (Hollister, 2005; (Vats et al., 2003). There have been many studies into the morphological design of scaffolds to stimulate cellular growth. Factors such as pore shape and size, as well as interconnectivity and spatial distribution through the scaffold, are important in the design of the scaffolds for optimised cellular growth (Wang et al., 2009). Foam and honeycomb-like structures with interconnecting and large pores are ideal templates for tissue engineering scaffolds. Recently, microbubbles have been used as pore generators in the biomedical field (Wang et al., 2009). It has been shown that a uniform pore size in scaffolds promotes more cell migration and distribution in the scaffold.

Same size scaffold pores leads to an increased cell proliferation, especially when the pore size is the same as the cell diameter, as the cells can sit in the holes and grow (Vats et al., 2003; Di Maggio et al., 2011). Scaffold prepared by Nair et al. using protein microbubbles was shown to be an excellent candidate for use as tissue engineering scaffolds, as well as drug/growth factor delivery vehicles.

#### **2.8.4 Scaffold-based 3D cultures as an *in vitro* model for BM**

The HSC is enriched in a specialised microenvironment in the BM, called niche. Stem cell niches are microenvironments in BM that maintain HSC and regulate the function of the HSC. BM niches produce cytokines, and these cytokines affect HSC and influence their activity (Morrison & Spradling, 2008). HSCs are rare populations in BM which have self-renewal and multipotent progenitor activity. HSCs give rise to a group of progenitors. Progenitors will proliferate and gradually differentiate to mature cells. Niches are believed to regulate various characters of the HSC, such as quiescence, self-renewal and differentiation. The function of the niches is regulated by their various components. These components are either cellular or molecular (Figure 20). The cellular components are mainly osteoblasts, osteoclasts, endothelial cells, mesenchymal cells and progenitors. The main molecular factors are stem cell factors, osteopontin, TPO, stromal derived factor-1 (SDF-1) and N-cadherin (Di Maggio et al., 2011). The commonly used methods of cell culture do not have the required components to form a niche-like structure and therefore are not a suitable model for studying HSC or LSC. It is important to keep the HSC in culture for a long term as various phenotype of these cells

develop within weeks. Various cytokines such as stem cell factor (SCF), FLT3 ligand, TPO and IL-11 are required for growth and survival of the HSC, and this indicates the necessity for the presence of various cytokines in the *ex vivo* culture of these cells (Fraser et al., 1990). In addition to cytokines, stroma cells are required for expansion of CD34<sup>+</sup> cells (HSC/progenitors). To include the cytokines and stromal structure, 2D cultures supplemented with stromal cells and cocktails of cytokines have been used in HSC studies. In spite of these improvements, this kind of culturing supports only the expansion of more differentiated cells and does not support the long-term culture of HSC (Haylock et al., 1992). To overcome the deficiency of 2D cultures in having a niche-like structure, 3D cultures have been introduced to mimic the BM microenvironment by having 3D structure, scaffolds, molecular matrix and cellular components (Braccini et al., 2005). An example would be ceramic-based 3D cultures, where BM nucleated cells are added to the ceramic scaffold to form a 3D cell network within the scaffold pores, followed by seeding of HSC (Di Maggio et al., 2011). Molecules such as segment-1 (CS-1) and RGD motifs, which mimic the fibronectin domains of the ECM if added to the scaffold, will help the expansion of CD34<sup>+</sup> cells (HSC/progenitors) (Di Maggio et al., 2011). The structure of the scaffold will determine how the stromal cells form the network in the 3D culture (Di Maggio et al., 2011). A 3D culture with various stromal cell types has a better chance of having a self-maintaining system with little dependence on external supply of essential cytokines. A 3D culture supporting the growth and maintenance of HSC would also be a good system for studying haematological malignancies, such as AML which has a hierarchical organisation similar to that of normal haematopoiesis.

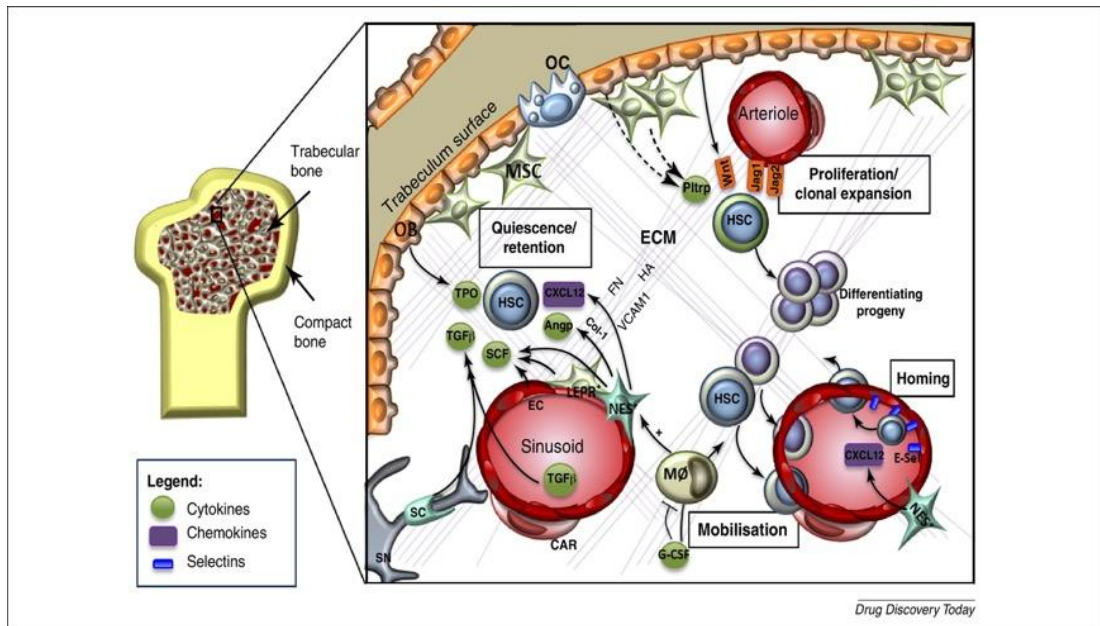


**Figure 20: The BM haematopoietic niche.**

The BM haematopoietic niche and its molecular interactions are shown here. The signals from the sympathetic neurons (SN) control the movement of HSCs into and out of the niche. CXCL12 is a chemokine secreted by some of the stromal cells (Nes+). It binds to the endothelial cells (EC) through E-selectin. Reduced expression of CXCL12 and other chemokine, and an increased expression of granulocyte colony-stimulating factor (G-CSF), are considered the stimulations for mobilisation of the HSC and progenitors. Interaction of the HSCs with CXCL12 and ECM components, such as vascular cell adhesion molecule-1 (VCAM-1), fibronectin (Fn), collagen-1 (Col-1), and HA, is the known mechanism for keeping the HSCs in the niche. Transforming growth factor beta (TGFβ), angiopoietin (Angp), SCF, and TPO protect the long-term HSCs in a quiescent state in the BM. TGFβ is secreted in an inactive form into the blood circulation and is converted by Schwann cells (SC) to an active form. EC, Nes+ mesenchymal stromal cells (MSC), and leptin receptor-expressing (LEPR+) MSCs secrete stem cell factor (SCF). Osteoblasts (OB) produce TPO. Various signalling pathways such as Wnt signalling, Notch ligands, Jagged-1 (Jag-1), Jagged-2 (Jag-2), and the cytokine, pleiotropin (pltrp), control the proliferation of HSCs and the various blood cell populations in BM. The image was modified and adapted from Dhimi et al. (Dhimi et al., 2016).

### **2.8.5 The significance of a BM-like culture for studying AML**

LSCs initiate the leukaemia and are capable of having unlimited self-renewal activity in AML (Krivtsov et al., 2006; Rossi, Jamieson, & Weissman, 2008; Essers & Trumpp, 2010). Among various types of leukaemia, AML is of special interest for *in vitro* investigations because of the little progress in its management and treatment (less than 50% successful treatment), despite recent progress in understanding its molecular genetic abnormalities. One of the main reasons for the low response rate of therapy for AML patients is believed to be due to our poor understanding of the molecular interactions between LSCs and their microenvironment (BM niche). The identification of the interactions between the AML cells and their microenvironment provides a therapeutic opportunity.

These interactions can be targeted by various drugs, resulting in AML cells suppression. It is important to identify the interactions between normal HSCs and their microenvironment, to direct treatment specifically towards LSC and save normal haematopoiesis. A 3D culture mimicking BM microenvironment would provide the opportunity to dissect the mechanisms related to LSC maintenance and would represent a useful platform for drug screening (Dhami et al., 2016).

## 2.9 Flowcytometry

Flowcytometry is a sophisticated method that measures multiple physical characteristics of a single cell. The size and granularity are measured simultaneously as the cell flows through a measuring device. The principle of flowcytometry is based on the light-scattering features of the flowing cells. The light scattering comes from the dyes added to the cells, or the fluorescent dyes attached to the monoclonal antibodies located on the surface of the cells, or to intracellular molecules inside the cells (Adan et al., 2017). Flowcytometry is the method of choice for analysing differentiation of normal and leukaemia cells. Flowcytometry, by using two light-scattering (size and granularity) and colour immunofluorescence signals from the added antibodies, can characterise the developmental stage of the cells in either normal or leukaemia condition.

At each stage of differentiation, maturing cells have a specific pattern of molecules (antigen) on their surface, and this antigenic pattern on the surface, along with molecular alteration in their morphology, establishes a unique pattern for each stage of differentiation and maturation. This unique pattern for each stage of differentiation under normal conditions provides a basis for making a distinction between normal and leukaemia cells. These normal patterns are disrupted in leukaemia such as AML. Flowcytometry helps to ascertain which population of cells is dominant and at which stage of differentiation the arrest has happened; this information provides a guide for the classification of leukaemia. Accurate classification will provide guidance towards a better treatment and management of the disease.

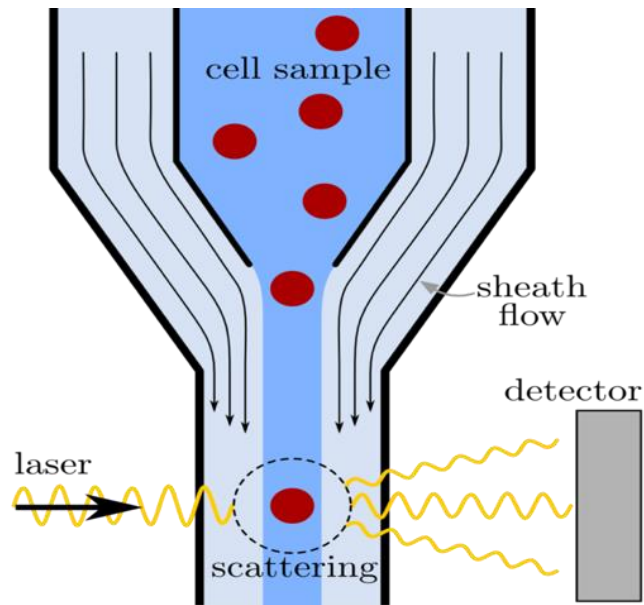


**Figure 21: Schematic diagram of the working principle of flowcytometry.**

*This figure shows how flowcytometry characterises the various qualities, such as size and density, of the investigated particles. The investigated particles (which are mainly cells in this thesis) pass individually through a capillary system, where they are exposed to a laser beam. The laser beam is scattered and is recorded by a detector.*

*The recorded information provides information about the size and complexity of the cell (<https://www.ptb.de/cms/en/ptb/fachabteilungen/abt8/fb-84/ag-841/flowzytometrie-841.html>, 01 August 2018, 9.24am).*

# Chapter 3

## Experimental details

### Methods and Materials

#### 3.1 Introduction

This chapter covers materials, product details and suppliers, as well as an introduction to the details of the experiments and the applied procedures during the investigative process. To ensure reproducibility, all the experiments were repeated at least three times. All equipment was calibrated, and measurements checked against known values as instructed by the supplier. All the biomaterial processing work has been done in the Edirisinghe lab (UCL Mechanical Engineering).

#### 3.2 Materials for evaluation of bubble formation

The main materials in the experiments were aqueous sodium alginate solutions combined with surfactants, such as polyoxymethylene glycol 40 stearate (PEG 40S). The production process was done using the capillary-embedded V-junction. For the experiments conducted to produce foam scaffolds, sodium alginate bubbles were cross-linked with calcium chloride.

##### 3.2.1 Sodium alginate

Sodium alginate is purchased in powder form from Sigma-Aldrich. The colour

of the sodium alginate powder is between white and pale yellow. The source of sodium alginate is seaweed. The extracted alginic acid from seaweed is neutralised to make the alginate biocompatible. The biocompatible alginate has been used extensively in biomedical and pharmaceutical systems. It has been used for encapsulation of delicate macromolecules such as proteins, cells and nucleotides.

The encapsulation with sodium alginate protects the structure and consequently the function of the particles it covers. The encapsulating character of the alginate seems to be due to its cross-linking capacity (Gombotz & Wee, 2012; Lee & Mooney, 2012).

The selection of alginate for drug delivery purposes in the gastrointestinal tract is due to its tendency for interaction with mucosal surfaces. The interaction between the sodium alginate and the mucosa is thought to be due to the charge distribution around the sodium alginate molecule, which gives it a mucoadhesive property and makes it a good choice for drug delivery through mucosa.

There are reports from other investigations, showing that alginates are comparable to other known mucoadhesive polymers such as carboxymethyl cellulose, polystyrenes and chitosan (Chickering & Mathiowitz, 1995). From these findings, it is expected that nanofibers which have alginates in their structure have superior performance for drug delivery aims, as this increases their attachment to mucosa.

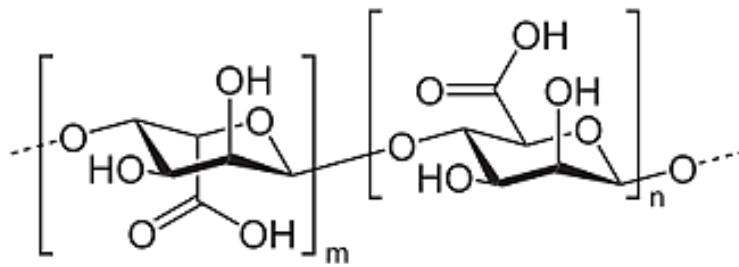


**Figure 22: Molecular structure of sodium alginate.**

*The structure of alginate acid is shown in this figure. This polymer confers substantial mucoadhesion capabilities to captopril microcapsules for prolonged release in the stomach. The relatively mild cross-linking structure makes alginate a preferred biopolymer for encapsulation of delicate macromolecules, including proteins, cells and nucleotides, as the structure and function of these biologics remain intact to a significant extent within the alginic systems (Nair and Laurencin, 2007; Gombotz and Wee, 2012).*

### **3.2.2 Surfactants**

To facilitate microbubble formation, surfactants were used to reduce the surface tension. The following surfactants were used for this study:

*Tween 40:* This product was purchased from Sigma-Aldrich. It is a non-ionic detergent with a wide range of applications in the food industry and in drug developments. It is usually used for solubilising oils in water-based products. Tweens are categorised as being biodegradable materials.

*PEG 40:* Polyoxyethylene glycol 40 stearate density; 1300 kg/m (which is also called PEG 40S) was purchased from Sigma-Aldrich. Since it is non-toxic, it has been used in the production of drugs, foods and cosmetic products, and has been approved by FDA.

### **3.2.3 Phospholipid**

L- $\alpha$ -Phosphatidylcholine was purchased as lyophilised powder from Sigma-Aldrich (Sigma-Aldrich, UK). The average molecular weight is approximately 768 g/mol. Phosphatidylcholine is the major structural component of cellular membranes. It also serves as a reservoir for several lipid messengers and is used for the preparation of vesicle suspensions, known as liposomes, or as monolayers.

### **3.2.4 Phosphate buffered saline (PBS)**

Dulbecco's phosphate buffered saline (DPBS) was purchased from Sigma-Aldrich, UK. It is an iso-osmotic buffer and is used for washing cells, dissolving drugs, during the staining cells with various chemical agents or fluorescent antibodies, or as a drug delivery release medium. Phosphate buffering maintains the pH in the physiological ranges and can be used to wash and rinse suspended cells.

### **3.2.5 Glycerol**

Glycerol ( $C_3H_8O_3$ , density  $1,261 \text{ kg/m}^{-3}$ , molecular weight 92.09, viscosity  $1.4 \text{ Pa s}$ , Sigma-Aldrich, UK), with 99% purity, was diluted with distilled water. Aqueous glycerol solutions are widely used in experimental studies of flow experiences. Experiments conducted with glycerol solutions facilitate the investigation of flows in a different range of Reynolds numbers.

### **3.2.6 Ethanol**

Ethanol ( $C_2H_5OH$ ) was purchased from Sigma-Aldrich. Ethanol was used for various applications in this study, such as for the cleaning of capillary needles (which were essential components of the experimental setup) and for sterilising foam scaffold for cell culture.

### **3.2.7 Calcium chloride**

Calcium chloride ( $CaCl_2$ ) was purchased from Sigma-Aldrich in powder form (anhydrous, beads, -10 mesh,  $\geq 99.9\%$  trace metals basis).

### **3.2.8 Gold nanoparticle and gold coating**

Additionally, gold nanoparticles were added to alginate microbubbles in the experiment in order to increase the stability of microbubbles. An aqueous gold suspension was used as the base for the microbubble coating. Gold nanoparticles (average diameter  $\sim 10$  nm) in phosphate-buffered saline (PBS) solution were obtained from Sigma-Aldrich, U.K. Gold nanoparticles (with average diameter  $\sim 10$  nm and spherical shape) can cover the surface and act as a chain around the bubble shell.

In order to coat the shell of the alginate bubbles, microfluidic V-junction was used. Gold suspension was provided via one of the liquid inlets and from the other inlet solution, and the surfactant was made to flow in, in order to form the bubble in the intersection zone of the polymer junction.

### **3.3 Material and solution preparation for microbubble production**

Three series of alginate solutions with concentration of 1, 0.5, 0.25 wt.% were prepared from sodium alginate powder (Sigma-Aldrich Poole, UK) dissolved in deionised water. Polyethylene glycol-40-stearate (PEG-40S, Sigma-Aldrich, Poole, UK, density; 1,300 kg/m<sup>3</sup>) was added as a surfactant to all solutions. The concentration of surfactant (PEG) for all solutions was 0.5 wt.%. All solutions were prepared at room temperature (20 °C). Microbubbles were collected through four different mediums: in deionised water, calcium chloride (20 vol%), glycerol (80 vol%) and hydrochloric acid (2 vol%) (Chemicals supplied by Sigma-Aldrich Ltd).

### **3.4 Characterisation of the solutions**

#### **3.4.1 Surface tension**

The surface tension for each solution was measured using a Drop Shape Analysis System (Figure 23), Model DSA100 (Kruss GmbH, Hamburg, Germany). In order to ensure accuracy of measurement, a secondary reading was taken using a Kruss Tensiometer K9 (Standard Wilhelm's plate method). The plate was completely submerged in the solution. The plate was gradually lifted, and the surface tension noted precisely as the plate was separated from the liquid surface. In order to reduce measurement errors, the plate was cleaned thoroughly with ethanol and completely dried before each

measurement. The mean value of three readings was taken to represent the surface tension of each sample.

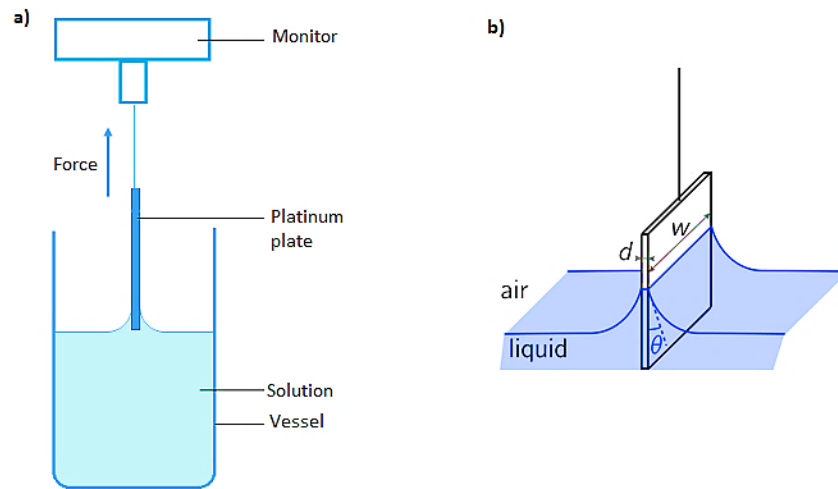


**Figure 23: Schematic illustration of a) tensiometer, and b) 3D of the plate's interaction with liquid sample.**

*This image was taken from the published paper by Butt et al. (2006).*

### 3.4.2 Viscosity

Solutions with viscosities higher than 15 mPas were measured using a Brookfield DV-111 Ultra programmable Rheometer (Brookfield Engineering Laboratory Inc., USA). The apparatus operates on the principle of proportionality between the shear rate and torque applied to a quiescent liquid. In this technique, a cylindrical spindle is spun at a specific speed within the solution in which viscosity is to be quantified. To guarantee accurate measurement of the kinematic viscosity of each solution, U-tube viscometers (BS/U type) were used. This value was subsequently multiplied by the density (in  $\text{gcm}^{-3}$ ) of the solution to calculate its dynamic viscosity. The process was repeated three times and the mean value of all readings was reported. For solutions of lower viscosity, the U-tube technique was found to be more

accurate.

### **3.4.3 Electrical conductivity and pH**

A Jenway 3540 pH/conductivity meter (Bibby Scientific Limited, Staffordshire, UK) was used to measure the electrical conductivity, and pH of the solutions were determined. The electrodes were kept immersed in the solution for ten minutes and then the reading shown on the meter was recorded. The mean value of three readings was taken as the electrical conductivity and pH of the sample.

## **3.5 Characterisation methods**

### **3.5.1 Optical microscopy**

All images were taken using a JVC KY-F55B digital camera, attached to a Nikon Eclipse ME 600 optical microscope. Image processing was carried out using a computer running the Image Pro v3.0 software. The microscope was calibrated using a standard microscope ruler slide and all samples were collected on micro slides at 5X, 10X and 20X magnifications. All micrographs were captured, and all sizes were measured via the Image Pro v3.0 software with the above-mentioned processing parameters. Each experiment was repeated three times and based on the expected bubble lifetime. Pictures were captured at different time intervals, as documented in chapter 4.

### **3.5.2 Confocal laser scanning microscopy**

Zeiss LSM 710 was used as a confocal microscopy imaging system and is equipped with a 405 nm/488 nm/561 nm Krypton-Argon ion laser. It was used to record confocal laser scanning microscopy images. Micrographs were obtained using a laser power of 2.0 mW with a box size of 2048x2048 pixels at 8-bit resolution. Zen software was used for image processing. The single channel images and the merged images were obtained.

### **3.5.3 Fluorescence microscopy**

Fluorescence microscopy is an optical microscope-based technique. It is used for examining the objects that emit fluorescent light, either in their natural form (autofluorescence) or in the form prepared to fluoresce as a result of combining with chemicals that can fluoresce (secondary fluorescence). The application of this type of microscopy is one of the fastest-growing areas. The mechanism of action for the fluorescent microscope is the emission of light with specific wavelength when the light of sufficient energy strikes an object. Fluorochromes are certain types of chemicals with delocalised electrons and are often used to stain materials for production of secondary fluorescence. The fluorochromes may be used for dyeing specific constituents of materials in polymeric or biological samples. This is termed fluorescent labelling and is used for various biomedical applications (<https://www.microscopyu.com>). A fluorescence microscope (Life Evos XL, ThermoFisher Scientific) was used for characterization of bubbles and their structure.

### **3.5.4 Scanning electron microscopy (SEM)**

The surface morphology and diameter of the bubbles and scaffolds were analysed by using scanning electron microscopy (Hitachi S-3400N and JEOL JSM-6301F field emission scanning electron microscopes, SEM). A JEOL JSM- 6301F field emission scanning electron microscope was equipped with an emitter that can achieve a resolution of ~1.5 nm. The accelerating voltage was set at 6 kV and the working distance between the emitter and the sample was 20 mm. The bubbles or the bubble/particle structures were collected and studied by optical microscopy immediately, and after 15 and 30 minutes of production, to detect any changes in their size and morphology. Then they were left to dry for 24 hours, and then scanned using electron microscopy at an acceleration voltage of 3–5 kV. All the samples were vacuum-coated with gold for 120s beforehand, using a sputtering machine (Edwards sputter coater S 1 50B) to obtain SEM images. This process enables conduction of the sample surface and avoids charging, which can cause damage when gold is used to make the surface conductive. The samples were then placed on an aluminium stub with a carbon sticker and were placed in the SEM chamber. Analysis of the products was carried out using the Image-Pro Insight software (Media Cybernetics Ltd., Marlow, UK) and the image-processing program UTHSCSA Image Tool (Image Tool Version 2, University of Texas, USA).

### **3.5.5 Hot-stage microscopy**

Hot-stage microscopy studies were conducted using a Leica DM 2700 M microscope (Leica Microsystems, Wetzlar, Germany). This microscope was equipped with an Infinity2 digital camera (Lumenera Corporation, Ottawa, Canada). This system was used to observe the microbubble bursting process. A heating stage unit was controlled by a FP90 central processor unit, both from Mettler-Toledo Ltd, Leicester, UK. Microbubbles were examined under two different temperatures, 20 °C and 37 °C.

### **3.6 Microfluidic experimental setup**

A diagram of the microfluidic setup is shown in figure 24 and the junction geometry is shown in figure 25. This device consists of four Teflon fluorinated ethylene polypropylene (FEP) capillaries with fixed internal diameters of 200  $\mu\text{m}$  (for experiments conducted to investigate the effect of variations in gas pressure and flow ratio), inserted in a polymer block (Figure 24).

The top capillary was connected to a gas regulator, fitted to a pressurised air tank via a 6 mm diameter pipe, where the gas was supplied to the junction at a constant pressure. A digital manometer was connected to the pipe to measure the in-line air pressure. A gas regulator was used to vary the gas pressure supplied to the V-junction. The side capillaries inserted into the junction supplying liquid was connected to a 20 ml stainless steel syringe (KD Scientific, Holliston, MA, USA). Two Harvard syringe PHD-4400 pumps (Harvard Apparatus Ltd., Edenbridge, UK) were used to force liquid through

the capillaries at a constant flow rate.

In order to produce microbubbles, the nitrogen gas from the top inlet and liquids from the side ducts of the junction meet at the intersection zone and bubbles are formed. Bubble formation was monitored at the junction in the 200  $\mu\text{m}$  gap between the main capillaries, where the liquid and air phases meet to start bubble formation. Each capillary is secured mechanically to the block via a standard high-performance liquid chromatography (HPLC) connector to prevent any slippage at the junction during operation at high pressure. All connections were checked for leakages and blockages prior to executing the experiments. Bubbles were collected from the bottom of the polymer junction on a glass slide coated with deionised water.

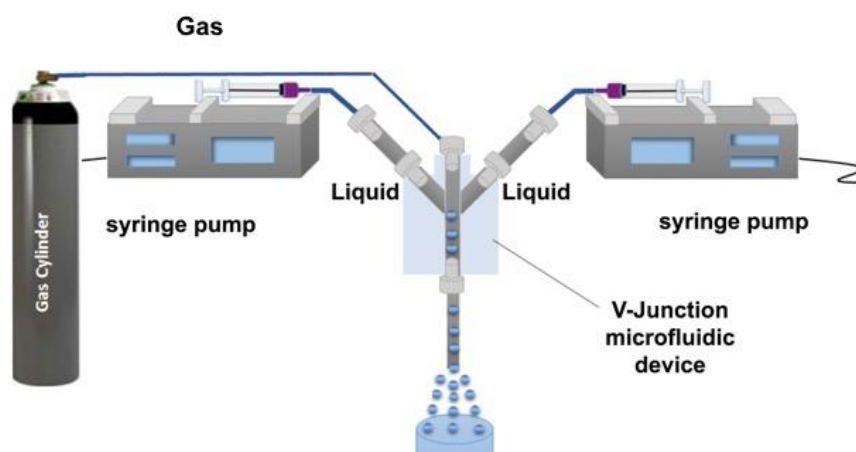


**Figure 24: Microfluidic setup.**

*Microfluidic V-junction device for the production of microbubbles.*

### 3.6.1 V-junction device

The polymer V-junction microfluidic device (Figure 25) was used to fabricate the microbubbles. This device is fabricated using polymethylmethacrylate

(PDMS) block manufactured at UCL mechanical engineering workshop. The polymer V-junction consisted of two Teflon capillaries in the side ducts, with a 30° angle to the top (gas) inlet. The two vertical capillaries have a constant inner diameter of 200 μm. The top inlet provides the gas and the produced microbubbles are collected from the bottom inlet.

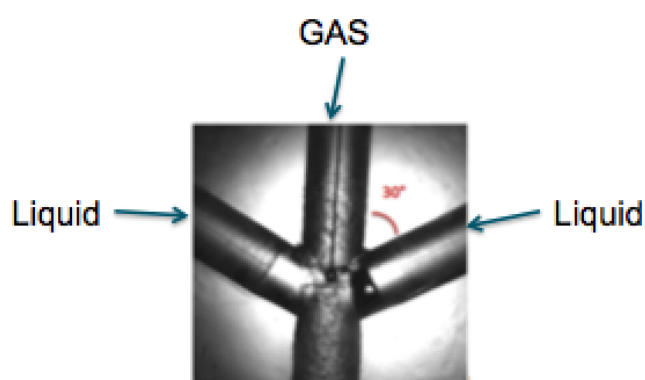


**Figure 25: Microfluidic V-junction device.**

*High-speed camera was used to capture an image of the V-junction microfluidic device.*

### **3.7 Apparatus design**

Figure 26 illustrates the apparatus used to determine the retention of an alginate dose on oesophageal tissue. A Perspex<sup>®</sup> mounting block was manufactured at UCL School of Pharmacy workshop, with dimensions of 100 mm length by 60 mm width and 15 mm deep. A groove was cut into this block in a central position; the dimensions of the groove were 100 mm long by 12 mm wide and 5 mm deep.

The mounting block was permanently attached to a clamp that was able to rotate through approximately 120°. The clamp was attached to a stand and placed to fix and hold the tissue sample. This apparatus mimics the angle and position of the oesophagus.

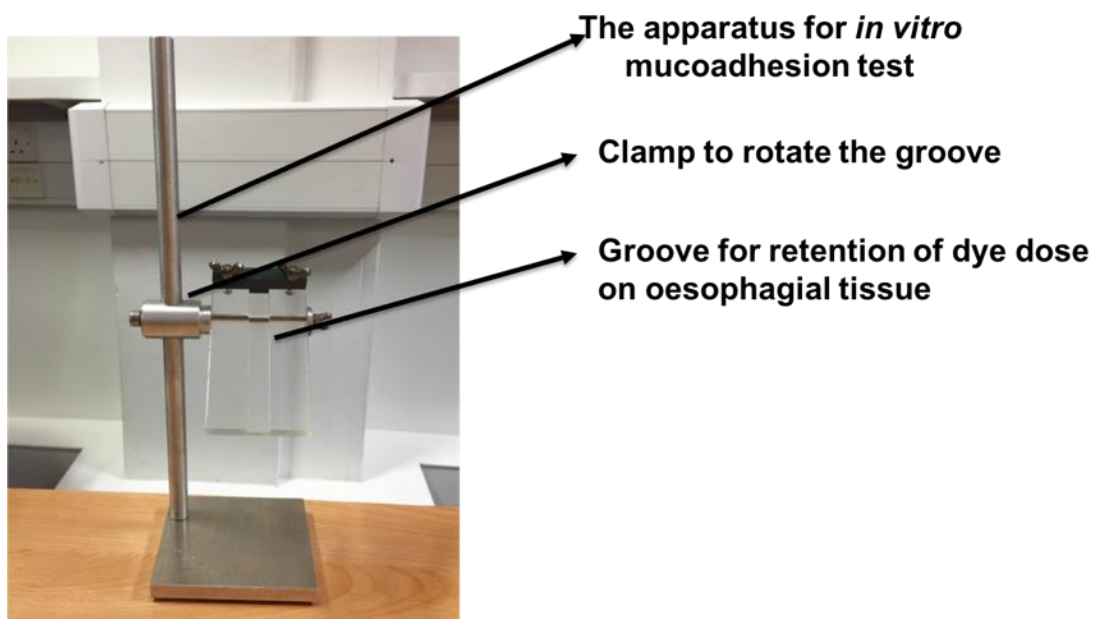


**Figure 26: Apparatus for bioadhesive studies.**

### **3.8 Membranes for mucoadhesive study**

Cellulose acetate of pore size 0.2  $\mu\text{m}$ , used as an artificial membrane in mucoadhesive studies, was obtained from Sartorius, Gottingen, Germany. Fresh mucosa for mucoadhesive study was from porcine oesophageal tissue, arranged and delivered from a local abattoir in London, UK.

## **3.9 Requirements of the cell cultures**

The requirements for cell culture have not changed since the first cell culture a century ago. Nutrients should be provided, as well as oxygen and a means for the removal of carbon dioxide.

### **3.9.1 Medium**

The common media have a basal saline medium to which various components are added. Cells require various components for growth and survival, such as amino acids, vitamins, metal ions, trace elements, and in particular glucose as the source of energy. A buffer is also required to control the pH of the medium (HEPES is particularly common). To indicate the acidity of the culture, phenol red is usually added to the medium. A basic medium was developed by Moore et al. (Moore & Glick, 1967; Moore & Pickren, 1967) at Roswell Park Research Institute and is called RPMI1640. It is the most widely used cell culture medium.

Eagle's basal medium (BME) is another widely used synthetic basal medium for supporting the growth of many different mammalian cells. BME was originally developed by Harry Eagle for HeLa cells and mouse fibroblasts. However, this medium does not have HEPES buffer and glutamine. BME was modified by adjusting the amino acid concentration, which led to the production of a new medium called Eagle's minimum essential medium (MEM). MEM was further modified by Dulbecco through increasing the concentration of the amino acid and vitamin to produce a new

medium called Dulbecco's minimum essential medium (DMEM). To support haematopoietic cells and produce a medium with even more amino acids and vitamins, as well as selenium, pyruvate and HEPES buffer, Iscove's modification of DMEM was developed (IMDM).

### **3.9.2 Serum-containing media**

To replace the missing requirements in the medium for culturing mammalian cells, serum is often added to the media. Serum provides proteins, lipids and carbohydrates, as well as growth factors and attachment factors. The concentration of components present is often variable. Serum obtained from newborn or foetal bovine is usually used for cell culture purposes. Serum is added at 5–20% of the total medium volume, depending on the cell type. Sera are usually prepared in aliquots and frozen at -20 °C.

### **3.9.3 Serum-free media**

There is a large variety in the composition of different sera. This can lead to different experimental outcomes, depending on which serum is being used for the experiment. The uncertainty that various serum supplementation might be introduced to cell culture has led to the exploration of serum-free media by many researchers. Two different approaches have been taken – one (Bottenstein & Sato, 1979; Sato et al., 1988) is to add specific supplement to the medium, while the other (Ham, 1963; Bettger & Ham, 1982) is to increase the concentration of various components of existing basal media. Insulin, transferrin, selenite, hydrocortisone and cytokines have

been the common components which are added to media as a serum replacement, while albumin has been used as the source for improving the protein content of the media and its addition has been shown to be useful. Components such as fibronectin have been useful when added to the media as they were shown to promote adhesion signalling (Prasad & Kumar, 1975; Allegra & Lippman, 1978; Barnes & Sato, 1979; Murakami & Masui, 1980).

#### **3.9.3.1 Source of media**

Media are available as commercial products. A specific type of medium should be selected, depending on the experiment and the cell line that is used in the experiment. The shelf life of the media is usually between 9–12 months.

#### **3.9.4 Cell culture plates**

There are many different sizes and forms of cell culture plates. Many of them are made from polystyrene. This type of plate allows the cells to adhere to the surface of the plate. For some experiments, it is better to prevent the cells from attaching to the plastic. For this application plates made from polypropylene is preferred. Plastics designed to promote adherence have a charged surface, resulting from chemical treatment or irradiation. For cell culture experiments in chapter 5, polystyrene 12 and 24 well culture plates have been used.

### **3.9.5 Environment for cell culture**

37 °C is the suitable and optimal temperature for the incubators where cells are kept for growth and maintenance. Temperature can change 1 degree around 37 °C, but the cells will die rapidly if the temperature rises to 40 °C. Culture media usually have buffering capacity because buffer is added to them as one of their essential components; however, this is insufficient and additional buffer is needed during the culture. This additional buffer is provided by 5% CO<sub>2</sub> to ensure optimal performance and to ensure the pH is kept between 7.2 and 7.4. The phenol red, which is a component of the medium, detects acidification through the changes in its colour. At pH 6.5, 7.0, 7.4 and 7.8, the colour of the phenol red converts to yellow, orange, red and purple respectively. The other critical factors for the cell culture environment are humidity and sterility.

## **3.10 Basic Laboratory Design and Equipment**

Cell culture requires a clean and well-designed laboratory with sufficient equipment to allow safe and sterile working.

### **3.10.1 Laminar flow cabinets**

Laminar flow cabinets are essential for safe and reliable culture of the cells. The Class II safety cabinet is ideal, as this provides operator and sample protection.

### **3.10.2 Centrifuges**

Most cell culture laboratories have benchtop centrifuges as they are required for cell pelleting. Centrifuges are essential for the cell work. To suspend a certain number of cells in a certain volume of culture medium, the volume which has that specific number of cells is removed and transferred into a tube, followed by spinning. The cells form a pellet at the bottom of the tube. The supernatant is removed with the cell pellet sitting at the bottom of the tube. The desired volume of medium is added to the cell pellet.

### **3.10.3 Incubators**

Incubators provide the carefully regulated environment for growing cells. In the incubators CO<sub>2</sub> and temperatures are carefully regulated.

### **3.10.4 Counting cells**

Cell counting is important for the cell works. Most of the cell culture experiments are based on observation of a specific condition on the viability or proliferation of a particular cell type, and the requirement for this aim is cell counting. This is usually performed using a haemocytometer and microscope, but recently a number of simple instruments have been used in the laboratories for cell counting and they provide greater accuracy. These new systems have a CCD camera system, and a disposable or reusable slide chamber or cassette which can be filled with cell suspensions in the laminar flow hood.

Flowcytometry can be used for cell counting, although it becomes an expensive method if it just uses for cell counting. In this work, for counting the cells, both the cell counter and the haemocytometer methods have been used.

### **3.10.5 Storage and other facilities**

The cells can be stored as frozen at -80 °C for a few weeks or in liquid nitrogen tanks for longer periods. The cells are usually suspended in freezing medium.

### **3.10.6 Solution preparation for scaffold production**

All the polymers in this study were purchased from Sigma-Aldrich (Poole UK) unless stated otherwise. To prepare the aqueous alginate solution, 1% wt. sodium alginate powder was dissolved in deionised water followed by the addition of 0.5% wt. polyethyleneglycol-40 (PEG- 40S, Sigma-Aldrich, Poole, UK, density; 1,300 kg/m<sup>3</sup>) as a surfactant. The mixture was stirred using a magnetic stirrer (KIKA, Labor-Technology RCT basic stirrer) for two hours to allow for even dispersion of the compounds. 0.5% wt. phospholipid (hydrogenated powder) was weighed and added to the solution, followed by further stirring for approximately another two hours until a homogenous solution was obtained.

### 3.10.7 Scaffold preparation

A V-junction microfluidic setup was used to obtain alginate bubbles (Figure 27). Previous work has been carried out on scaffold preparation by Ahmed et al. (Ahmad, Stride and Edirisinghe, 2012). In the current study, the microfluidic method was used to obtain porous scaffolds, where the bubbles were deposited into arrays to produce the foam. The temperature and relative humidity during processing was 21 °C, and 40%, respectively. The foam scaffold was dried (as observed by optical microscopy) after 10 days of incubation in a desiccator.

The average microbubble diameter was determined by measuring their diameters at ~100–200 µm points in the SEM images using the ImageJ software (Version 3.00). To allow the cell growth and support the biocompatibility features, the scaffolds have high porosity, and HA nanoparticles are incorporated into them.

In this study to support cell compatibility, HA nanoparticles (diameter < 200 nm, 5% wt.) were added to the scaffold structure (Phipps et al., 2011). This was achieved by adding the HA to the alginate solution prior to forming bubbles using the V-junction. Figure 27 indicates the scaffold preparation method. In the experiment, from inlet 1 alginate solution was applied, and from inlet 2, HA suspension was applied to coat the bubbles in the shell.

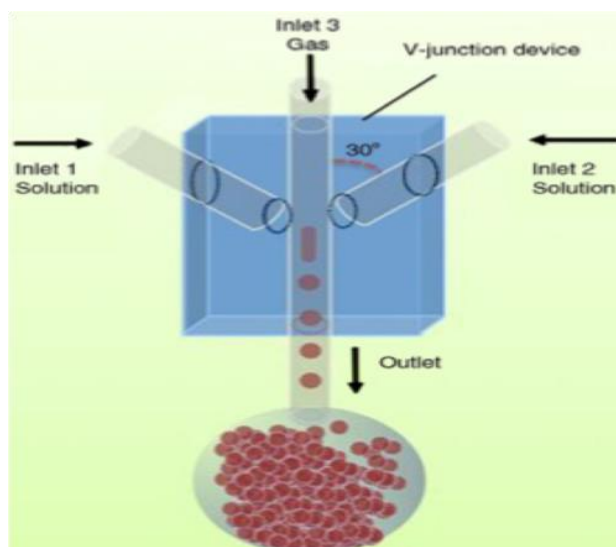


**Figure 27: Alginate bubbles sample produced via V-junction.**

### **3.11 The method for drying foam-based scaffold**

A desiccator was used in order to dry the produced foam to obtain the scaffold. Desiccators are sealable enclosures, used for preserving moisture-sensitive items such as cobalt chloride paper. A common use for desiccators is to protect chemicals which are hygroscopic, or which react with water from humidity. In order to dry foam scaffold, the microbubbles samples have been kept for 10 days in a desiccator.

#### **3.11.1 Preparation of normal haematopoietic and AML cells**

Informed signed consent was obtained from the patients for using their samples for research. Mononuclear cells (MNCs) were separated by density centrifugation in a Ficoll-Hypaque (Nycomed, Zürich, Switzerland) from peripheral blood of newly diagnosed AML and CML patients, and then cryopreserved. To separate MNC from the whole blood (as MNC is the

template for CD34+ cells), 15 ml blood was diluted with equal volume of PBS. The 30 ml diluted blood was transferred drop by drop into a 50 ml Falcon tube containing 20 ml Ficoll-HyPaque™ Plus (GE Healthcare, Uppsala) and centrifuged for 30 minutes at 1,800 rpm in a bench centrifuge (Heraeus Megafuge) at room temperature. The spinning finished with a non-brake status to avoid disturbance of the different layers of the cells.

As can be seen in figure 28, five layers can be distinguished at the end of the Ficoll separation. From the top to bottom, these layers are: plasma, a cloudy layer of MNC, Ficoll, and a white layer of granulocytes sitting directly on red cells. MNCs were transferred from the inter-phase of Ficoll and Plasma to a new tube and counted by a haemocytometer.

CD34+ cells were separated from MNC using a CD34+ collection kit (StemCell Technologies) as recommended by the manufacturer (<https://www.miltenyibiotec.com/>, 02 August 2018, 9.24am). For the AML samples, the information about the percentage of the leukaemia cells was provided by the diagnostic lab. CD34 marker is measured routinely, along with other major myeloid markers for the AML MNC samples. As the majority of the MNC from AML patients were leukaemic, no further purification was performed after separation of MNC.

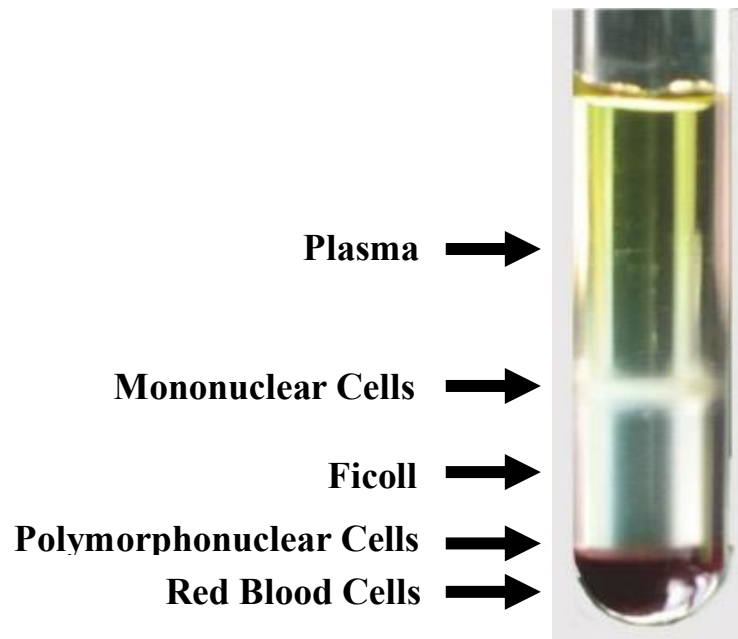


**Figure 28: Cell separation by Ficoll.**

*This figure shows the five different layers formed following fractionation of whole blood cells using Ficoll. Plasma stands on the top of other components. Then the MNCs stand as a cloudy layer between the plasma and Ficoll. Polymorphonuclear cells appear as a whitish layer under Ficoll, and finally red blood cells sit as the last layer.*

### **3.11.2 Cell lines**

A cell culture developed from a single cell, and therefore consisting of cells with a uniform genetic make-up, is commonly used for studying various aspects of cell behaviours. As mentioned earlier, due to the short life of many cells when cultured outside the body physiological condition, cell lines have been used as they can survive long enough for various investigations. In particular, cell lines have been investigated extensively for leukaemia research and the exploration of the therapeutic targets.

For this thesis, AML and CML were studied in regard to their response to the related antileukaemia agents. Three types of cell lines were used: K562,

HL60 and HS-5 (BM-derived mesenchymal cell line) (Figure 29). K562 and HL60 cell lines were kindly provided by Professor Nicholas Cross (University of Southampton).

HS-5 cells were purchased from ATCC (United States). K562 is a cell line model for CML. HL60 is a cell line derived from a patient with AML and is used as a model for this type of leukaemia. To simulate a BM microenvironment HS-5 cells were used, which are bone marrow-derived mesenchymal stromal cells.

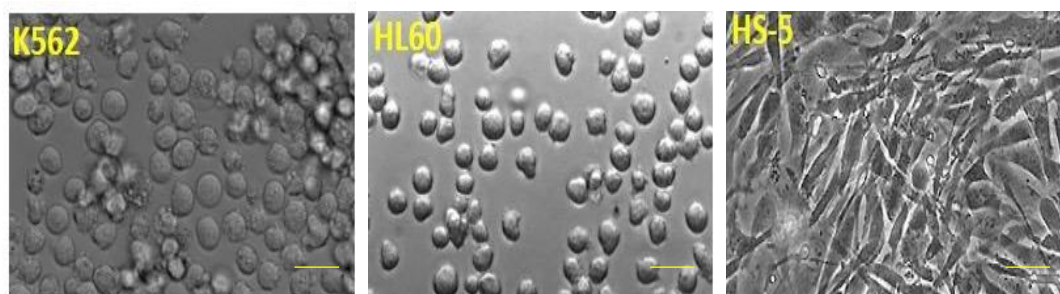


**Figure 29: Optical microscopic images of the K562, HL60 and HS-5 cell lines.**

*K562 and HL60 cells are suspension cells which are round, as shown in the figures. HS-5 is a mesenchymal stromal cell derived from human BM. They are adherent cells which have spindle morphology when they are in culture and attached to the culture dish. The presented scale (yellow line) is 20  $\mu$ M.*

### **3.11.3 Sterilisation of the foam-based scaffold**

Inside the laminar flow cabinet, scaffold pieces with an average diameter of  $\sim$ 0.5 cm were cut into appropriate pieces using a sharp cutter, and were transferred to each well of a 24-well plate using a fine-point forceps. A UV lamp (UV-C 60W Tube Unit Aluminium) with 254nm peak output, used for

disinfection of air and surfaces, was put in the laminar flow cabinet. The UV light was kept on for two hours (60W) while the scaffold was exposed to it.

After two hours of UV exposure the scaffolds were washed with PBS. 1 ml PBS was added to each well and then removed after one minute. This was repeated three times. Then 1 ml cell culture medium (please see the cell culture section) was added to the scaffold in each well and the plate was kept in the incubator overnight. The next day the medium was removed, and the scaffold was ready for adding the cells.

#### **3.11.4 Cell culture**

All the cell culture work has been done in the Centre for Haematology, Department of Medicine, Imperial College, Hammersmith Hospital, Du Cane Road, London, W12 0NN, UK. The method for drug sensitivity and cell work study from the Imperial Lab, have been optimised by Khorashad group working in this Lab. For 2D culture, K562 and HL60 cell lines were cultured in RPMI medium, supplemented with 10% Foetal Bovine Serum (FBS), 2 mm L-glutamine and 100 U/mL penicillin/streptomycin (RF10). Primary AML cells were cultured in StemSpan (Thermofisher) supplemented with CC100 (StemCell Technologies). The cells were cultured at a concentration of  $25 \times 10^4$ /ml. For 3D culture, the prepared scaffolds were transferred to 24-well culture plates and sterilised by exposure to UV light inside a laminar flow cabinet for two hours, followed by three times PBS washing. After the third wash, 1 ml RF10 (or StemSpan for primary AML) was added to each well, followed by incubation of the plates at 37 °C in a cell culture incubator for 24 hours. Subsequently, the medium was removed. Primary AML cells, K562 or

HL60 cell lines were suspended at  $25 \times 10^4$ /ml concentration and then 1 ml of the cell suspension was added to each well. For the drug sensitivity study, a final concentration of 0.5, 1 or 2  $\mu$ M imatinib or 0.1, 0.2 or 0.4  $\mu$ M doxorubicin was used. Doxorubicin should be handled very carefully. All the preparation for various dilutions of this drug was done in the air cabinet. Two layers of gloves were worn while handling doxorubicin. Imatinib and doxorubicin were purchased from Selleckchem (TX, USA). Two independent experiments with triplicate for each condition (control and various doses of drugs) were performed. T-test was used to measure the significance of the difference between the two conditions.

### **3.11.5 Measuring the lowest inhibitory dose of doxorubicin or imatinib on HL60 or K562**

In order to assess anticancer drug on the samples, various doses of imatinib were used to identify the lowest inhibitory dose of imatinib for K562. Without prior knowledge about the potential induced level of resistance by the foam-based scaffold, the lowest inhibitory concentration of imatinib was used in the experiments. K562 cells were cultured at the concentration of 5,000 cells per 100  $\mu$ l with or without 0.1, 0.2, 0.5, 1, 1.5 and 2  $\mu$ M imatinib in a 96-well plate. The inhibitory effect of imatinib was measured after 72 hours by methanethiosulfonate (MTS)-based viability assay (CellTiter 96 AQueous One; Promega). HL60 and HS-5 cell lines were treated with or without 0.1, 0.2, 0.5 and 1  $\mu$ M doxorubicin for 72 hours in triplicates, followed by viability/proliferation measurement using MTS assay (as will be described later in this chapter).

### 3.11.6 Co-culture of HS-5 with HL60 or K562 cells

Experiments to examine the effect of 3D culture have all been done in the centre for Haematology, Department of Medicine, Imperial College, Hammersmith Hospital, and the proposed method was designed by the auteur of this thesis and the help of the Khorashad research group.

Foam-based 3D culture was further developed by adding HS-5 cells to calcium alginate foam scaffolds.  $15 \times 10^4$  GFP<sup>+</sup> HS-5 cells were suspended in 500  $\mu$ l RF10 and transferred to each well of the 24-well plates containing the scaffold foam. 24 hours later  $5 \times 10^5$  K562 or HL60 cells were suspended in 500  $\mu$ l RF10 and added to each well. 24 hours was given to the K562 or HL60 cells to settle down and make contact with the scaffold and HS-5 (Figure 30). After this 24 hours, the drug treated groups were given 0.5 or 1  $\mu$ M imatinib or 0.1 or 0.2  $\mu$ M Doxorubicin. 72 hours later, the live K562 or HL60 cells were counted using Countess II FL (Life Technologies, USA). To do the counting, the supernatants from each well were transferred to the related tubes.

The wells containing the scaffold were washed with 1 ml PBS and the resulting supernatant was added to the related tubes containing the original supernatant. 100  $\mu$ l Trypsin-EDTA solution was added to each well and incubated for five minutes at 37 °C. It was followed by adding 900  $\mu$ l PBS and pulling it up and down a few times, before passing the solution through a cell strainer (Corning) into the related tube. Now each tube had all the cells from each associated well (Figure 31).

After shaking each tube well, 10  $\mu$ l was removed and mixed with 10  $\mu$ l trypan blue. 10  $\mu$ l of the mixture was added to the Countess II FL slides, followed by insertion of the slide into the counter and recording the count readings. HS-5, like any other BCR-ABL1 negative cells, is not sensitive to imatinib and its proliferation is not affected as a result of exposure to imatinib.

Regarding the doxorubicin experiment, we showed that HS-5 was not affected by the dosage of doxorubicin applied in this study, and because of the equal number of HS-5 cells in all the wells, the differences in the counts were related to the leukaemia cells (primary or cell line). Each condition was performed in triplicate and the experiment was done twice. T-test was used to compare the differences.

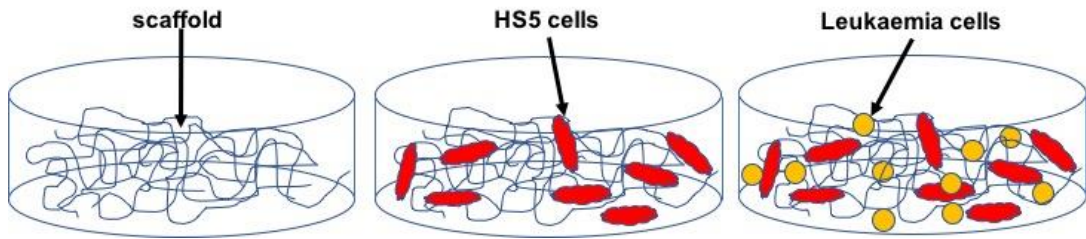


**Figure 30: The process for developing a 3D culture.**

*This figure shows the process for developing a 3D culture. The calcium alginate foam scaffolds were sterilised by exposure to UV light for one hour inside an air cabinet. It was followed by washing the scaffolds three times with PBS. After washing with PBS, the scaffolds were washed with cell culture medium three times. After the third wash the HS-5 cells (shown in red) were added to the scaffolds. The HS-5 are adherent cells, which have spindle shape but lose their shape after they are detached from the surface of the culture dish. The HS-5 were left in the scaffolds for 24 hours. During this time, they attached to the scaffolds and also to the surface of the culture dish and secreted cytokine into the medium. At the end of the 24-hour culture of HS-5, the investigated leukaemia cells, such as K562, HL60 or primary AML cells (shown as round yellow circles), were added to the scaffold. If any drug experiment is planned, it will be done 24 hours after adding the leukaemia cells. This 24 hours gives an opportunity for the leukaemia cells to make contact with the HS-5 cells and the scaffold, and also to being influenced by the secreted cytokines in the medium. For this experiment the HS5 cells were labelled with GFP (green fluorescent protein). GFP marker helped in distinguishing the HS-5 from the leukaemia cells under fluorescent microscope.*

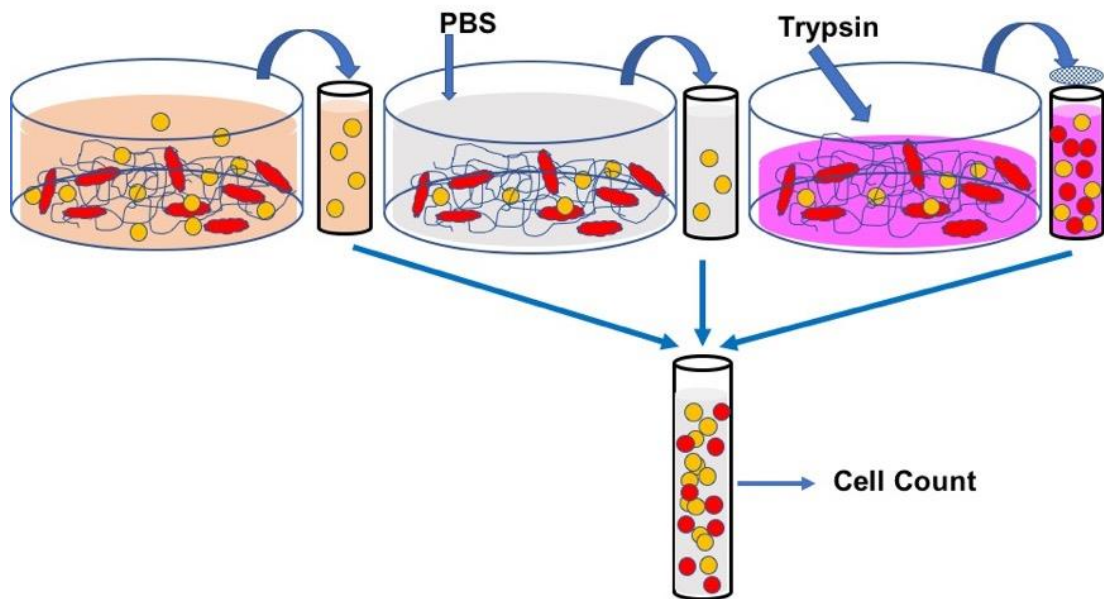


**Figure 31: Removing the cells from the 3D culture.**

*This figure demonstrates the process for removing the cells from the 3D culture before counting. The scaffold is shown as blue curvy lines. HS-5 stromal cells in 3D culture are shown as long red cells. The white blood cells (normal CD34, primary leukaemia cells or cell line) are shown as yellow round cells. HS-5 in culture looks like long and stretched cells because they are attached to the surface of the scaffold plate. Following the addition of trypsin, the HS-5 cells lose their contact to the microenvironment and become round in shape. Adding trypsin also degrades the calcium alginate scaffold because EDTA in the trypsin solution chelates the calcium, resulting in degradation of the scaffold. To remove the degraded scaffold from the cells before counting, the trypsin-treated cells are passed through the cell strainer. The colour of the medium, PBS and trypsin have been shown to be orange, grey and pink respectively.*

### **3.11.7 Differentiation of the cells using flowcytometry**

CD34 is the marker found usually on the surface of the haematopoietic stem cells and progenitor cells. CD34 gradually disappears during differentiation of

the haematopoietic cells. The loss of this marker is one of the indications for differentiation. In addition to CD34 marker, a wide range of cell surface markers are investigated to characterise differentiation of the blood cells. As for this study, the differentiation of AML was investigated, and the cell surface markers related to myeloid lineage were measured. The appearance or increased expression of CD13, CD117, and HLA-DR indicate the enhanced differentiation of the myeloid lineage. Detection and measurement of the myeloid markers was done by flowcytometry. To distinguish each cell marker, specific antibodies for each cell marker were used. Each antibody has an attached unique fluorescent marker which can be recorded by the flowcytometry instrument (Terstappen & Loken, 1990).

CD34+ cells from one normal and three AML patients were cultured in StemSpan (Thermofisher) supplemented with CC100 (StemCell Technologies) in foam-based 3D and 2D culture. Foam-based 3D cultures were prepared in 24-well plates by sterilising the scaffold using UV, washing with PBS and medium, followed by culturing the cells. Myeloid markers were measured at the time of culture to determine the baseline level of myeloid markers and then reassessed after three days to demonstrate the alterations in the expression of the myeloid markers under 2D and 3D conditions. To retrieve the cells, the supernatant was removed from the 3D culture to collect the suspending cells in the culture. To collect the leukaemia cells attached to the scaffold, the scaffold was washed with PBS and then treated with Trypsin-EDTA (Sigma-Aldrich). During the incubation time trypsin disrupts the adhesion of cells to the scaffold, leading to their release into the medium. After five minutes of incubation at 37 °C, the supernatant contains the

remaining cells which could then be collected. Trypsin contains EDTA, which is a chelating agent that leads to degradation of the calcium alginate foam scaffold. This makes it difficult to retrieve the cells by centrifuging as the alginates precipitate with the cells following spinning. To collect the cells and remove the alginates, the supernatant was removed and passed through a filter. The filtered cells were then added to the cells collected from the medium. The collected cells were centrifuged, followed by washing with PBS. The cells were stained with the fluorescent-labelled antibodies and incubated for 15 minutes at room temperature for the formation of the antibody/antigen bond. After the incubation, the cells were washed to remove the unbound antibodies; then measurements were taken for the presence of various myeloid cell markers by flowcytometry. Immunophenotype was determined using 8-colour Euroflow AML/MDS antibody panel tube 1 (CD16 FITC, CD13 PE, CD34 PerCP-Cy5.5, CD117 PE-Cy7, CD11b APC, CD10 APC-H7, HLA-DR V450, CD45 V500). Data was acquired using a BD FACSCanto II flowcytometer (BD) and analysed with Infinity software (Cytognos).

### **3.11.8 MTS assay**

This is a colorimetric method for determining the number of viable cells in proliferation, cytotoxicity or chemosensitivity assays. The CellTiter 96<sup>®</sup> AQueous One Solution Reagent contains a tetrazolium compound [3-(4,5-dimethylthiazol-2-yl)-5-(3-carboxymethoxyphenyl)-2-(4-sulfophenyl)-2H-tetrazolium, inner salt; MTS] and an electron coupling reagent (phenazine ethosulfate; PES). PES has enhanced chemical stability, which allows it to be combined with MTS to form a stable solution. Assays are performed by

adding a small amount of the CellTiter 96<sup>®</sup> AQueous One Solution Reagent directly to culture wells, incubating for one to four hours and then recording absorbance at 490 nm with a 96-well plate reader. The quantity of formazan product is measured from the amount of 490 nm absorbance, which is directly proportional to the number of living cells in culture. This is one of the most commonly applied assays for investigating the inhibitory effect of antileukaemia agents in *in vitro* studies (Figure 32).

Cells ( $10^4$ ) were suspended in 200  $\mu$ L medium  $\pm$  inhibitor and cultured in triplicate in a 48-well plate in the presence or absence of inhibitors (imatinib or doxorubicin) at indicated concentrations. After 72 hours, CellTiter 96 AQueous One Solution MTS Reagent (Promega) was added according to the manufacturer's instructions. After one hour, 100  $\mu$ L of the medium was transferred from each well to a 96-well plate. The dye absorbance was then measured at 490 nm using a Multiskan GO Microplate Spectrophotometer (ThermoFisher Scientific). The reduction of MTS tetrazolium compound by viable cells generates coloured formazan product that is soluble in cell culture media. This conversion happens through NAD(P)H-dependent dehydrogenate enzymes in metabolically active cells. The dye produced in viable cells is quantified by measuring absorbance at 490/500 nm.

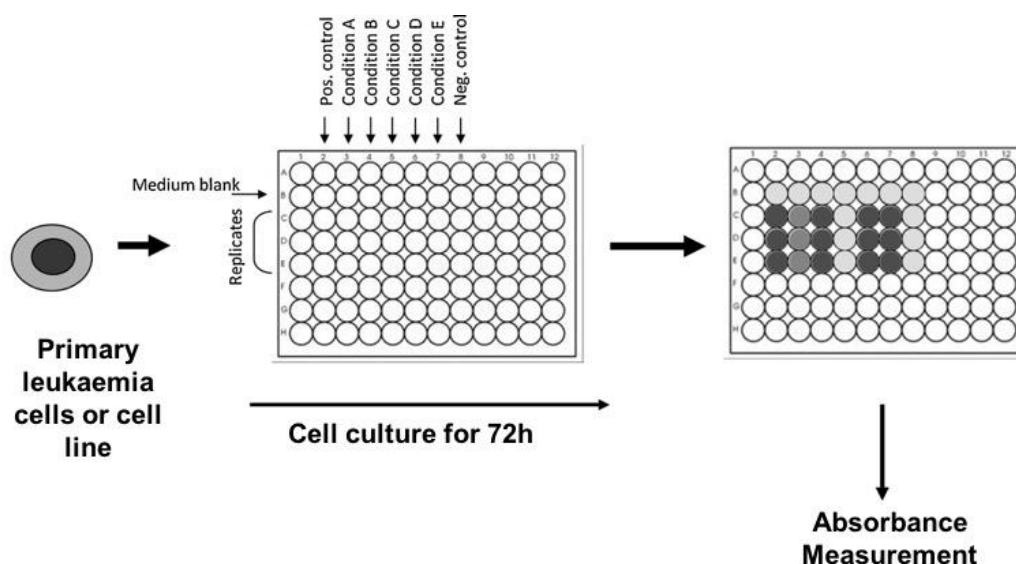


**Figure 32: The principle of MTS assay.**

*This figure outlines the setup and measurement principle of MTS assay. The principle of MTS assay is based on comparing the colour changes in the test condition compared to control, measured by spectrophotometry. For drug sensitivity studies in leukaemia, the cells are treated with various doses of the investigated drugs along with untreated control, followed by culturing for various periods. The number of tested cells depends on the type of the investigated cells. For cell line, usually between  $2-5 \times 10^3$  per  $100 \mu\text{l}$  medium, and for primary cells,  $20-30 \times 10^3$  cells per  $100 \mu\text{l}$  medium is used. After the desired time, the MTS assay dye is added to the cells, followed by keeping the cells in the incubators from 30 minutes to several hours. The incubation time for primary cells is usually longer than cell lines (adopted from Boehm and Bell (2014)).*

### 3.11.9 Statistical analysis

All the statistical analysis was done using Graphpad prism software version 7. A 2-tailed Student *t*-test was used for assays with cell lines and primary cells. For 3-(4,5 dimethylthiazol-2-yl)-5-(3-carboxymethoxyphenyl)-2-(4-sulfophenyl)-2H-tetrazolium (MTS) assays, three independent experiments,

each with three replicates per concentration, were performed in unique plates with untreated controls.

### **3.12 UV-Vis spectroscopy**

Ultraviolet-visible spectroscopy (UV-Vis) is a method for drug release investigations. The principle underlying this method is the absorption of light by the tested substance in the specific UV-Vis spectral range. The span for the UV-Vis spectral region is in the range 200–700 nm in the electromagnetic spectrum (Figure 33). Energetic excitement causes electronic transition in the atoms and molecules within the specific UV-Vis spectral region. This affects the electronic structure and the interrelated colour of the tested material. Energy from a light passing through a substance is absorbed by the molecules of the substance which is in the solution. This causes the electrons in the highest occupied molecular orbital (HOMO) to be excited to the lowest unoccupied molecular orbital (LUMO). The molecules with double bonds and conjugations usually have an easier electronic transition because there are more available delocalised electrons for excitation. Higher conjugation results in a shift towards the visible range from UV for the emission wavelength (Abou-Taleb, 2014). The transmitted light's intensity through a substance in solution is measured by a UV-Vis spectrophotometer.

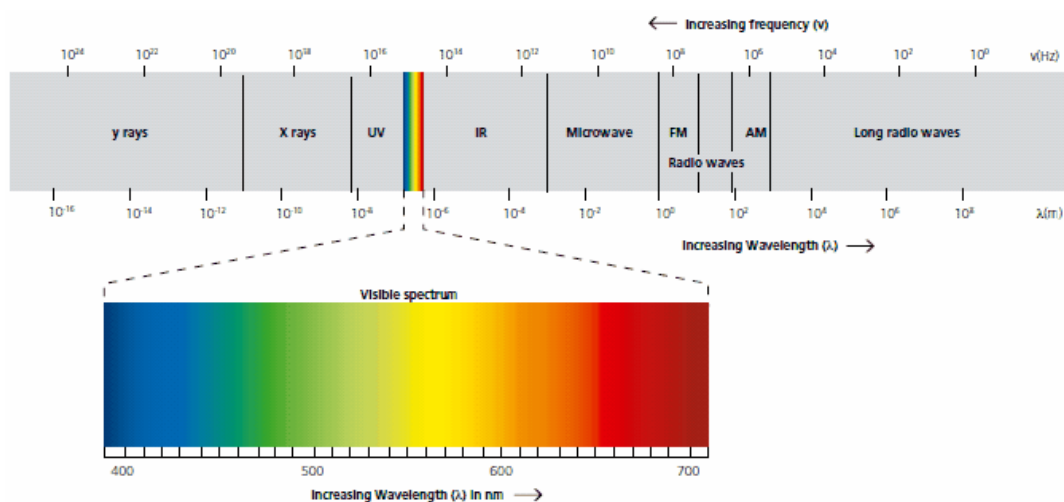


**Figure 33: Different zones in the electromagnetic spectrum with a magnified visible range (Jeitziner, 2014).**

*The medium performance Perkin Elmer Lambda 35 (Perkin Elmer, UK) UV-Vis spectrophotometer is a double-beam spectrophotometer and was used throughout this work. The halogen lamp in this spectrophotometer generates visible wavelengths between 354–700 nm, and the deuterium lamp is responsible for 200–354 nm wavelengths. Quartz cuvettes were used for sample measurements. Scan rates of 300 nm/min, and a slit width of 1 nm were used throughout, while the wavelength range 200–700 nm was selected for dye substances.*

## Chapter 4

# Creating microbubbles using microfluidic technology for potential and therapeutic use in healthcare

### 4.1 Introduction

Ultrasound imaging modality is commonly used for diagnostic purposes because of the excellent image quality combined with lack of ionizing radiation, cost effectiveness and being non-invasive. Therapeutic and diagnostic capacities of ultrasound can be further improved through the application of microbubbles. Microbubbles enhance the targeted delivery and localization of the drugs when used with ultrasound.

The aim of this study was to characterise the microbubble formation process in microfluidic channels and to optimise the bubble stability using different methods, followed by analysing the stability of microbubbles under gastric condition. Geometry and angle position of the oesophagus makes oral drug access to this region difficult. Various methods of oral drug delivery have been investigated to improve the drug delivery to the gastroesophageal region. In this study alginate microbubbles as a vehicle for drug delivery to the oesophagus was investigated. The microbubbles were generated using V-junction microfluidic techniques and were optimised by increasing their stability through modification of the collection medium and coating with solid nanoparticles. The data in this study confirmed that the collection of the alginate microbubbles using glycerol and incorporation of gold nanoparticles

into the microbubble shell increase their stability. To simulate the gastroesophageal condition, the stability of the microbubbles was investigated in the presence of acidic pH and body temperature. The generated microbubbles were able to deliver the model drug to the porcine oesophageal tissue and also to artificial membranes as demonstrated by mucoadhesive test, suggesting the microbubbles as a bioadhesive agent for drug delivery to oesophageal tissue. In order to facilitate bubble formation, microfluidic V-junction techniques were used in this work. There are different methods for microbubbles production such as lithography and wet etching (Garstecki, Gañán-Calvo, & Whitesides, 2005; Zhang & Wang, 2009). The regular blockage and clogging of the flow channels and the consequent need for expensive replacement and cleaning processes of the devices is one of the challenges that these devices face (Mustin & Stoeber, 2008). Compared with other methods, the microfluidic setup in the current study provides a low-maintenance system for bubbles/droplets production. Any problem related to the blocked channel can be easily solved by replacing capillary tubes. The bubble/droplet size can be controlled using the microfluidic setup as described in this study, and it is very important as microbubble size plays a significant role in drug delivery. In order to investigate the alginate bubble formation process and optimise this system, a detailed investigation was performed to study the effect of solid nanoparticles on the microbubbles surface. It was done by adding gold nanoparticles to the bubble's shell. In addition, the effect of collection medium on the bubble stability was studied. Glycerol and calcium chloride solutions were chosen for this purpose. In the present work alginate microbubbles were prepared using a V-junction microfluidic device and the microbubbles were collected under different

conditions. The variations for different conditions included medium, acidity and temperature were studied in this part. The stability of the microbubbles was studied under ambient conditions and at body temperature (37 °C).

#### 4.1.1 Characterisation of alginate solution

The viscosity and surface tension of the alginate-PEG solutions, which are crucial factors for the production of microbubbles, were measured and documented in Table 1. It is important to measure and check the properties such as surface tension and viscosity because they affect bubble size and lifetime. These properties are explained in further detail later in this chapter. With the increase of the alginate concentration from 0.25 to 1%, the viscosity of the alginate-PEG-40S solution increased from 12 to 24 mPa s. The surface tension also increased from 43 to 47 mN/m. All experiments were carried out at room temperature (21 °C) and repeated on three separate occasions to achieve the accurate measurements.

Solution (wt%)	Viscosity (mPa s) ±2	Surface tension (mN/m) ±2	pH± <sub>1</sub>	Bubble size (µm) ±2	Temperature (C) ±1	Humidity (%) ± <sub>1</sub>
1wt.% Sodium Alginate+PEG	24	47	5	66	21°	42
0.5wt.% Sodium Alginate +PEG	19	45	5	70	21°	42
0.25wt.% Sodium Alginate +PEG	12	43	5.3	80	21°	42

**Table 1: Characterisation of alginate microbubbles solution.**

*Three series of alginate solutions with concentration of 1, 0.5, 0.25 wt.% were prepared from sodium alginate powder dissolved in deionised water. Polyethyleneglycol 40 was added as a surfactant to all solutions. The concentration of surfactant (PEG) for all solutions was 0.5 wt.%.*

#### **4.1.2 Microbubble preparation using microfluidic V-junction**

Experiments showed that by increasing alginate concentration from 0.25 to 1 wt.%, the viscosity of alginate- PEG-40S solutions were increased from 12 to 24 mPa s. The surface tension was varied between 43 and 47 mN/m. A microfluidic V-junction device was used for microbubble preparation.

Sodium alginate is a natural, biocompatible and bioadhesive polymer, and was chosen in this study for microbubbles production (Stops et al., 2008). Alginate solution from the side inlet was applied to the V-junction and nitrogen gas was applied from the top inlet; liquid and gas met in the intersection of the junction and microbubbles were formed. Same size alginate bubbles were collected from the outlet of the polymeric junction. Alginate microbubbles were collected on a glass slide covered with deionised water.

The bubble-bursting process is shown in Figure 34. As a function of time, the diameter and population of alginate microbubbles were reduced, and after almost 45 minutes all of microbubbles disappeared through the bursting process.

It can be seen that after 45 minutes only the dried alginates and nanoparticles remained on the glass slides. An image by optical microscope shows the dried particles following the burst of the alginate bubbles (Figure 35).

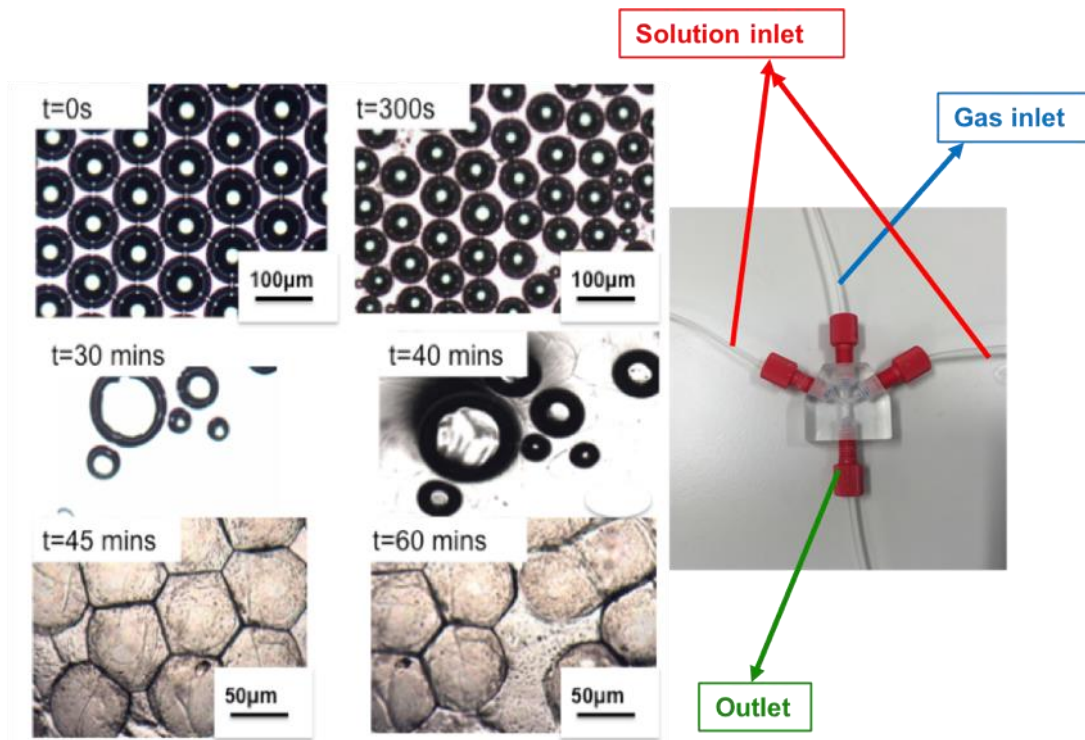


**Figure 34: Optical microscope image of alginate bubbles.**

*The top left-hand group of the optical microscope images show the alginate microbubbles as a function of time (5, 30, 40, 45 and 60 minutes). The top right-hand image shows a V-junction. The bottom images show a decrease in bubble population and diameter over time.*

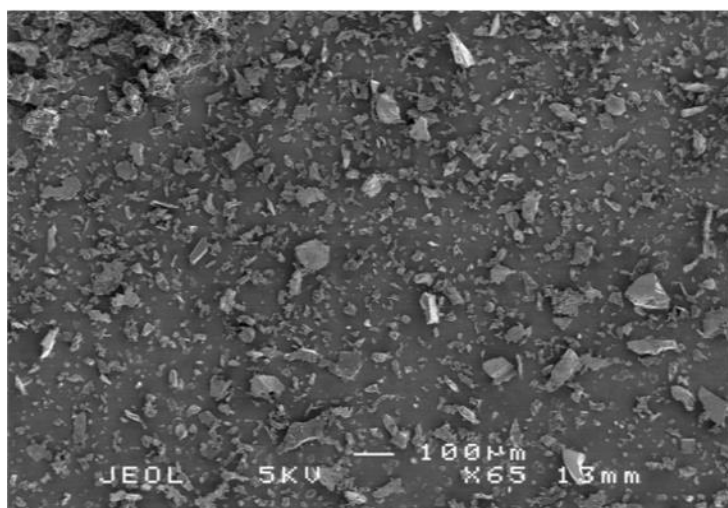


**Figure 35: SEM image of alginate particles from burst bubbles.**

This image is taken from bursting alginate bubbles kept on a glass slide.

### **4.1.3 Microbubble size**

Microbubble size is important to ensure the delivery of accurate drug dose in drug delivery studies as it influences the drug release process (Stride & Edirisinghe, 2008). The size of the microbubbles can be controlled by changing gas pressure and the liquid flow rate. The results indicated the impact of various factors on the size of the bubbles during the microfluidic process. The bubble size was increased as the gas pressure rose. The bubble size was reduced as the liquid flow rate increased.

#### **4.1.3.1 Effect of gas pressure on size of the microbubble**

This experiment was done to assess the effect of gas pressure on the bubble diameter. Alginate solution was tested with gas pressure in the range of 75 to 125 kPa and liquid flow rate was constant in all cases. The result showed that monodisperse microbubbles were produced by controlling gas pressure and

liquid flow rate within a specific range. The bubbling gas pressure was set and adjusted using a monometer connected to a gas tank. This made obtaining the required size of bubbles a simple task. Increasing the bubbling gas pressure caused a corresponding rise in the size of the produced microbubbles, at a constant flow rate. As it can be seen in figure 36a, figure 36b and figure 36c, monodisperse microbubbles of size 140  $\mu\text{m}$ , 60  $\mu\text{m}$  and 35  $\mu\text{m}$  were produced under the gas pressure of 125 kPa, 100 kPa and 75 kPa respectively.

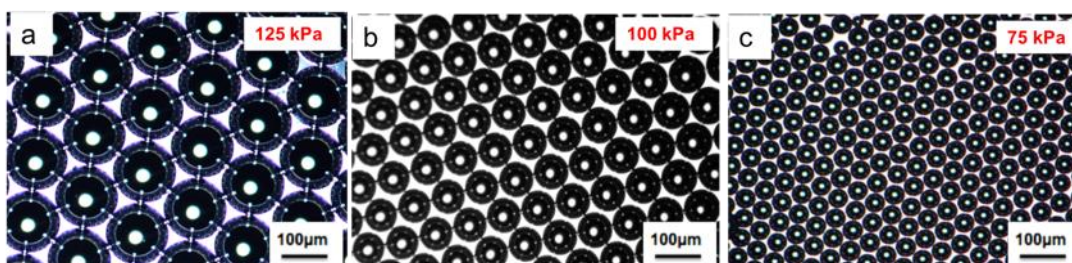


**Figure 36: Alginate bubbles with the different gas pressure.**

*Increasing gas pressure will increase size of the microbubbles. a) Gas pressure at 125 kPa; b) Gas pressure at 100 kPa.; c) Gas pressure at 75 kPa.*

#### **4.1.3.2 Effect of liquid flow rate on size of microbubble**

The other factor that was found to have an influence on the size of the produced bubbles was the flow rate of the solution, which was set and controlled using a controlled syringe pump. By testing different flow rates ranging from 150 to 500  $\mu\text{l}/\text{min}$ , the size of the microbubbles was found to be inversely proportional to the flow rate, at a constant bubbling gas pressure. This conclusion is in agreement with the experiment, showing higher flow rates results in microbubbles with smaller diameters, ranging from 140  $\mu\text{m}$  to 60  $\mu\text{m}$  (Figure 37).

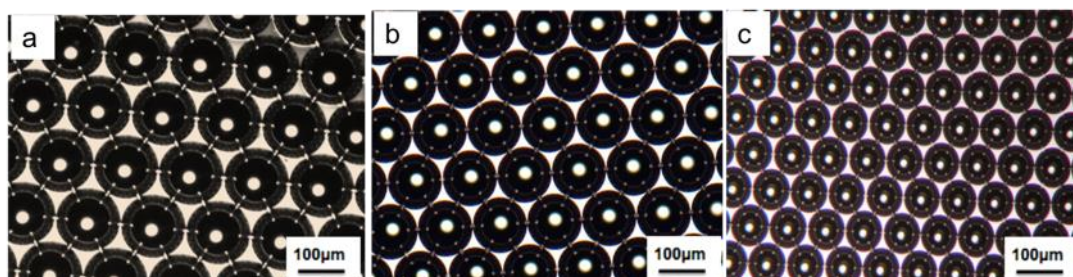


**Figure 37: Effect of liquid flow rate.**

*The diagram indicates microbubble production using three different liquid flow rates (a:150 µl/min, b:300 µl/min, c:500 µl/min). The bubble size was reduced by increasing the flow rate.*

#### **4.1.3.3 The impact of surfactant type on the size of the microbubble**

The size of microbubbles was found to be influenced by the concentration and type of the surfactant; it was directly proportional to the surface tension of the solution (Xu et al., 2009). The size of the microbubbles could change with the magnitude of the solution surface tension, even when the same combination of the flow rate and bubbling pressure was used. In order to investigate the effect of surfactant type on bubble stability, two different surfactants (PEG 40 and Tween 20) were used with the same amount of each in the alginate solution. It was found that bubbles produced with Tween and collected on glass slides lasted for 35 minutes, while the produced bubbles using PEG lasted for 45 minutes. The increased stability of the bubbles produced using PEG is shown in figure 38. This longer lifetime of the microbubble is due to steric stabilization by the non-ionic surfactant at the adjacent bubbles (Napper, 1977; Atta et al., 2004).

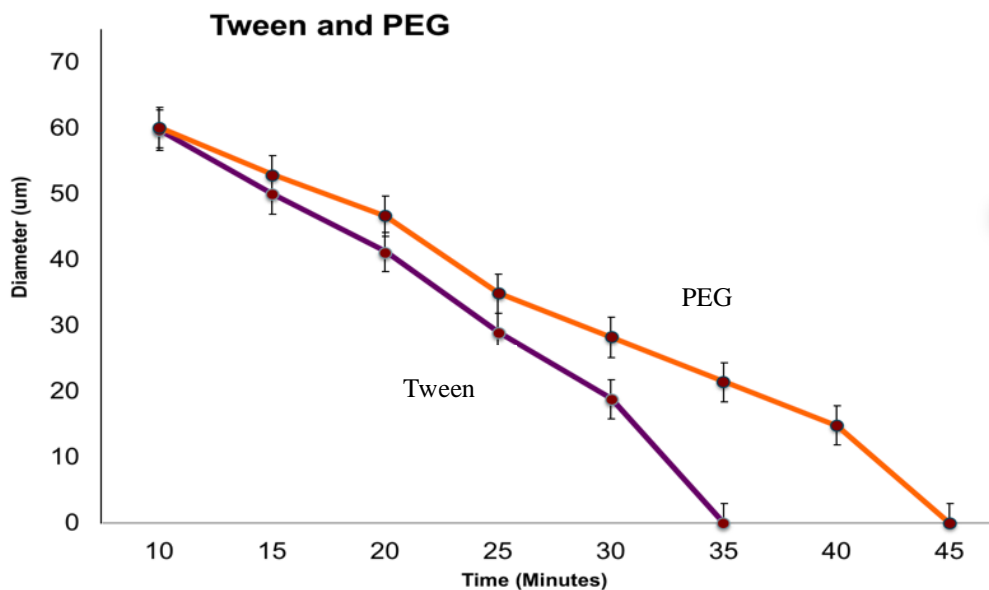


**Figure 38: Time study graph.**

*The graph indicates using surfactant PEG (orange) compared to same percentage of surfactant Tween (purple) in the alginate bubbles.*

#### 4.1.3.4 The effect of the capillary size on the microbubble size

Polymer V-junction consisted of two perpendicular Teflon FEP (Fluorinated Ethylene Polypropylene, Upchurch, USA) capillaries with a constant inner diameter (200 µm). The top vertical capillary is connected to a gas cylinder. The gas cylinder is connected to a digital manometer to control the pressure supplied to the junction. A schematic of the V-junction setup and the junction geometry is shown in figure 39. The impact of the capillary diameter on the bubble size was investigated using the two capillaries with tubing inner diameter sizes of 150 and 200 µm. Each set of the experiment was performed twice with constant gas pressure and liquid flow rate. It was observed that by increasing the capillary diameter, the bubble size increased, and bubble formation occurred within a larger range of flow ratio. The liquid flow rate was constant during the experiment while the capillary size increased, leading to

the formation of bubbles within a bigger diameter, as shown in figure 40.

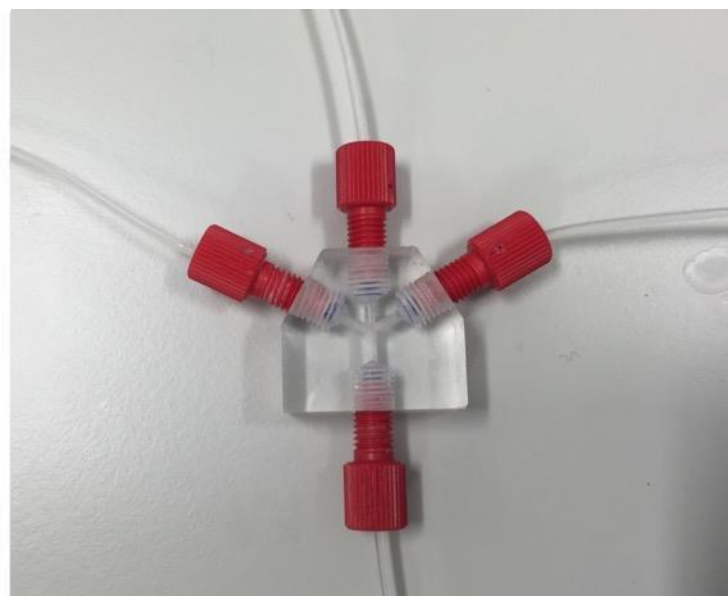


**Figure 39: Microfluidic V-junction, bubble preparation process and collection.**

*This figure shows the process of producing bubbles in microfluidic device (top) with the V-junction (bottom).*

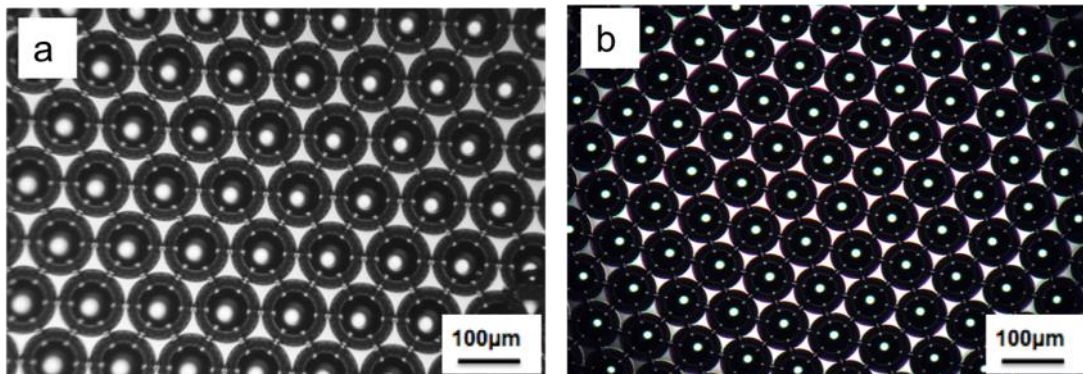


**Figure 40: The effect of capillary size on the bubble size.**

*Alginate microbubbles prepared by microfluidic. Figure (a) shows bubbles produced via capillaries with inner diameter of 200  $\mu\text{m}$ , and figure (b) shows bubbles produced via capillaries with inner diameter of 150  $\mu\text{m}$ .*

#### **4.1.4 Preparation of microbubbles for drug delivery**

Alginate microbubbles were collected on a glass slide which was covered by deionised water. Over time the populations of the bubbles and their diameters reduced. The gas inside the bubbles expanded overtime and resulted in the shell fragmentation and bubble disruption.

Figure 41 shows the bubble-bursting process. Gradually the gas inside the bubbles evaporated, leading to microbubble shrinkage and eventually bubbles with smaller size compared to the initial ones.

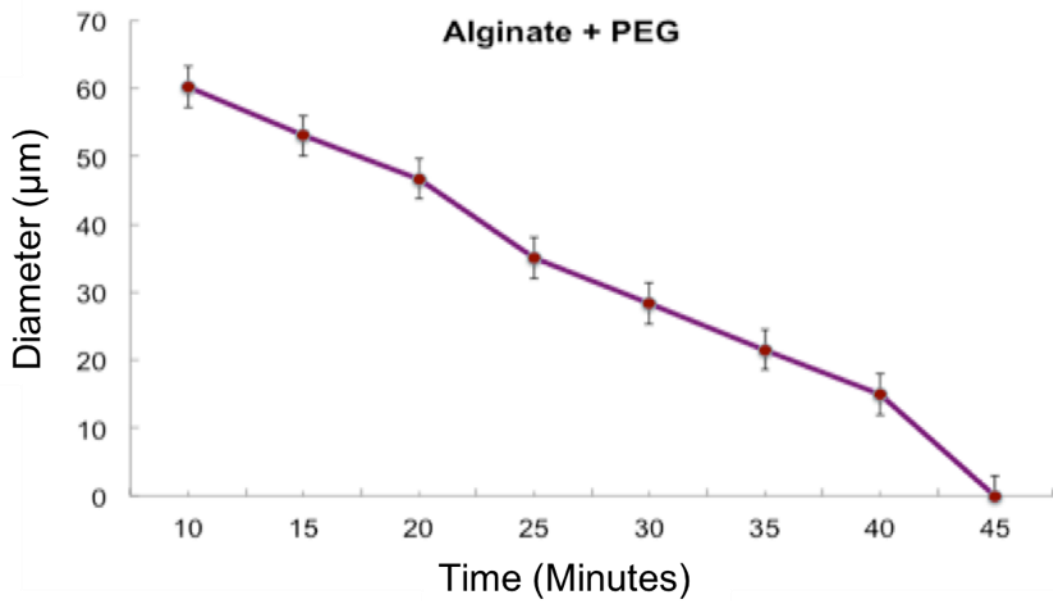
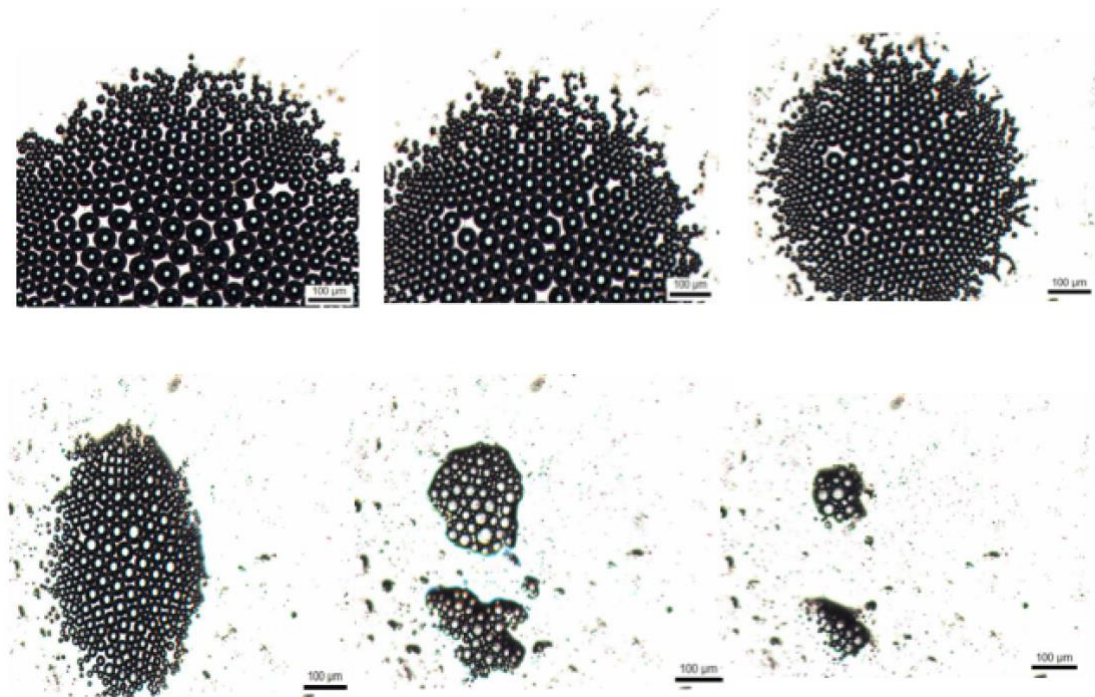


**Figure 41: Alginate microbubble bursting process.**

*Optical microscope images taken from alginate microbubble sample (five minutes apart) from formation to burst. The top figures are microscopic images from the microbubbles over time. The graph at the bottom shows the alteration in the size of the bubbles as time passes.*

#### 4.1.5 Monodispersity and polydispersity

One of the main advantages of using the microfluidic devices is the ability to generate monodisperse bubbles. Monodisperse and polydisperse bubbles refer to the same size and various size bubbles respectively. To obtain monodisperse microbubbles (80  $\mu\text{m}$ ), as shown in figure 42 (left), the flow rate of the solution and the gas pressure were adjusted concurrently; otherwise polydisperse microbubbles with various sizes (10–80  $\mu\text{m}$ ) would have been formed, as shown in figure 42 (right). In addition to flow rate and gas pressure, the size of microbubbles can be influenced and controlled using other processing variables such as the properties of the solution, like surface tension (Yobas et al., 2006).

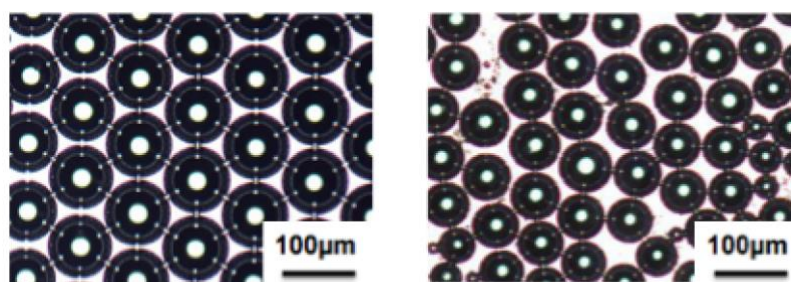


**Figure 42: Monodispersity versus polydispersity.**

*Monodisperse microbubble and polydisperse microbubbles are shown on the left and right respectively. Monodisperse and polydisperse bubbles refer to the same size and various sizes of microbubbles respectively.*

#### 4.1.6 Microbubbles stability

The stability of microbubbles in biomedical applications is very important. By increasing stability, efficient and accurate dosing as well as minimisation of

unwanted side effects can be achieved, allowing for more effective treatments (Mohamedi et al., 2012a). Two methods were tested to achieve microbubble stability in the current study. These were the modification of the alginate solution and the collection media.

#### **4.1.6.1 Modifying alginate suspension: the effect of gold nanoparticles on the stability of alginate microbubbles**

Previous work has been done using gold nanoparticle suspension to coat microbubbles (Mohamedi et al., 2012b; Mahalingam, Meinders and Edirisinghe, 2014). It was shown previously through theoretical modelling as well as experimental investigations that incorporating solid nanoparticles into the solution results in increased stability and life span of the microbubbles (Mohamedi et al., 2012b). The incorporated nanoparticles increased stability through preventing gas diffusion and coalescence in the microbubbles (Mohamedi et al., 2012). The experiments in this chapter confirmed that by adding gold nanoparticles to the alginate solution, the size reduction of the microbubbles decreased and therefore the microbubbles' size remained unchanged for a longer period. Comparisons were conducted between bubbles coated with and without gold nanoparticles. Near-monodisperse microbubbles (~100  $\mu\text{m}$  diameter) were prepared using a microfluidic device, with and without adding a suspension of spherical gold nanoparticles (~0.3  $\mu\text{m}$  diameter). It was observed that the stability of the microbubbles was enhanced for 30 minutes by the presence of the gold nanoparticles (Figure 43). In accordance with the ripening process, a small amount of the second component with a very low solubility was incorporated

into the system which led to a heterogenous population of microbubbles and this resulted in a lower lifetime (Figure 44). This result demonstrates that the presence of gold particles leads to more homogeneous microbubbles, which is associated with more stable microbubbles.

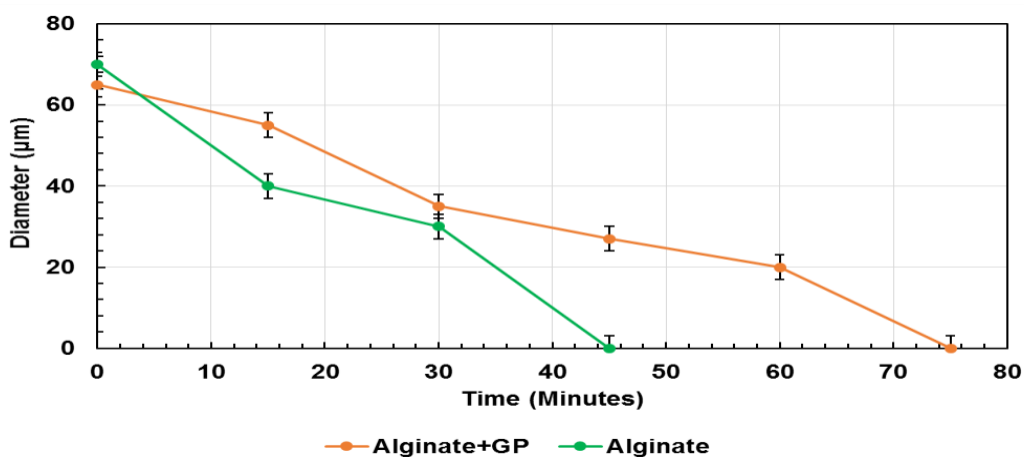


**Figure 43: Microbubbles coated with nanoparticles.**

The presence of gold nanoparticles (GP) increased the bubbles' lifetime, compared to alginate microbubbles without gold nanoparticles. The X and Y axis represent microbubble diameter and time respectively.

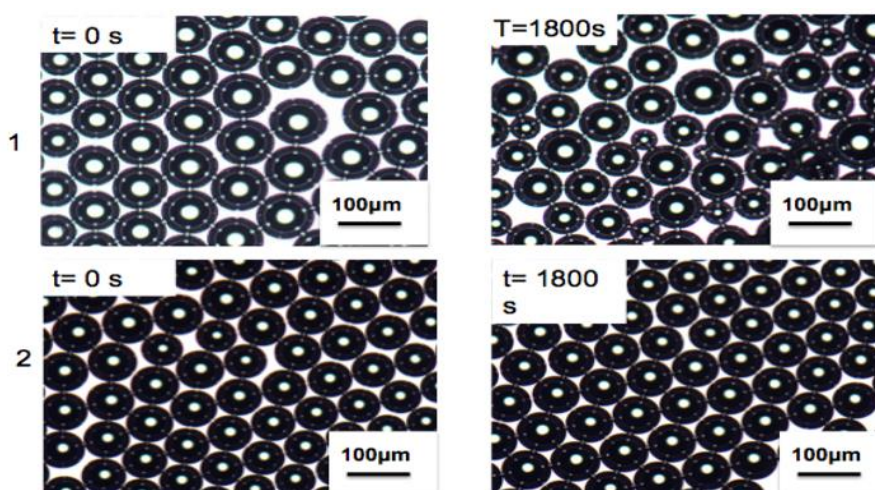


**Figure 44: Optical microscope images from alginate bubbles.**

Optical microscope images show the alginate microbubbles without (first row) and with GP (second row). GP on the surface of microbubbles led to increased microbubbles lifetime.

#### 4.1.6.2 Modifying collection media

In order to investigate the effect of collection media on the stability of microbubbles, they were collected in calcium chloride. Calcium chloride cross-links the shell of the bubbles. When sodium is put into a solution of calcium chloride, the calcium ions replace sodium ions in the polymer, as each calcium ion can attach to the two polymer strands. This process is called cross-linking, which makes the shell of the bubbles firmer and consequently makes them more stabilised (Ahmad, Stride, & Edirisinghe, 2012). From the experiments performed in this thesis it was found that alginate microbubbles collected in calcium chloride solution remained stable for nine hours, compared with alginate microbubbles which were collected in water. The collected microbubbles in water were stable for only 45 minutes.

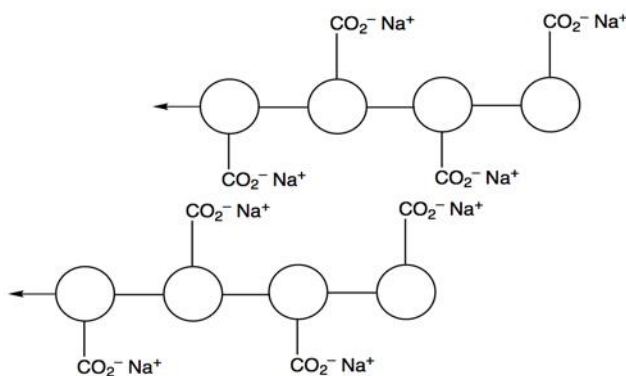


**Figure 45: Cross-linking process.**

*The figure shows the principle underlying molecular interaction during the cross-linking and how the bubbles' shell cross-links in calcium chloride.*

Microscope images representing the stability of the microbubbles collected in calcium chloride over time are shown in figure 46. However, bubbles collected in calcium chloride showed promising results with regards to stability in

comparison to bubbles collected in deionised water, as the bubbles' shell became harder after the cross-linking process by calcium chloride.

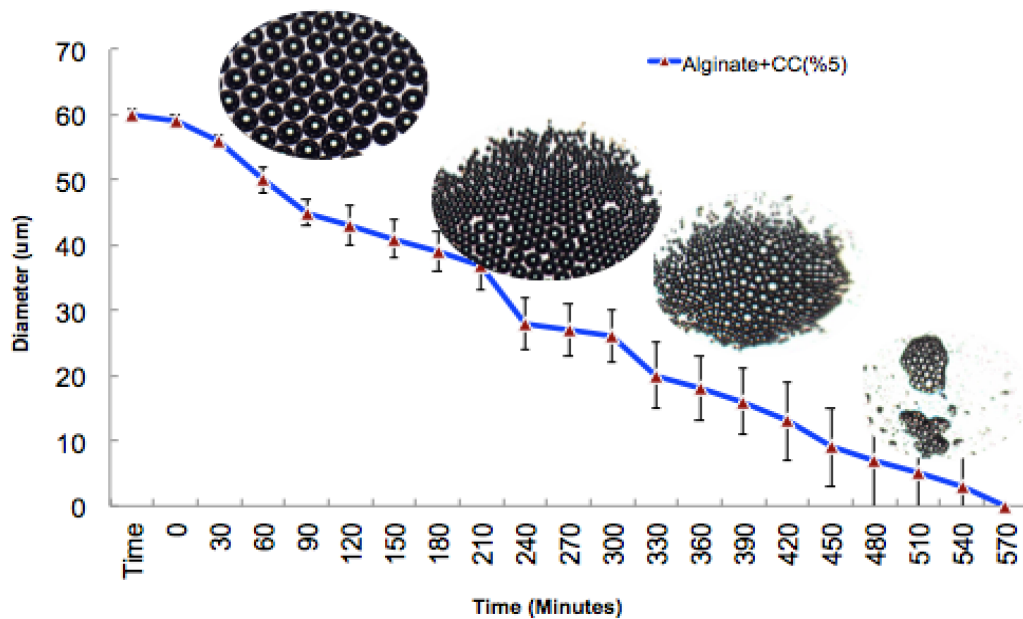


**Figure 46: Cross-linking shell of the bubbles.**

*The graph shows that alginate microbubbles collected in calcium chloride by cross-linking process survived up to nine hours over time. The microbubble images were prepared by optical microscopy.*

#### 4.1.6.3 Collection of alginate microbubbles in glycerol

To make the bubbles stable, in different experiments alginate microbubbles were collected in glycerol. The collected microbubbles in glycerol could survive up to 48 hours. Glycerol reduces surface tension in the bubbles and by minimising interfacial tension it can prevent gas diffusion, which is the cause of bubble shell collapse and burst (Borden & Longo, 2002). Figure 47 shows the optical microscope images from alginate microbubbles collected in glycerol over time. This figure demonstrates that the collection of microbubbles in glycerol increased the lifetime of the alginate microbubbles.

The graph in figure 48 demonstrates that the bubbles were still detectable after 48 hours. This was a longer lifetime compared to the collection in calcium chloride bubbles, which was up to nine hours.

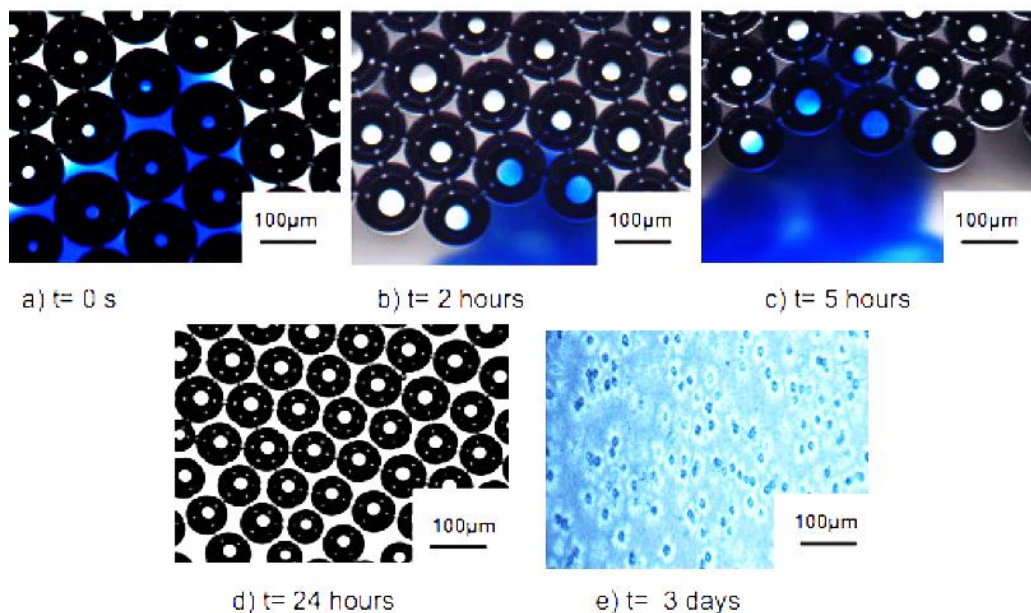


**Figure 47: Alginate microbubbles collected in glycerol.**

*This figure demonstrates optical microscopy images taken over a three-day period. The alteration of the size and the number of the microbubbles collected in glycerol is observed in this experiment. The size and the number of the microbubbles was reduced as time progressed. In three days, nearly all the microbubbles lost their structure and only dried alginate particles were observed on the glass slide. Using glycerol to make the surface molecule chain more packed, led to making the surface stronger and prevented gas diffusion from the bubble core.*

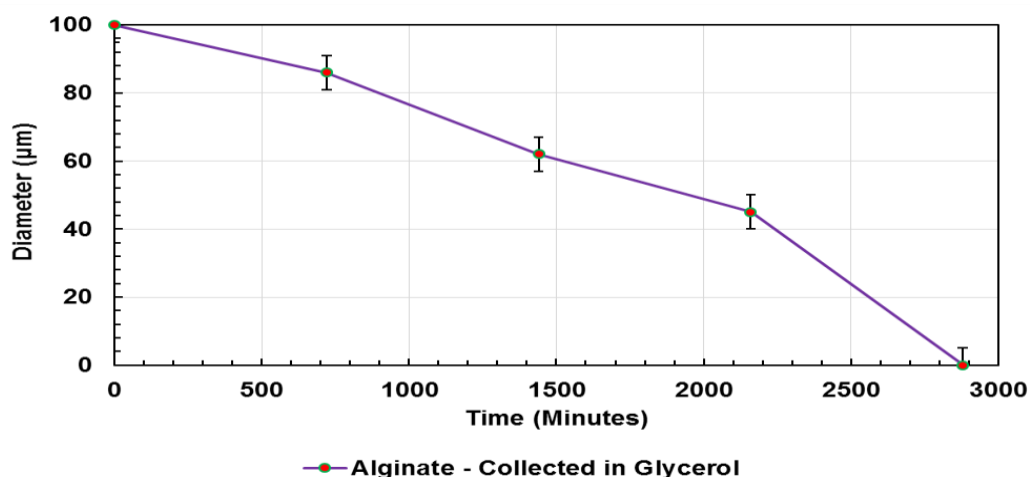


**Figure 48: Microbubbles in glycerol.**

*The alginate microbubbles collected in glycerol could be detectable for 48 hours. The microbubbles' lifetime was increased due to the reduced surface tension by the introduction of glycerol.*

#### **4.1.7 Collection of alginate bubbles in gastric condition**

It is important to examine alginate microbubbles in gastric conditions because the acidic condition of the stomach might accelerate the microbubbles' bursting and disappearance. In fact, it is difficult for the microbubbles to resist the gastric conditions (Borden & Longo, 2002). Therefore, in order to achieve an accurate treatment (which improves therapeutic performance) it is important to produce stable microbubbles in the acidic condition of the stomach (Szíjjártó et al., 2012). To study alginate microbubbles in gastric condition, the microbubbles were collected in hydrochloric acid, which had a comparable pH to that of the stomach (around 2–3 pH) in this study. Figure 49 shows the method of microbubbles collection in hydrochloric acid and figure 50 shows that these bubbles could be detected up to six hours later.

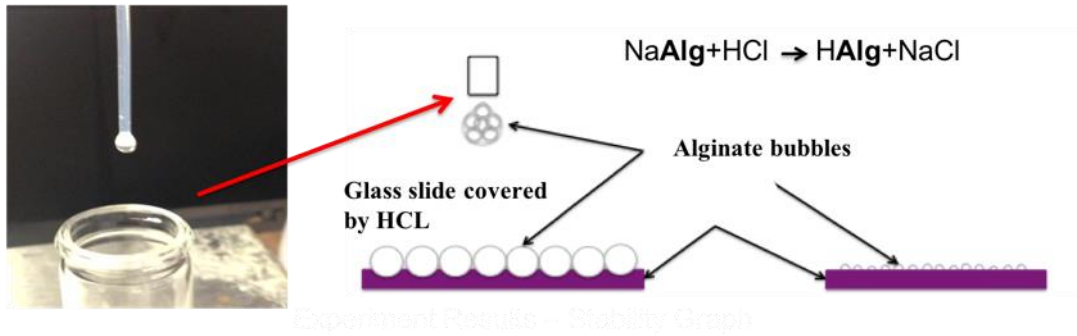


**Figure 49: Collection of alginate microbubbles in hydrochloric acid.**

*Alginat microbubbles, prepared by microfluidic V-junction, and collected in hydrochloride acid on glass slide. The glass slides were covered by HCl, followed by collection of microbubbles on the glass slides. The chemical reaction between the sodium alginat and the hydrochloric acid is shown here.*

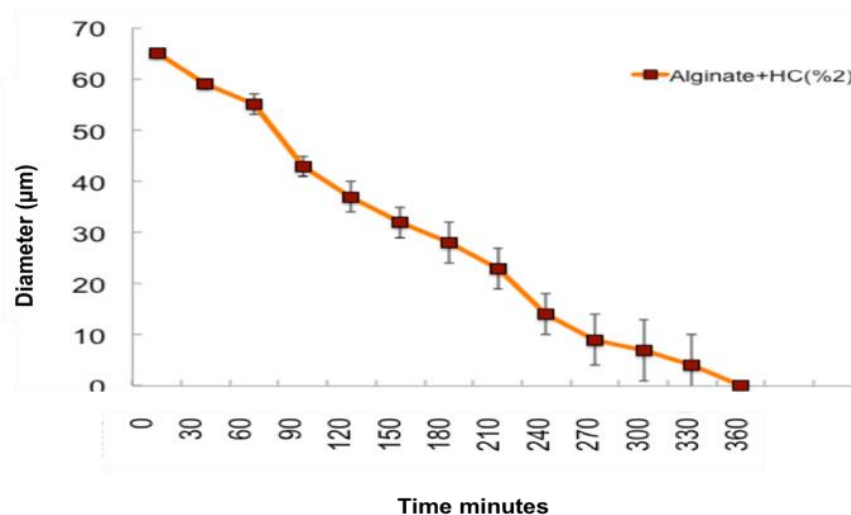


**Figure 50: The lifetime of the microbubbles collected in gastric condition.**

*This graph represents the alteration in the diameter of the microbubbles collected in gastric acid condition over time. The Y-axis and X-axis represent the diameter of the microbubbles (micrometres) and the time from the collection (minutes) respectively. The bubbles could be detected up to six hours later.*

#### **4.1.7.1 Introduction to effect of temperature**

In the current section the effect of temperature on the stability of alginate microbubbles was investigated. Alginate microbubbles are air bubbles covered with alginate shell; this shell is comprised of alginate molecules that are non-covalently linked (Azmin et al., 2012).

The results of these experiments showed that the number of microbubbles started to decrease and the average size of the diameter started to increase at higher temperature. The stability of microbubbles is considered to be highly associated with the shell structure, providing a barrier to gas exchange. For instance, Guiot et al. (Guiot et al., 2006) reported an increase in the mean bubble diameter with increasing temperature and a decrease in bubble concentration. They suggested that changes in the surface tension and shell elasticity with increasing temperature contribute to bubble expansion through the admission of gas molecules from the surrounding liquid. Rising temperature changes the physical properties of the bubble coating, causing reduced stability via mechanisms of gas diffusion and mostly leads to the collapse of the shell.

The destabilization of microbubbles with increasing temperature was attributed to alterations in the microstructure of the shell, which resulted from conformational changes in the hydrophilic polymer chains, as well as weakened van der Waals interactions in the hydrophobic tails of the microbubbles. Mulvana et al. (Mulvana et al., 2010) investigated the effect of temperature on the nonlinear behaviour of Sonovue microbubbles and reported that the majority of bubbles at room temperature oscillated

approximately spherically, while the same-sized bubbles at body temperature oscillated more violently, leading to nonspherical expansion, shell fragmentation and gas expulsion, ending up with complete bubble destruction.

#### **4.1.7.2 Effect of temperature on microbubble stability**

In the present work, the aim was to elucidate the underlying phenomena taking place in the shell structure with increasing temperature so that the design of microbubbles with improved stability can be achieved. For this purpose, a parametric study was carried out on the alginate-based microbubble stability at temperatures ranging from 20 °C to 37 °C.

A mixture of sodium alginate and PEG40 was dissolved in deionised water. The solution was kept in a sonicator water bath tank at room temperature overnight to obtain homogenous solution. Alginate bubbles were produced by microfluidic V-junction, collected on the glass slide and placed on the hot-stage at constant temperature. One droplet of the bubble samples was taken intermittently from the tubes to estimate the size and concentration. Images of microbubbles were captured using a hot-stage microscopy using a Leica DM 2700 M microscope (Leica Microsystems, Wetzlar, Germany). This microscope was equipped with an Infinity2 digital camera (Lumenera Corporation, Ottawa, Canada). This system was used to observe the microbubble bursting process at higher temperature. A heating stage unit was controlled by a FP90 central processor unit, both from Mettler-Toledo Ltd, Leicester, UK. Microbubbles were examined under two different

temperatures: 20 °C and 37 °C. Time-lapse images were acquired using a high-resolution CCD camera and analysed by ImageJ software (Figure 51).

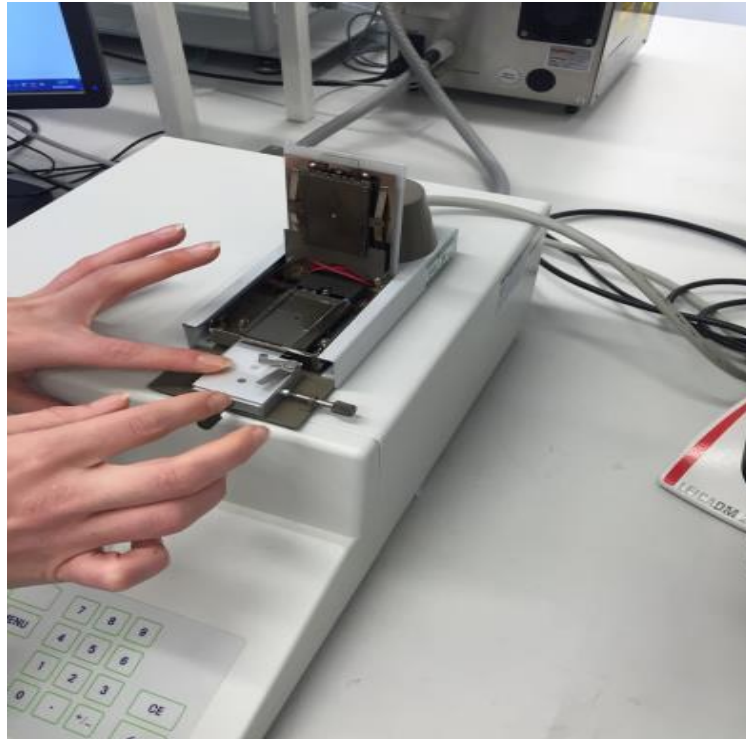


**Figure 51: Hot-stage microscopy.**

*This figure shows a hot-stage microscope which is used to observe the samples under various temperatures.*

The optical images of the bubbles were acquired at intervals of 30 minutes over a period of six hours at 20 °C and 37 °C and it was shown that microbubbles at 37 °C have a tendency to exhibit increased rates of dissolution compared to those at 20 °C.

The results showed that microbubble size and concentration changed by increasing the temperature. Figure 52 shows that at 37 °C the mean bubble diameter decreased after an initial and temporary size-increase (compare to

bubbles at 20 °C) indicating the adverse impact of temperature rise on bubble lifetime.

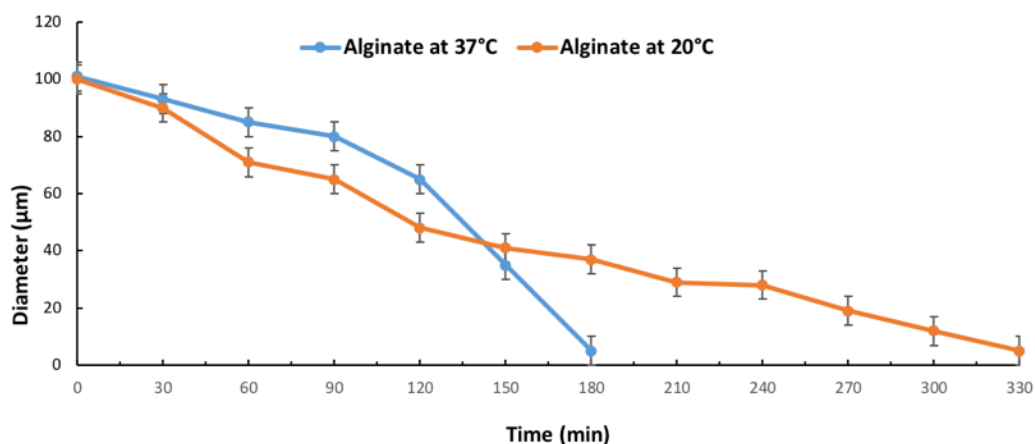


**Figure 52: Effect of temperature.**

*The Y and X axes represent the bubble diameter (micrometers) and the time (minutes) respectively. The blue and the orange lines represent 37 and 20 °C respectively. The graph indicates that temperature rise was associated with the reduced lifetime of the alginate bubbles.*

In conclusion, this result showed that by increasing temperature the size and concentration of the microbubbles changed simultaneously, resulting in the decreased number of bubbles.

The observed changes in the size and number of microbubbles were attributed to the dilation of the microbubble shell, not only resulting from weakened van der Waals forces between hydrocarbon tails but also conformational changes in the PEG chains at increasing temperatures. Transformation of the polymer chains from an extended phase to a collapsed form with increasing temperatures indicated diminished hydrophilicity of the PEG chain, and a suppressed amphiphilic character of the molecules to orient and self-assemble at the gas-liquid interface.

## **4.2 Mucoadhesive study**

### **4.2.1 Introduction to mucoadhesive test**

This part of the study examines the feasibility of oesophageal adhesive drug delivery using the model which is based on alginate microbubbles delivering rhodamine B (Fluorescent dye).

The oral route is one of the preferred methods of drug delivery for various pathological conditions. However, due to short gastric retention time, this approach faces challenges such as incomplete drug release. In order to overcome the aforementioned issue, the application of a bioadhesive drug delivery system using alginate microbubbles is proposed in the current study. This method has a potential application in the treatment of gastro-oesophageal reflux disease and oesophageal cancer. Fluorescent dye (rhodamine B) was used as a model drug in alginate solution with the aim of detecting the structural features of the microbubbles and to track them during the drug delivery on oesophageal porcine tissue.

In this part of the work, a novel approach to produce microbubbles from polymers with inherent mucoadhesive properties was applied. The generated microbubbles were characterised for determination of their morphology and size distribution. Furthermore, they were assessed for mucoadhesive performance and then the candidates with the best prospects were selected for drug loading. The drug-loaded bubbles were examined for drug release and mucoadhesive performance.

In conclusion, this work has demonstrated the possibility of generating drug-

loaded bubbles as potential constructs for developing oral dosage forms. Furthermore, a new approach to quantify mucoadhesion between bubbles and mucosa using confocal imaging method was developed, with an outcome correlating favourably with those from established methodologies.

For oral drug delivery there are different controlled methods that have been designed to overcome the unpredictable difficulties caused by gastric emptying time. Indeed, gastric retention has received significant interest in the past few decades, as most of the conventional oral delivery systems have shown some limitations related to fast gastric emptying time and GRT. Fast GRT leads to a lower bioavailability and incomplete release of drug, which may in turn lead to a reduced efficacy of the administered dosage.

The current study was performed in this context to investigate the potential use of alginate microbubbles as bioadhesive agents to support oral drug delivery. This study has a particular interest in evaluating the possibility of using a mucoadhesive coating agent to develop a method for assessing the absorption of coated dye particles into the oesophagus tissue sample. The main purpose of examining the bioadhesive system here is to offer the prospect of local drug delivery to the oesophageal area.

The geometry and angle position of the oesophagus in the gastric system makes this area difficult to access for drug delivery. Therefore, the main focus here is to characterise the bubble formation process by microfluidic techniques to develop a novel drug delivery system with bioadhesive ability. Upon consumption, lightweight air-filled alginate microbubbles may attach to the oesophageal system. This forms the main idea for the proposed

approach, as this approach is expected to help the drug to be released and become effective within a specific area of the body within a particular time frame. In fact, the alginate microbubbles attach to mucosal surface and the bubble-bursting process results in drug releasing within the region of a specific target, leading to improved drug delivery.

#### **4.2.2 Microbubble preparation for the mucoadhesive test**

A comparative study was performed, using suspensions of the alginate microbubbles within rhodamine B 0.005 %w/v, and also suspension of the same amount of alginate (without microbubbles) with the same concentration of rhodamine B.

To obtain monodisperse alginate microbubbles within the fluorescent dye in the shell, a microfluidic V-junction setup was used (Figure 53) to generate alginate bubbles. To create bubbles with the dye in the shell structure, a suspension fluorescent dye was mixed within the bubble shell at the intersection zone of the V-junction. A coated microbubble sample was collected and stored in the glass vial for the bioadhesive test.

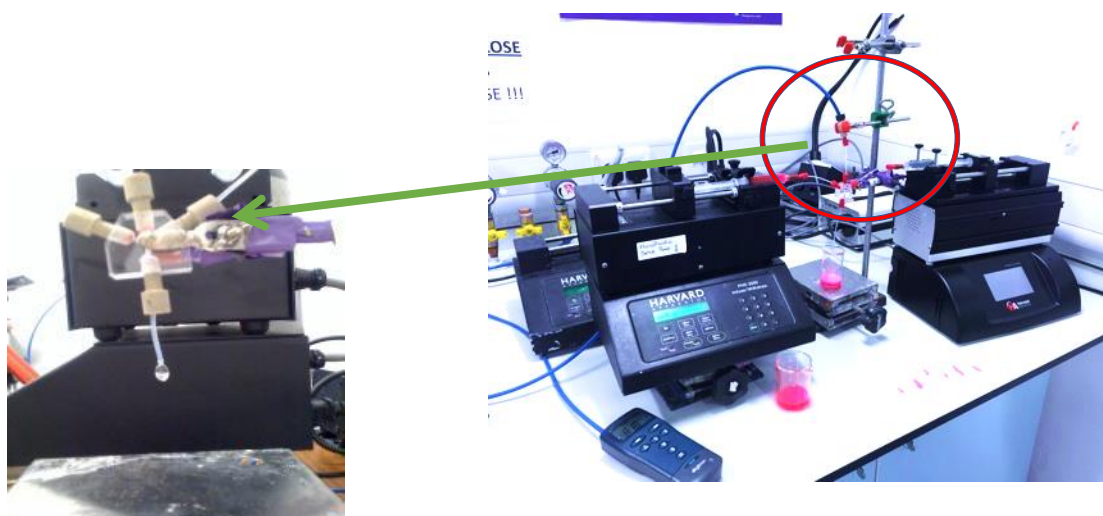
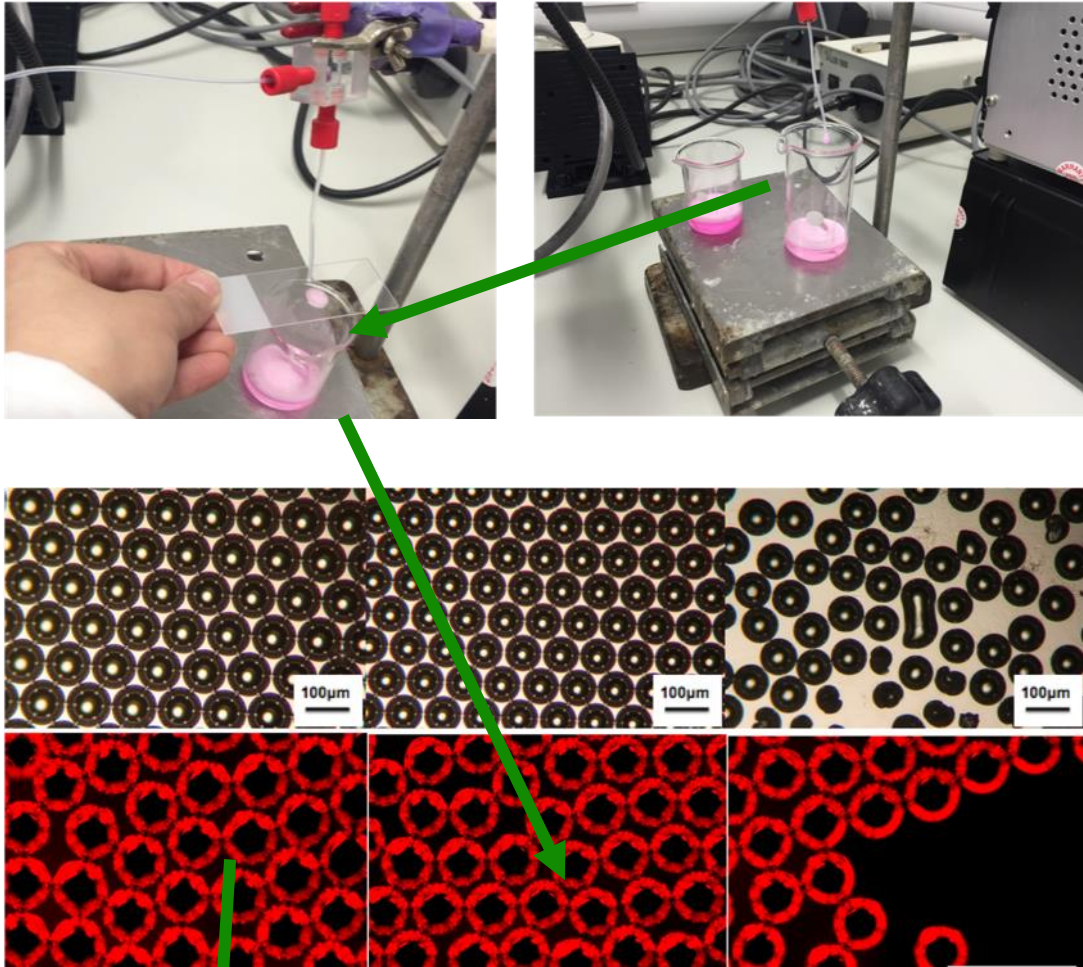


**Figure 53: Fluorescent dye encapsulation.**

*This figure demonstrates the preparation of alginate microbubbles loaded with the fluorescent dye (the pink colour in the glass container is rhodamine B). The green arrow points to the magnified picture of the V-junction.*

#### **4.2.3 Incorporation of rhodamine B**

Rhodamin B was added to the bubble-coating material to detect the structural feature of the alginate microbubbles and to track them in future drug delivery studies. Fluorescent microscopy imaging confirmed the presence of dye in the shell (Figure 54). Rhodamin B was dissolved in water and was added through one of the side inlets; the alginate was added through the other side inlet. The alginate and the rhodamine B suspension meet at the intersection zone of the junction, where the alginate and rhodamine B form the microbubbles with rhodamine B that is incorporated into the shell.



## Fluorescent dye (rhodamine B)

**Figure 54: Fluorescent microscopy imaging study.**

*The collection of the microbubbles with rhodamine B is shown on the top row. The figure on the top left shows the collection of the microbubbles on the glass slide for optical microscopy and the one on the top right presents the collection of the microbubbles in a glass container for applying to the porcine oesophageal tissue. The figures in the middle are optical microscopy of the microbubbles over time (from left to right). Fluorescent microscopy imaging indicates the presence of fluorescent dye in the shell of the bubbles (bottom figures).*

#### 4.2.4 *In situ* studies

Porcine oesophageal tissue was used as the tissue model for delivering the drugs. The fresh tissue was collected from an abattoir and kept frozen at  $-24^{\circ}\text{C}$  in the freezer. The day before the experiment, the tissue was removed from the freezer and was allowed to thaw overnight in the fridge.

The next day the tissue was removed from the fridge, cut to an appropriate size of 8 cm lengths and orientated onto section holders for positioning within the groove, as shown in figure 55.

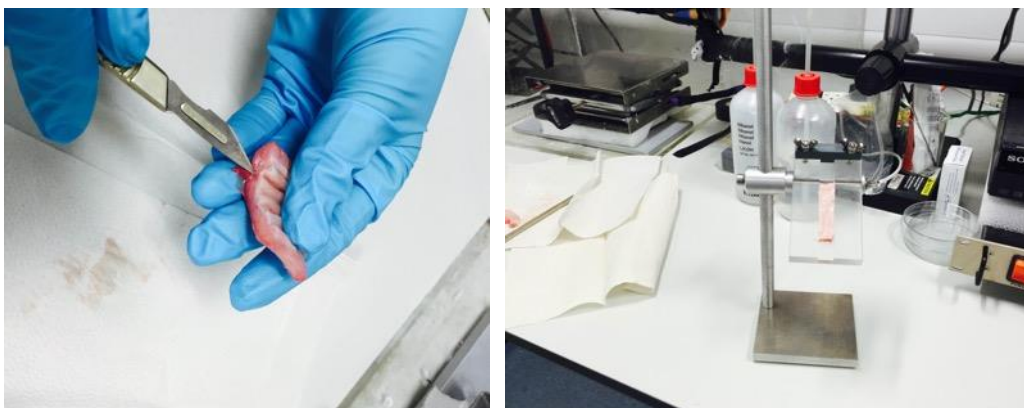


**Figure 55: Tissue preparation.**

*This figure shows tissue preparation (Left) from porcine oesophagus and its fixation on the apparatus (Right).*

This comparative test was performed under two conditions. In the first condition, alginate bubble solution with the dye (rhodamine B) in the shell was applied to measure the absorption into the oesophagus tissue. In the second condition, the same concentration of the dye suspension mixed with alginates solution (no bubbles) were applied at a specified rate to oesophageal tissue under the same experimental conditions. The tissue sample was fixed to an

apparatus to mimic the angle and position of the oesophagus (Figure 56). The syringe containing the bubble solution was fixed to a pump (Harvard, PHD 4400) to control the flow rate of the microbubble solution and also the flow rate of the rhodamine B, at the rate of 500  $\mu\text{l}/\text{min}$ . Applied materials were collected from the porcine tissue at the bottom of the apparatus in a glass container for dye measurement studies. Once the first applying material (alginate microbubbles with dye) was finished, the second experiment consisting of the same concentration of the dye suspension with alginate (no bubbles) was applied with the same method. Both tissue samples on the day of the experiment were analysed by confocal imaging system method.



**Figure 56: Bioadhesive test study.**

*The vitro mucoadhesive test is shown in this figure. Alginate solution (with or without microbubbles) with the dye in the shell was applied to the animal tissue surface. The applied alginate solution which slipped over the tissue was collected in the glass container (pointed to by the green arrow).*

#### 4.2.5 Confocal imaging studies

The tissue samples from both experiments were compared using the confocal imaging microscopy to show the absorption of fluorescent dye into the porcine oesophageal tissue, as shown in figure 57. Confocal imaging analysis confirmed that alginate microbubbles with dye helped to increase the tissue absorption of the dye. Comparing the images from the two experiments showed a different colour intensity. The higher intensity of the colour means more absorption of the dye. This data showed that there was a higher absorption of the rhodamine B into the tissue when delivered using microbubbles. This confirms that adhesive alginate microbubble is able to support the dye particles' delivery and its application can increase the absorption of the dye into the targeted tissue.

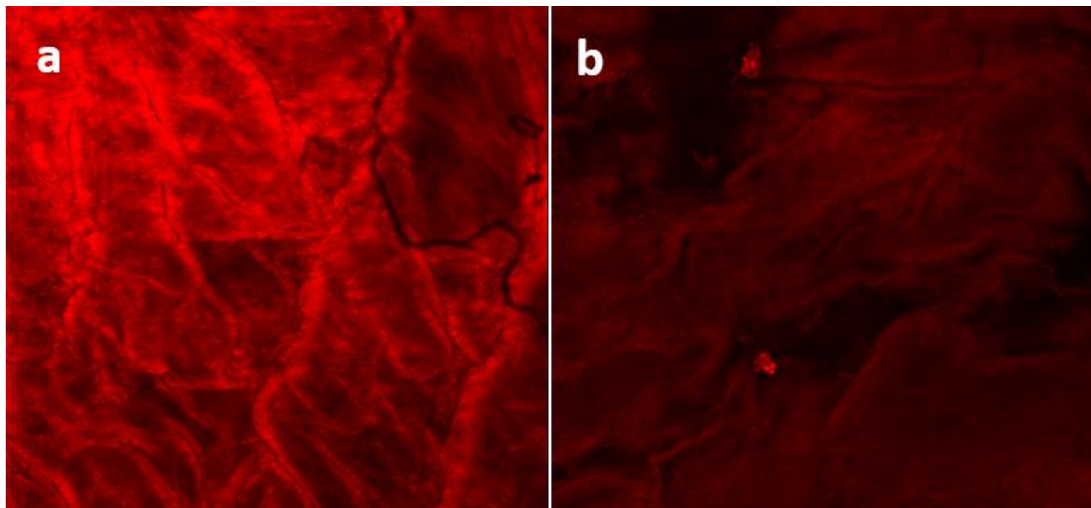


**Figure 57: Confocal imaging study.**

*The image on the left (a) illustrates the confocal imaging microscopy from the oesophageal porcine tissue with the applied alginate microbubbles containing dye in their shell. The image on the right (b) illustrates the confocal imaging microscopy from the oesophageal porcine tissue treated with the applied dye suspension mixed with alginate (no bubbles).*

#### 4.2.6 Calibration curve and calculation for UV analysis

The second approach for measurement of absorbed dye into the tissue was through measuring the non-absorbed dye and subtracting it from the starting solution. This was achieved by collecting the unabsorbed solutions from both experiments and measuring their dye content. The measurement of the dye in the collected solution was achieved using UV studies. The principle of dye measurement using UV is to correlate the UV absorption of the solution with the dye concentration. This correlation was achieved through a calibration curve. The calibration curve was established using known concentrations of the rhodamine B dye and measuring the associated UV absorption (Figure 58). Following the establishment of the calibration curve, the UV absorption of the collected dye from tissue was applied to the formula from the calibration curve to calculate the concentration of the dye in the collected solution.

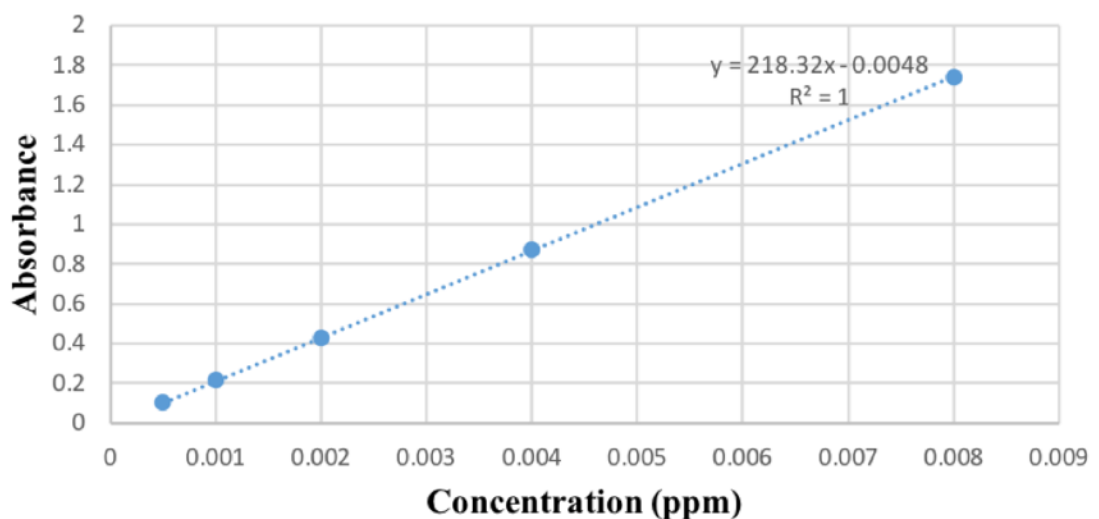


**Figure 58: Calibration curve of rhodamine B in SBF solution.**

*Calibration curve and equation used to calculate the amount of rhodamine B in alginate solution.*

#### 4.2.6.1 UV analysis of dye content within the animal tissue sample

The rhodamine B content within the bubbles was determined following the standard assay procedure of dissolution in water for detection by UV at 558 nm (NCBI, 2004). 5 ml of bubble solution and suspension which have 0.02 g dye in the solution were applied on both the actual tissue and artificial membrane surface. Applied material was collected from each sample. All samples were dissolved in 25 ml water and analysed spectrophotometrically at 558 nm using a Jenway 6305 UV/Visible spectrophotometer (Bibby Scientific, Staffordshire, UK).

The absorbance of the solutions with known concentration was taken at 558 nm ( $\lambda_{\text{max}}$  of dye) to obtain a calibration curve (Figure 58) from which the dye contents of the bubbles could be quantified. Using the equation of the calibration curve,  $y = 218.32x + 0.0048$ , concentrations ( $x$ ) from absorbance readings ( $y$ ) were obtained by the equation:

$$(\text{Absorbance} - 0.0048) \div 218.32$$

##### *Calculation example*

5 ml of sample was applied to the testing tissue. The collected material was diluted with water by bringing the volume to 25 ml; the absorbance was recorded as 0.374 when measured at 558 nm. Then using the calibration curve equation, which is  $[(\text{Absorbance} - 0.0048) \div 218.32]$ , the dye concentration in the diluted collected solution was calculated. The calculated

concentration was multiplied by the dilution factor to obtain the real concentration of the dye in the collected solution.

Therefore, the dye in the collected material was equal to  $(0.374 - 0.0048) \div 218.32 = 0.001735 \times 25 \text{ ml} = 0.0434 \text{ mg}$ .

The same experiment was done using artificial tissue membrane with mucoadhesive properties, to support the experiment done using actual tissue sample. The results obtained from the *in-situ* studies show that the remaining solution collected from the first condition (Table 2) had lower absorption compared to the second condition of no-bubble sample. Table 3 shows the results from the same experiment but with the artificial tissue. This also indicates that more dye was absorbed into the surface of the oesophagus tissue using microbubbles due to the higher adhesive characteristic of the alginate bubbles.

<b>Dye measurement animal tissue</b>	<b>Concentration of the dye in initial material</b>	<b>Concentration of the collected dye</b>	<b>Concentration of the absorbed dye in the tissue</b>
<b>Applied alginate microbubbles</b>	<b>2.500 ± 0.002 mg/ml</b>	<b>0.127 ± 0.002 mg/ml</b>	<b>2.373 ± 0.002 mg/ml</b>
<b>Applied alginate solution</b>	<b>2.500 ± 0.001mg/ml</b>	<b>0.134 ± 0.001mg/ml</b>	<b>2.366 ± 0.001mg/ml</b>

**Table 2: Dye measurement in actual animal tissue.**

*This table presents the calculation of the animal tissue dye absorption using alginate microbubble solution and alginate suspension using UV analysis.*

Dye measurement artificial tissue	Concentration of the dye in initial material	Concentration of the collected dye	Concentration of the absorbed dye in the sample
Applied alginate microbubbles	2.500 ± 0.002 mg/ml	0.110 ± 0.002 mg/ml	2.390 ± 0.002 mg/ml
Applied alginate solution	2.500 ± 0.001 mg/ml	0.128 ± 0.001 mg/ml	2.372 ± 0.001 mg/ml

**Table 3: Dye measurement in artificial tissue membrane.**

*The table presents the calculation of the artificial tissue dye absorption using alginate microbubble solution and alginate suspension using UV analysis.*

### 4.3 Discussion

In this section, the application of microbubbles as a tool for oral drug delivery to oesophageal tissue was investigated. This shows the application of microbubbles for oral delivery of drugs. This investigation started with optimisation of the methodology for production of the microbubbles. A microfluidic V-junction device was used for production because of the previous successful experience of using this device for the microbubble generation, leading to the production of more homogeneous microbubbles (Parhizkar, Stride, & Edirisinghe, 2014). The materials which were used for production of microbubbles was alginate because it is a natural substance which is not toxic to human cells and is the preferred method for medical applications (Elsayed, Huang, & Edirisinghe, 2015). The size of the microbubbles is of pharmacokinetic significance because it influences the

efficient delivery of the drugs (Wang et al., 2013). Therefore, it is important to know the influencing factors on the size of the microbubbles during the production. These parameters affect the physical mechanism of bubble formation during the microfluidic process. The results of the bubble formation process indicate that the balance between the air and the liquid flow were key factors in the production of microbubbles. Properties such as viscosity, density and surface tension, along with geometry of the device, are important parameters that influence the bubble formation process (Parhizkar, Stride, & Edirisinghe, 2014). Geometric features of the device, such as the diameter of the capillary, were influential factors affecting the size of the bubbles. Microbubble diameter ( $D_b$ ) is a function of:  $D_b = f(\mu_g, \mu_l, Q_g, Q_l, \sigma_l, \rho_l, L_{gap}, D)$ , where  $\mu_g$  and  $\mu_l$  are the respective gas and liquid viscosities,  $Q_l$  and  $Q_g$  are the respective liquid and gas flow rates, while  $\sigma_l$  and  $\rho_l$  denote liquid surface tension and density respectively.  $L_{gap}$  is the gap and  $D$  is the interior diameter of the capillary. There is a linear relationship between the diameter of the produced bubbles and capillary diameter. However, as the gap ( $L_{gap}$ ) increases, higher gas pressure is needed in order to generate microbubbles (Sirsi & Borden, 2009). The results from this work confirmed the significance of the gas pressure, liquid flow rate and capillary size on the size of the generated microbubbles and established how the size could be controlled during the production. The results from this work confirmed that higher gas pressure or larger capillary size increased the size of the microbubbles, while increased flow rate reduced the size of the microbubbles. The noticeable effect of the bubbling pressure can be attributed to the formation of a longer

bubble/slug at higher pressures, which eventually forms a larger bubble. The significance of control over the size of the bubbles is due to its role during the bursting process of the microbubbles (Parhizkar, Edirisinghe, & Stride, 2013).

The other factor that impacts the dynamics of bubble formation is the applied surfactant. Surfactant influences factors such as the channel surface character (i.e. hydrophilicity of channel walls) and the liquid-solid and liquid-gas interfaces in the microchannel (Parhizkar, Edirisinghe, & Stride, 2015). To choose the appropriate surfactant for the production of the microbubbles, two different types of detergents were investigated which are commonly used as surfactant for the microbubble studies. The comparison between the stability of the microbubbles produced by PEG and Tween showed better stability and duration of the microbubbles generated by PEG. This is due to the fact that this surfactant has a larger hydrophilic chain and therefore the wettability of the channel wall surface is affected in a different manner. The wettability of the channel wall surface consequently influences the dynamic interfacial tension and therefore the bubble formation leading to production of smaller bubbles. As smaller bubbles have been shown to stay for longer duration (Stride & Saffari, 2003), the microbubbles generated using PEG as a surfactant had a higher lifetime. This led to the application of the PEG as surfactant for microbubble generation in this study.

The stability of microbubbles as a drug delivery agent is important from the pharmacokinetics aspect. Various factors have been indicated through various studies to influence the stability of microbubbles. In this work, the role of solid nanoparticle, the type of collection media, pH condition and

temperature on the stability of microbubbles were investigated. Gold nanoparticles were used in this study to stabilise the microbubbles. Gold nanoparticles was chosen because of its favourable outcome in other medical applications, such as in the treatment of rheumatology disorders (Lee et al., 2011). The result showed that the presence of gold nanoparticles in the shell of the microbubbles increased the microbubbles' lifetime and stability. The nanoparticles act as a chain around the shell and give stability to the microbubbles, providing stronger resistance against the external and internal pressures (Mohamedi et al., 2012a). This led to gold nanoparticles being chosen for the preparation of the microbubbles for drug delivery purposes in this work.

The other factor that was investigated as being an influential factor on microbubble stability was the type of collection media. In this work calcium chloride and glycerol were investigated as collection media for the generation of the microbubbles. The reason for choosing these two materials was due to the unique quality of each regarding microbubble structure. Calcium chloride cross-links the alginate molecules on the surface of the bubbles (Ahmad, Stride, & Edirisinghe, 2012) and leads to their increased stability. Glycerol reduces the surface tension on the surface of microbubbles (Borden & Longo, 2002), and as a result the lifetime of the microbubbles increases. The microbubble time study in this work showed that generated microbubbles in glycerol had a longer stability and therefore led to the application of this material for the collection of microbubbles.

The drug delivery by microbubbles can be aimed at various targeted tissues. Specific modifications might be required for optimisation of the delivery, depending on which delivery route is used, and on which organ or tissue is targeted. Additional conditions were tested here because the aim of this project is the delivery of the drugs to the oesophagus. These additional conditions were the pH and temperature. The pH condition was tested because one of the targeted regions in the oesophagus is at the junction with the stomach. To deliver drugs to this section, it is suggested to deliver the microbubbles to the stomach. However, because of the floating character of the bubbles, and also the gastric muscle contractions and movements, the bubbles have a higher chance of hitting the junction and as a result releasing the drug. To mimic a gastric condition, the microbubbles were collected in hydrochloric acid (pH: 2–3). The time analysis showed that the microbubbles in the acidic pH could last up to six hours. This is shorter than when the microbubbles are collected in glycerol (48 hours) and longer compared to when the microbubbles are collected in water (pH: 6.5–8). Acid chemical reaction makes strong bonding between alginate and hydrogen, which results in the formation of more stable bubbles (Vakarelski et al., 2010). This stability was good enough for oral drug delivery purposes as the emptying time for the stomach is two to six hours, which is within the time range for the generated microbubbles as described here. Temperature is known to have an important influence on the stability of the microbubbles (Sagdic, Bolukcu & Kilic, 2015). The result from this work, along with earlier publications (Ahmed & Jameson, 1985), showed higher stability of the microbubbles when tested over time at room temperature compared to 37 °C. The microbubbles'

behaviour at different temperatures may be related to changes that temperature causes in the shell structure (Szekely et al., 2011). Stability variation in the microbubbles due to temperature changes was attributed to alteration in the microstructure of the microbubbles' shell. The main microstructures in the shell which are affected by the temperature are the hydrophilic alginate and PEG chain (Stepniewski et al., 2011). Change in the surface tension and shell elasticity with increasing temperature contributes to the bubble expansion through the admission of gas from surrounding liquid (Kučerka, Nieh, & Katsaras, 2011). This causes a reduction in bubble stability via a mechanism of gas diffusion in the shell (Szíjjártó et al., 2012). The majority of the microbubbles oscillate at a higher level at body temperature compared to room temperature. More violent oscillation results in increased shell fragmentation and destruction (Shen, Longo and Powell, 2008; Garg, Thomas and Borden, 2013).

However, the half-life of the collected microbubbles in the gastric condition and at physiological temperature (37 °C) was 180 minutes in this work, which still made it a suitable method for oral drug delivery.

The aim of this part of the project was to develop an oral drug delivery method to the oesophagus using adhesive alginate microbubbles. Therefore, the absorption of the drug delivered by microbubbles was investigated in this study. Oesophagus tissue was obtained from porcine. A condition similar to the physiological condition regarding the angle and position of the oesophagus was developed using an apparatus which mimicked the slope of the oesophagus. The absorption of the drug rhodamine B in this experiment

was measured using two different approaches. One is a direct method by observation of the absorbed dye into the tissue using confocal microscopy. The other method (UV study) is an indirect approach which measures the dye concentration in the collected liquid following exposure to the tissue. The results from these experiments showed that alginate microbubbles, prepared by microfluidic V-junction with fluorescent dye in the shell, could adhere to oesophageal tissue. Microbubbles adhesion helps to increase the absorption of fluorescent dye in the targeted region. This study demonstrated that alginate microbubbles suspension can have an application as a bioadhesive agent for localisation within the oesophageal tissue to improve drug delivery. Microbubble drug delivery to oesophageal tissue for treatment of malignancies can be applied, based on the results from this study.

The proposed drug delivery system using alginate bubbles will take advantage of both the mucoadhesive and floatable systems. Some of the alginate bubbles after administration will attach to the oesophageal surface, leading to increased drug absorption, and the remaining bubbles will enter the stomach where they remain floatable. Gastric waves make the floatable bubbles hit the gastroesophageal region, which in turn increases the contact of the delivering drugs to the mucosal surface of the gastroesophageal region (Figure 59).

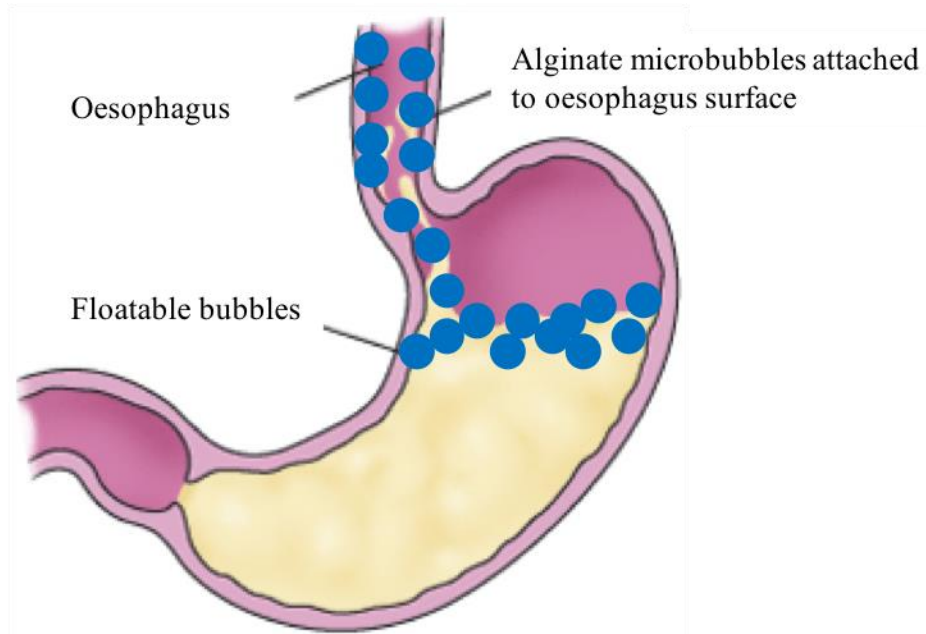


**Figure 59: Alginate microbubbles attached to mucosa.**

*This figure shows the mucoadhesive and floating model of drug delivery to the gastroesophageal region using microbubbles.*

## Chapter 5

# Drug resistance investigations in leukaemia using microbubbles

### 5.1 Introduction

Drug discovery for cancer is amongst the most popular types of research in medicine. Some of these drug discovery investigations are done to identify potential therapeutic targets in relapse or drug resistance following primary response to chemotherapy. One type of leukaemia which has been studied extensively for relapse or drug resistance is CML.

CML is a haematopoietic stem cell malignancy, driven by BCR-ABL1, an acquired fusion protein. BCR-ABL1 is a constitutively active tyrosine kinase that activates multiple signalling pathways, thereby promoting the expansion of myeloid cells. The recognition that BCR-ABL1 kinase activity is central to CML pathogenesis eventually led to the development of imatinib, a small-molecule adenosine triphosphate (ATP)-competitive TKI (Hochhaus et al., 2009; Fava & Saglio, 2010; Cortes et al., 2011).

Most patients who start imatinib in early-stage disease achieve good responses (Druker et al., 2006). However, it is estimated that approximately 20% to 40% of newly diagnosed patients will eventually require switching to newer second or third generation TKIs because of partial or complete relapse of therapy-resistant disease (Gorre et al., 2001; Baccarani et al., 2006; Lucas et al., 2008; Hochhaus et al., 2009; Fava & Saglio, 2010; Cortes et al., 2011).

Between 30% and 40% of patients who acquire imatinib resistance do so via the acquisition of missense mutations in the *BCR-ABL1* kinase domain (KD) that sterically inhibit TKI binding (Shah et al., 2002; O'Hare et al., 2005; Redaelli et al., 2009). The aberrant signalling pathways responsible for resistance in the patients with no *BCR-ABL1* KD mutations are unknown (de Lavallade et al., 2008; Khorashad et al., 2008).

Similar situations can be observed in other myeloid malignancies such as AML, in which patients may develop resistance to agents targeting other molecular drivers, such as aberration of the *FLT3* gene, via mechanisms that are equally poorly understood (Parmar et al., 2011; Smith et al., 2012).

Many lines of evidence support the presence of persistent low levels of quiescent LSCs as the source of eventual disease relapse. Indeed, even optimally responding CML patients who achieve "molecular remission" continue to harbour a low level of leukaemia, detectable by ultra-sensitive methods or *in vitro* assays. These LSCs reside in the BM niche and survive independent of their tyrosine kinase activity, a feature that protects them against continued TKI therapy. Ongoing research is therefore focused on understanding the signalling pathways responsible for protection and self-renewal of quiescent LSCs. One plausible explanation for the persistence of quiescent LSCs in the presence of targeted therapy is their interaction with the surrounding microenvironment.

The BM microenvironment includes various types of cells and macromolecules which compose the scaffold of the BM niches, and which may confer a protective effect on LSCs. There is *in vitro* evidence that the

interaction of leukaemia cells with an artificial scaffold in 3D culture causes resistance to chemotherapeutic agents (Aljitawi et al., 2014). There is a hypothesis, that the influence of the bone marrow niches causes reduced sensitivity of the LSC cells to the anticancer agents (Aljitawi et al., 2014). However, a realistic culture matrix that accurately mimics the 3D structure of the BM is currently lacking.

Two-dimensional (2D) cell-based assays have long been used for drug discovery in cancer. However, they have limited value in predicting long-term clinical response to anticancer drugs because they do not effectively mimic the 3D nature of the tissue (Johnson et al., 2001; Kunz-Schughart et al., 2004). In particular, absence of the ECM, which plays a crucial role in normal and deregulated cellular homeostasis, is a major limitation of conventional 2D culture (Frantz, Stewart, & Weaver, 2010; Cox & Epler, 2011; Gilkes, Semenza, & Wirtz, 2014). Cells in 2D culture usually lose their ability to differentiate but this characteristic is recovered in 3D. Therefore, ECM-related cellular interactions have significant physiological relevance (Weaver et al., 2002; Baker & Chen, 2012; Friedl et al., 2012; Venugopalan et al., 2014).

To address this experimental limitation, attempts have recently been made to produce 3D culture systems, some of which have shown potential for better simulating the *in vivo* tumour microenvironment (Imamura et al., 2015). Studies on breast cancer cell lines have shown that 3D cultures provide superior *in vivo* simulation of important tumour characteristics, namely hypoxia, dormancy, anti-apoptotic features and their resulting drug resistance

(Kim, Ho, & Wu, 2011; Imamura et al., 2015). To date, however, a reproducible simulation of the BM microenvironment has not been published. The fact that resistant LSCs in CML have been observed *in vivo* but not *in vitro* 2D culture supports the notion that the 3D BM microenvironment might be responsible for the persistence of quiescent LSCs and subsequent emergence of overt TKI resistance. Considering the deficiencies of current 2D cultures (Fang & Eglen, 2017), recent efforts have focused on developing 3D cultures which can mimic the BM microenvironment by accommodating the essential components of the BM (Braccini et al., 2005). Lack of 3D structure and molecular matrix components are potential causes of their unsustainability for long-term HSC culture (Jiang et al., 2006). The development of an *ex vivo* 3D culture, mimicking the BM microenvironment in providing niche-like structures for the HSC to reside and proliferate, provides an opportunity to study haematological malignancies. The main challenge for studying AML cells for therapeutic target discovery purposes has been the difficulty in growing and maintaining these cells in an *in vitro* culture (Bendall et al., 1994). The majority of AML cells usually undergo spontaneous apoptosis and only a subpopulation of the cells proliferate during *in vitro* culture (Stolze et al., 1995). The proliferation and survival of the AML cells increases in the presence of haematopoietic growth factors, co-culture with stromal cells and a 3D environment (Bendall et al., 1994; Aljittawi et al., 2014; Tabe & Konopleva, 2015). It has also been shown that AML cells have reduced sensitivity to chemotherapeutic agents in 3D cultures (Bhatia et al., 2003).

Insufficient information on molecular interaction between the AML stem cells (SCs) and their microenvironment might be the main reason for the failure of the current therapeutic approaches (Karimpoor et al., 2017). The new approaches should be focused on selectively inhibiting LSCs by disrupting the interaction between them and their niche environment, but at the same time preserving the normal haematopoiesis. Long-term low-level *BCR-ABL1* oncogene detection by sensitive PCR techniques in CML patients who achieve major molecular response to tyrosine kinase inhibitors is believed to be due to the survival of LSCs in the BM niches, in spite of the inhibition of BCR-ABL1 kinase (Bhatia et al., 2003).

A 3D culture mimicking the BM microenvironment provides a model through which the mechanism of LSC maintenance can be explored, and this facilitates the investigations in developing drugs targeting the survival pathways activated by such interactions. Various 3D cultures have been developed so far for studying leukaemia cells. I have already developed PMMA-HA fibre-based scaffold to show the influence of 3D culture on the reduced sensitivity of leukaemia cells to the tested antileukaemia agents (Karimpoor et al., 2017; Medyouf, 2017; Pollyea & Jordan, 2017). The PMMA-HA scaffold provides a 3D structure by having HA to simulate some characteristics of the bone. However, it lacks the spongy structure of the BM. To develop a scaffold with pores similar to bone lacuna, a foam-based scaffold with spongy structure was developed using alginate biomaterial. Microbubble technology was applied to produce a foam with the expected size of the pores. This foam-based 3D culture supported the growth of both leukaemia and normal haematopoietic cells and promoted cell differentiation

similar to *in vivo* condition. This system reduced the sensitivity of the leukaemia cells to antileukaemia agents. Due to simulating the physiological condition, our foam-based scaffold can be used for drug sensitivity studies of the primary leukaemia cells.

## 5.2 The aims of this chapter

- 1) Development of a foam-based scaffold using microfluidic process.
- 2) Investigating the impact of alginate foam-based scaffold on differentiation of normal haematopoietic cells and also AML stem/progenitor cells.
- 3) Measuring the leukaemia cells' response to antileukaemia agents in alginate foam-based 3D culture in comparison to 2D cultures.

The aims of this section are summarised in the following diagram.

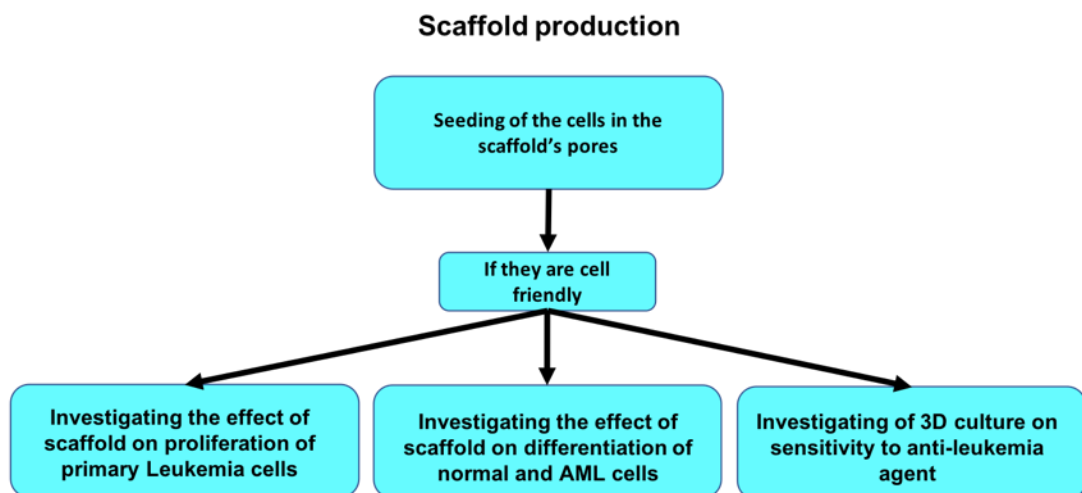


**Figure 60: Chapter 5 structure.**

The main aims of chapter 5 are summarised in this figure. As it is shown here, the final goal is to develop a 3D culture for investigating the drug sensitivity of leukaemia cells. To achieve this aim, foam-based scaffolds were

developed and their influence on the phenotype of the normal and leukaemia cells was investigated.

### **5.3 Characterisation of materials and solutions**

In the process of microbubble production using a microfluidic technique, parameters such as gas pressure, liquid flow rate and viscosity have a significant influence on the diameter size of the bubbles and their formation in the V-junction device. Monodisperse microbubbles with average diameter 150  $\mu\text{m}$  were obtained at gas pressure of 95-120 kPa and a flow rate of 200-250  $\mu\text{l}/\text{min}$ . In this study, to improve the stability of alginate microbubbles, they were collected in 2% wt. calcium chloride solution to cross-link the bubbles' shell. This made the shell stronger, and as a result the bubbles lasted longer and allowed time for the foam structure to evolve (Figure 61).

Physical properties such as viscosity and surface tension have a significant impact on the bubble formation process. In the current study, the surface tension of alginate-PEG liquid was measured to be 49 mN/m, using a Kruss Tensiometer (Model-K9, Kruss GmbH, Germany). The viscosity was measured to be 20 mPa s, using a Brookfield DV-11 Ultra programmable Rheometer (Brookfield Engineering Laboratory Inc., Middleboro, MA, USA). To obtain accurate results different measurements were performed at ambient temperature (22 °C) and the average of seven readings was taken to ensure accuracy.

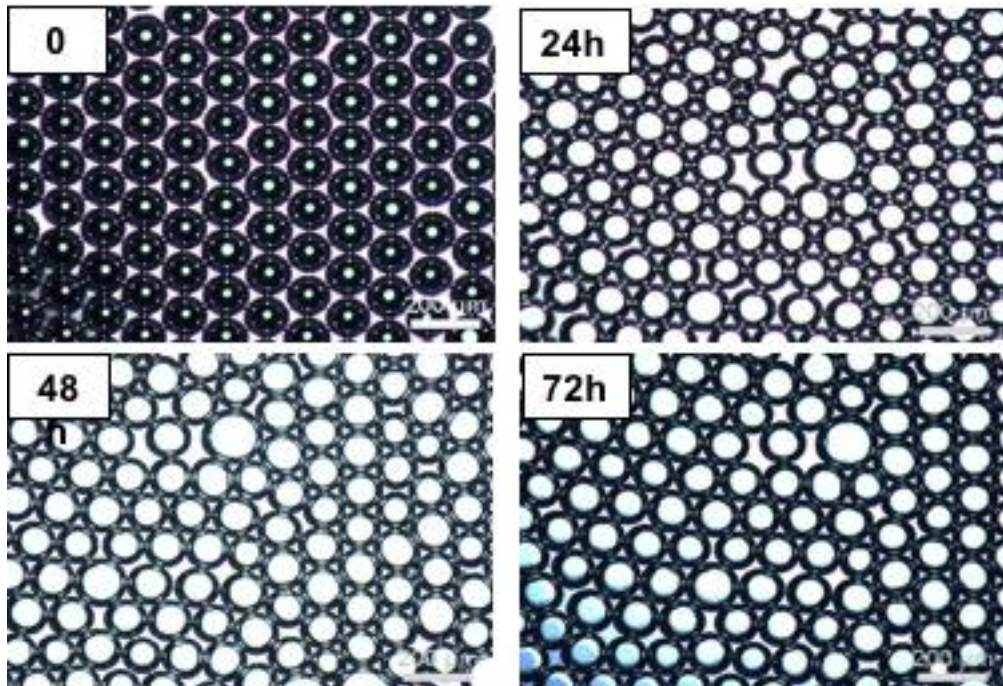


**Figure 61: Optical micrograph of the alginate microbubbles generated by a microfluidic device.**

*The image illustrates an optical micrograph of the alginate microbubbles generated by microfluidic, collected in calcium chloride to cross-link the shell of the bubbles and make them more stable. The image shows their changes during time-lapse, immediately after collection (zero time) and within the next 72 hours. Alginate microbubbles dried to porous foam shape structure, as shown at 72 hours.*

#### **5.4 Foam-based scaffold**

Foams are metastable inclusions of gas in a fluid phase and are frequently used in the food industry and biomedical applications. In this study, solid foam structures with high porosity were successfully prepared by cross-linking the alginate microbubbles (Figure 62). The foam scaffold was dried after ten days of incubation in a desiccator. Foam scaffolds typically show a spongy-porous like structure with pore size ranging between 20 and 200 $\mu\text{m}$  (Figure 63).

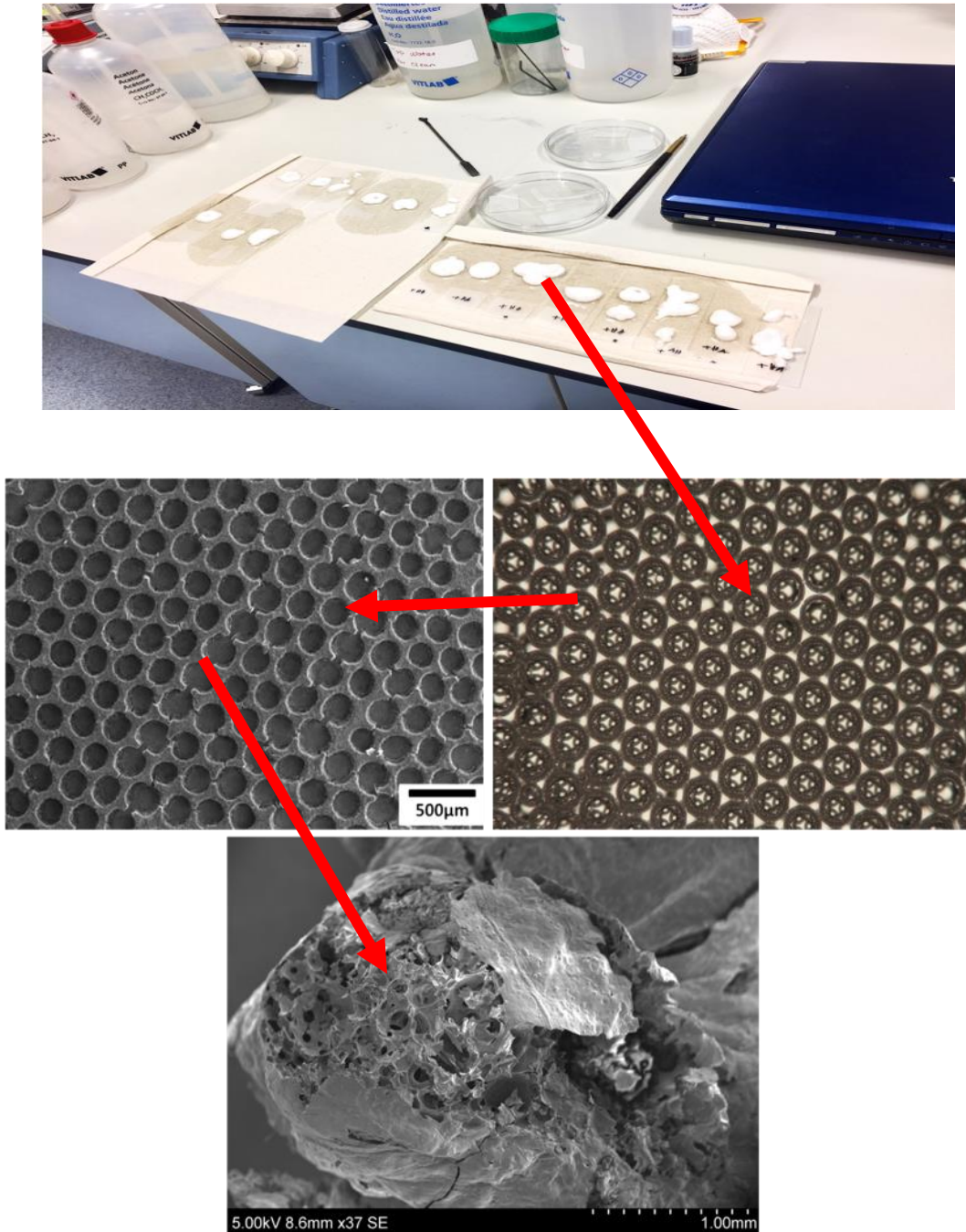


**Figure 62: Scaffold production process.**

*The photo on the top row shows the prepared foam from microbubbles, following cross-link, but before transferring to the desiccator. The right-hand image in the middle row is the optical microscopy from the alginate foams. The left-hand image shows dried foam bubble scaffold on the glass slide. The bottom image indicates a SEM image of a cross section of foam-based scaffold.*

## 5.5 Bioactivity and biocompatibility of scaffold

To allow the cell growth and support the biocompatibility features, it is critical that the scaffolds have high porosity and that bioactive nanoparticles are incorporated in them. HA is the main inorganic component of bone material and is widely used in various biomedical applications due to its excellent bioactivity and biocompatibility. In this study, to support cell compatibility, HA nanoparticles (diameter < 200 nm, 5% wt.) were added to the scaffold structure (Phipps et al., 2011).

This was achieved by adding the HA to the alginate solution prior to forming bubbles using the V-junction. We observed settlement of K562 and primary AML cells in the microcavities of the scaffold, which is an evidence for the biocompatibility of the prepared foams (Figure 64). The cells were concentrated in the microcavities and around the scaffolds, indicating the attraction of this scaffold to the leukaemia cells.

Bioactivity test has been done by adding the AML and K562 cells into in the well plates containing the foam scaffold and then putting the samples in the incubator for three days. A certain number of the cells were added to the wells, and in the first day of the experiment images were taken from the samples using an optical microscope After three days, images were taken from the samples again. The result from the images indicates that the microcavities have accommodated the K562-AML cells and provided a space and environment for both cells types to grow (Figure 64).

Interconnection between the pores allows the movement of the cells across the scaffold and distribution of the cells at different zones. These interconnections also provide a circulating system similar to sinusoids of the bone marrow.

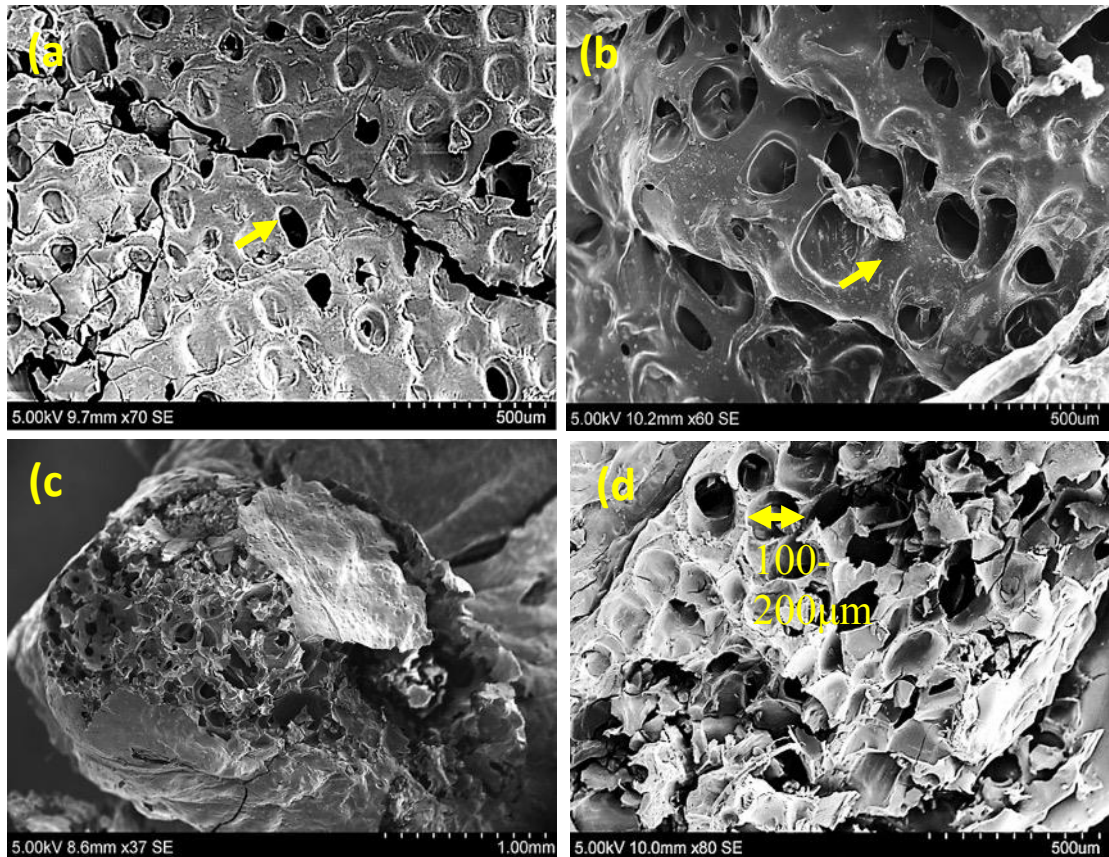


**Figure 63: SEM image of the foam-based scaffold.**

(a) SEM image of the foam-based scaffold (yellow arrows indicate pores). (b) Cross section of the scaffold. Bright dots in the SEM image marked by yellow arrows are HA nanoparticles on the surface of the scaffold. (c) This figure shows the porous structure of the scaffold and their interconnection. The pores and interconnection between the pores make this structure similar to spongy feature of the bone (d) The relative size of the microcavities (pores) in the scaffold has been shown here. This provide a space for settling down of the cells during the culture.

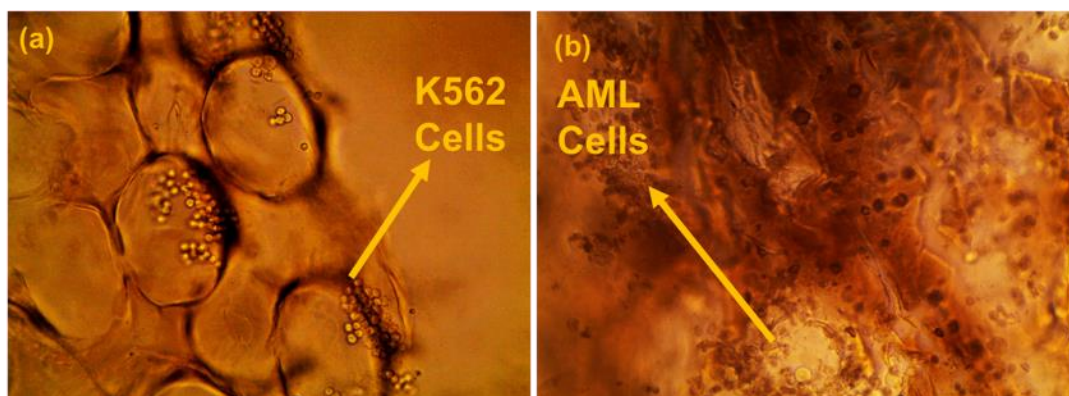


**Figure 64: Optical microscope images from cells growing in the foam scaffold.**

*Optical microscopy imaging shows the microcavities in the scaffold, acting like niches and accommodating (a) K562 and (b) primary AML cells. Figure (a) is an optical microscopic image from alginate foam with images of the K562 cells within the pores in the foam body structure. The spongy nature of the foam makes it similar to bone structure. The microcavities have accommodated the K562 cells and provided a space and environment for the K562 to grow. Accumulation of the K562 inside and at the walls of the microcavities indicates the cell-friendly nature of this scaffold. The presence of cells in several microcavities also indicates the connection between these microcavities, which is similar to the case of sinusoidal network inside BM. Figure (b) is an alginate foam optical microscopic image and shows AML cell proliferation inside the alginate scaffold. This confirms that the alginate foam-based scaffold is not only friendly to the cell line, but that it can also accommodate primary leukaemia cells and keep them alive.*

## **5.6 The lowest inhibitory dose of imatinib and doxorubicin**

Due to a lack of prior knowledge about the potential level of resistance which might be induced by the foam scaffold, we investigated various inhibitory concentrations of imatinib (Figure 65) or doxorubicin for K562 or HL60 and HS-5 cells (Figure 66). 0.5  $\mu\text{M}$  was determined as the lowest inhibitory dose

of imatinib for K562 in 2D culture and was consequently used for the experiments. The lowest inhibitory dose of imatinib was chosen to observe the potential minor response differences induced by the scaffold. To determine the lowest inhibitory dose of doxorubicin for HL60 cells which is not toxic to HS-5 stromal cells, both cell lines were treated with various doses of doxorubicin followed by MTS assay. This experiment identified 0.1  $\mu\text{M}$  as being the lowest inhibitory dose of doxorubicin for HL60 which had no inhibitory effect on HS-5 cell co-culture (for further details please see appendix). K562 cells were cultured at the concentration of 5,000 cells per 100 $\mu\text{l}$ , with or without 0.1, 0.2, 0.5, 1, 1.5 and 2 $\mu\text{M}$  imatinib, in a 96-well plate. The inhibitory effect of imatinib was measured after 72 hours by methanethiosulfonate (MTS)-based viability assay (CellTiter 96 AQueous One; Promega). HL60 and HS-5 cell lines were treated with or without 0.1, 0.2, 0.5 and 1  $\mu\text{M}$  doxorubicin for 72 hours in triplicates, followed by viability/proliferation measurement using MTS assay (as will be described later in this chapter).

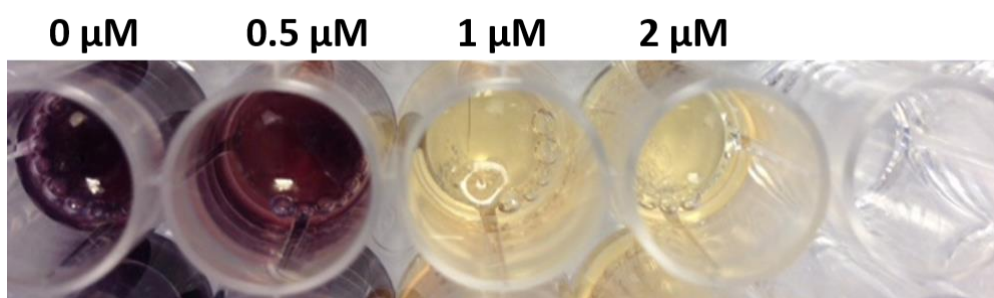


**Figure 65: MTS assay to measure lowest inhibitory dose of imatinib.**

*The colour of the MTS assay following 0.5–1 hour of incubation shows the reduced brownish colour in 0.5  $\mu\text{M}$  imatinib, indicating reduced proliferation of the K562 cells. The yellow colour of K562 cells treated with imatinib with 1*

and 2  $\mu\text{M}$  is due to the severe inhibitory impact of imatinib at these doses. The quantitative comparison was done by spectrophotometry.

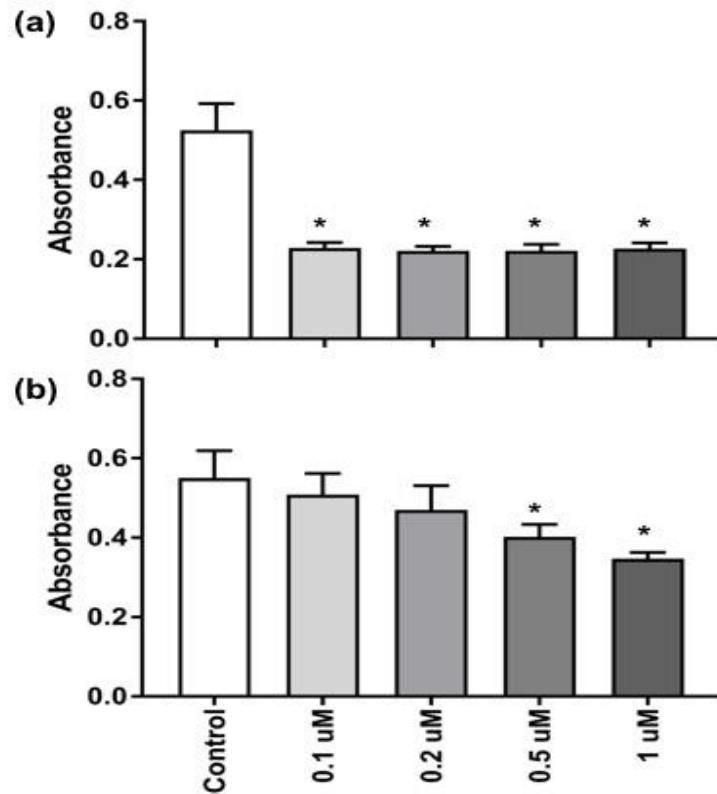


**Figure 66: The inhibitory effect of doxorubicin at various doses on (a) HL60 and (b) HS-5 cells.**

*The X-axis represents various doses of doxorubicin and the Y-axis represents the absorbance as measured by a Multiskan GO spectrophotometer.*

## **5.7 Differentiation of the primary haematopoietic cells and acute myeloid leukaemia cells**

Mononuclear cells from a newly diagnosed AML patient were cultured in the presence or absence of scaffold (in triplicate). The cell counts after five days of culture showed a larger number of AML cells in the scaffold compared to

no scaffold (Figure 67). This supported the cell-friendly nature of the alginate scaffold.

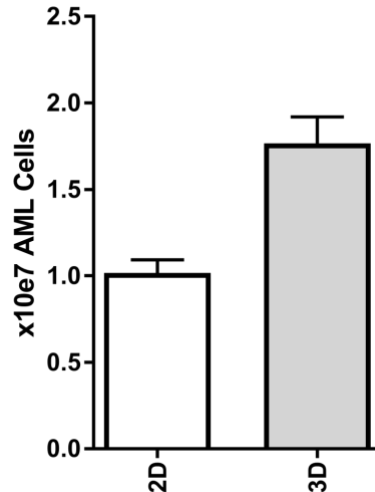


**Figure 67: The proliferation of primary AML cells in foam-based scaffold (3D) compared to 2D.**

*The relative proliferation of primary AML cells in foam-based scaffold (3D) compared to 2D is shown. The experiment was done in triplicate and shows higher proliferation of the cells in 3D compared to 2D culture.*

To investigate whether the scaffolds influences the differentiation of the leukaemia and normal stem/progenitors, the myeloid differentiation of the CD34<sup>+</sup> cells from one normal and two AML patients were investigated in the presence or absence of foam scaffolds for three days. The antigenic expression of primary normal haematopoietic cells (Figure 68) and two different acute myeloid leukaemia cells (Figure 69 and 70) from day 0 to 3 was measured by flowcytometry. CD16, CD13, CD34, CD117, CD11b, CD10, HLA-DR and CD45 markers were used to characterise myeloid differentiation in the presence of 3D and 2D culture. Myeloid differentiation progresses

along with reduced expression of CD34 or increased expression of myeloid markers in the CD34<sup>+</sup> stem/progenitor cells in normal or AML blast cells.

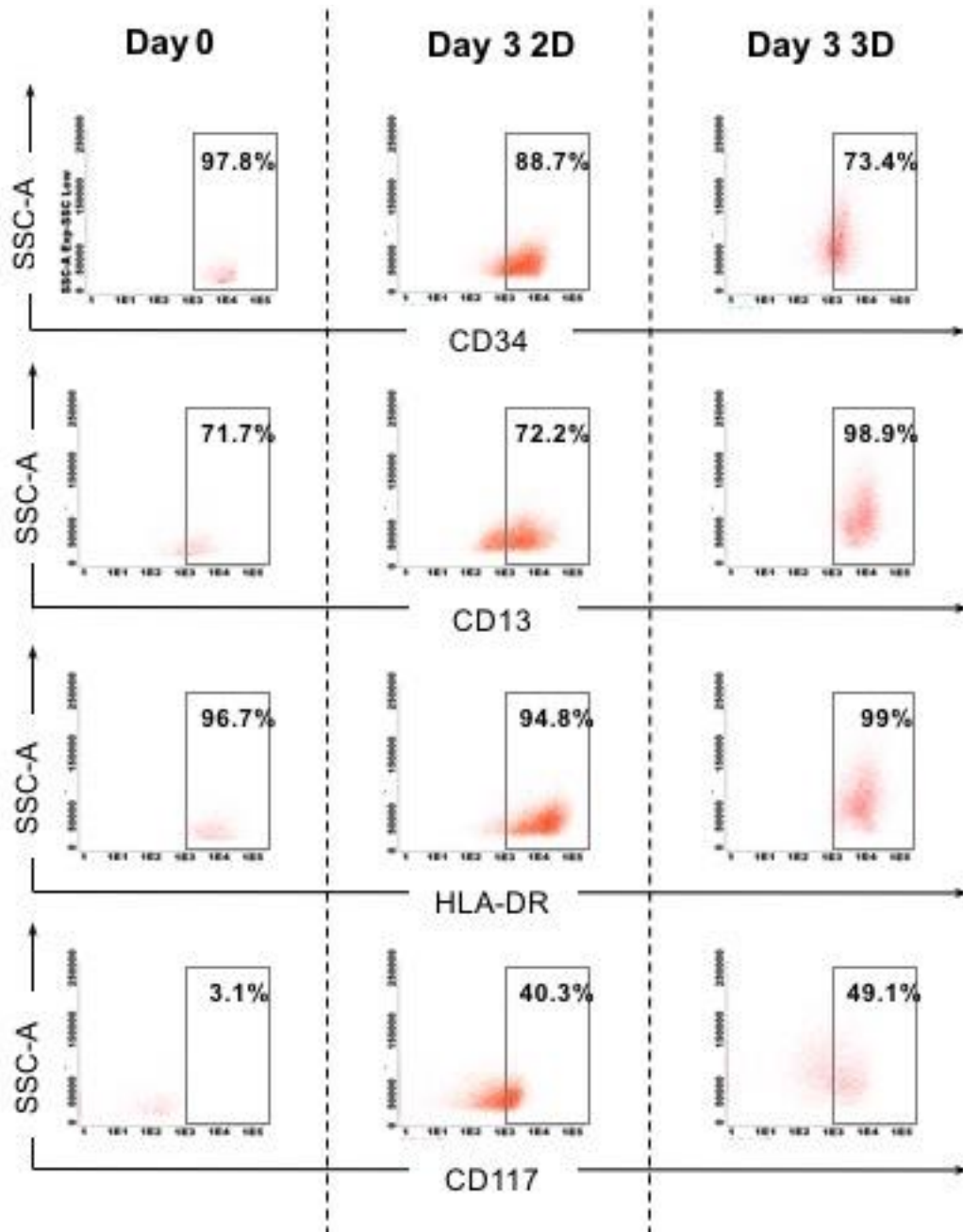


**Figure 68: Myeloid differentiation in 2D and 3D culture in normal donor cells.**

*This figure shows the expression of various myeloid differentiation markers in CD34<sup>+</sup> cells from a normal donor. CD13 and CD117 markers have increased in 3D compared to 2D and day 0.*

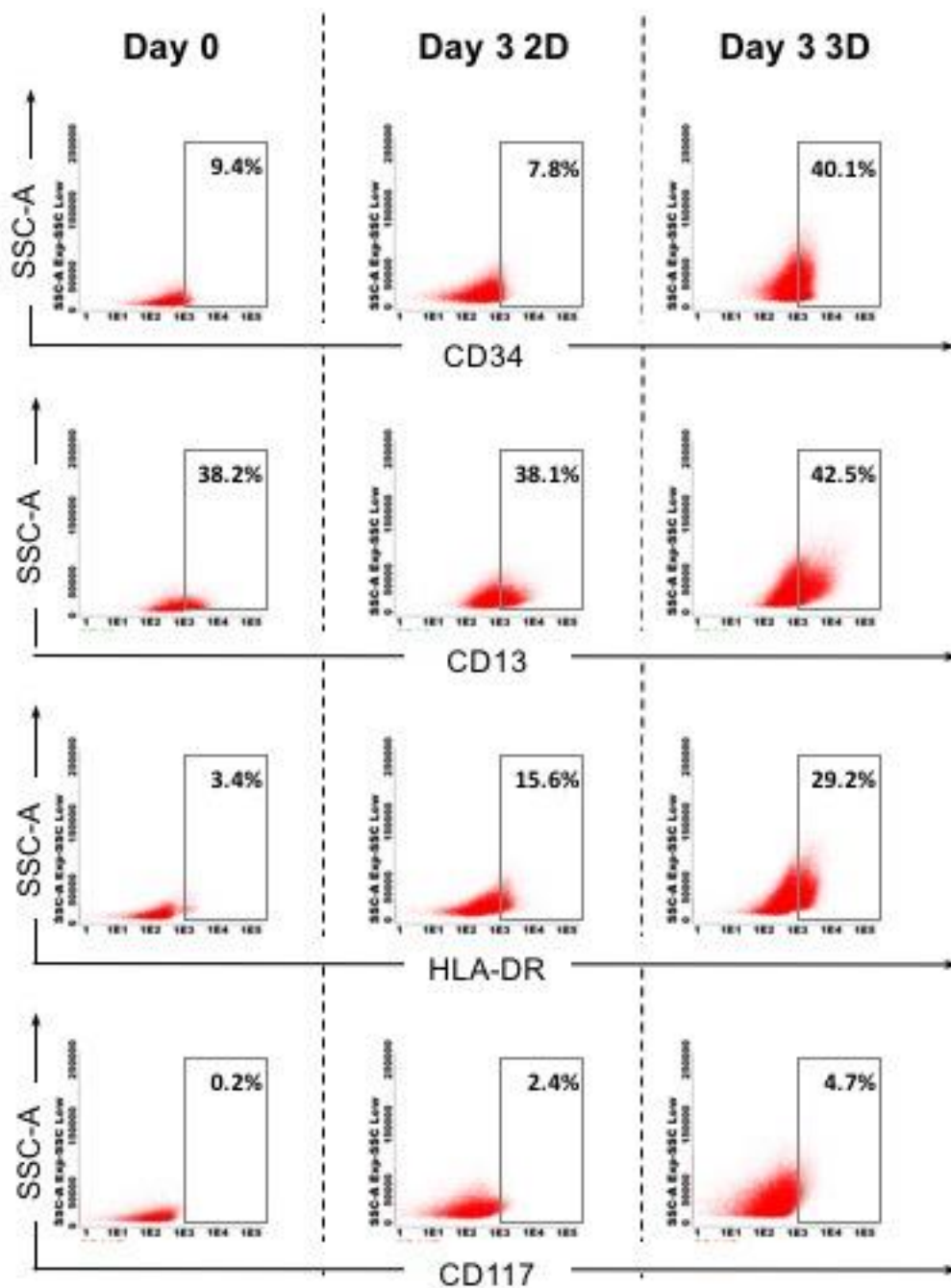


**Figure 69: Myeloid differentiation in 2D and 3D culture in AML cells (patient 1).**

*This figure shows the expression of various myeloid differentiation markers in blast cells from an AML patient (patient 1). CD13 and CD117 markers have increased in 3D compared to 2D and day 0, suggesting the role of 3D culture in promoting myeloid differentiation of the myeloid leukaemia cells.*

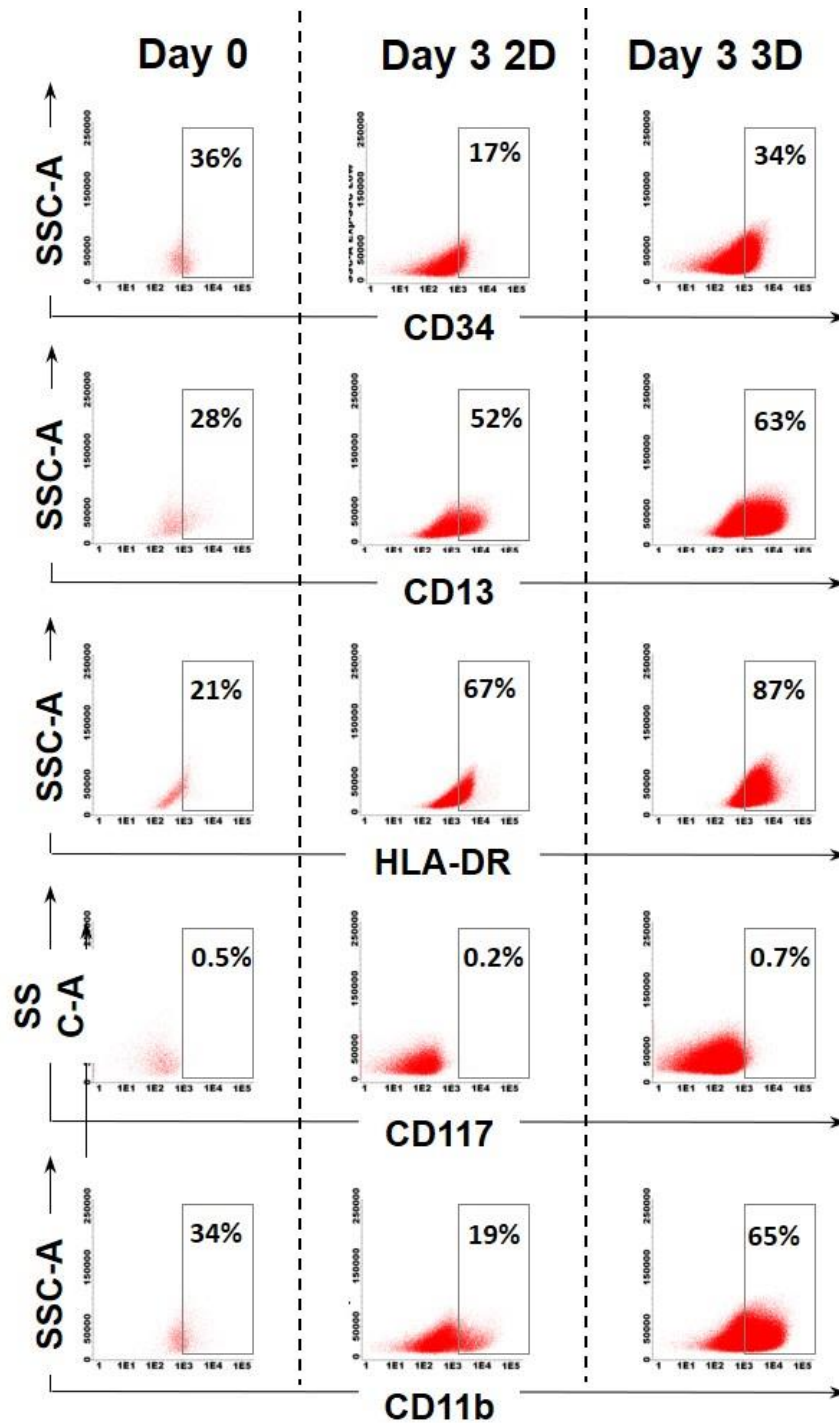


**Figure 70: Myeloid differentiation in 2D and 3D culture in AML cells (patient 2).**

*The expression of myeloid markers is shown for the blast cells from the AML patient 2 after three days of culture in the presence of 2D and 3D culture and also on day 0. Increased differentiation markers of CD11b, CD117, HLA-DR*

*and CD13 were observed after three days in AML cells cultured in 3D, compared to day 0 and also 2D culture.*

Normal CD34<sup>+</sup> precursors showed stronger and more homogenous expression of the myeloid associated antigens CD117 and CD13 after three days of culture in the foam-based scaffold compared to non-scaffold (2D) culture, indicating enhanced differentiation. Similarly, in figure 69, myeloblasts have augmented intensity of HLA-DR and CD13. This is even more evident in figure 70, where the blasts showed a profound monocytic differentiation compared to 2D culture, having stronger expression of HLA-DR and CD11b. The summary of the percentage of all the markers for the normal and the two AML patients have been presented in Table 5 along with their statistical analysis in figure 71, showing the significance of the altered expression of these markers in 3D culture compared to 2D. Although the small number of the sample in this work did not lead to significant p-value, the trend of the expression pattern indicated the impact of the 3D culture on induction of myeloid differentiation.

Enhanced differentiation of CD34<sup>+</sup> cells to more differentiated cells (represented as reduced CD34<sup>+</sup> expression) was also observed in myeloblasts from the third AML patient, which was performed in an independent experiment (Figure 72).

The findings from this observation suggest that foam-based 3D culture enhances myeloid differentiation in the normal CD34<sup>+</sup> cells and also in myeloblasts from AML patients.

Marker	Normal $\pm$ 0.1			AML1 $\pm$ 0.1			AML2 $\pm$ 0.1		
	0	2	3	0	2	3	0	2	3
CD13	71.7	72.2	98.9	38.2	38.1	42.5	27.9	51.6	63.3
CD117	3.1	40.3	49.1	0.2	2.4	4.7	0.5	0.2	0.7
CD11b	0	0	0	0	4.9	21.4	33.8	19.5	65.3
HLA-DR	96.7	94.8	99	3.4	15.6	9.2	21.3	64.3	86.7

**Table 4:**The percentage of myeloid markers on normal and two AML samples in 2D and 3D cultures.

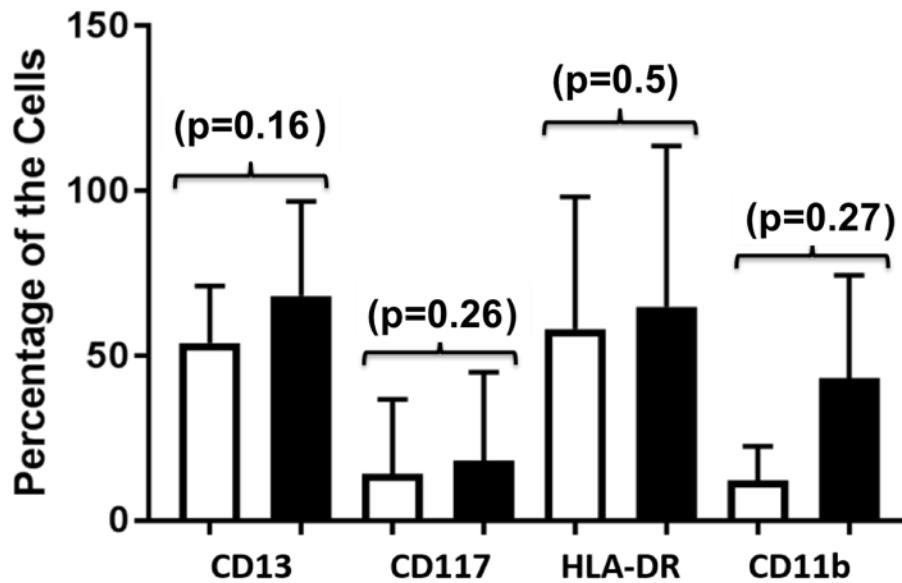


**Figure 71:** The statistical differences for the myeloid markers between 2D and 3D cultures.

*The p-value has been calculated using paired t-test analysis for the data from the normal and two AML samples cultured in 2D and 3D.*

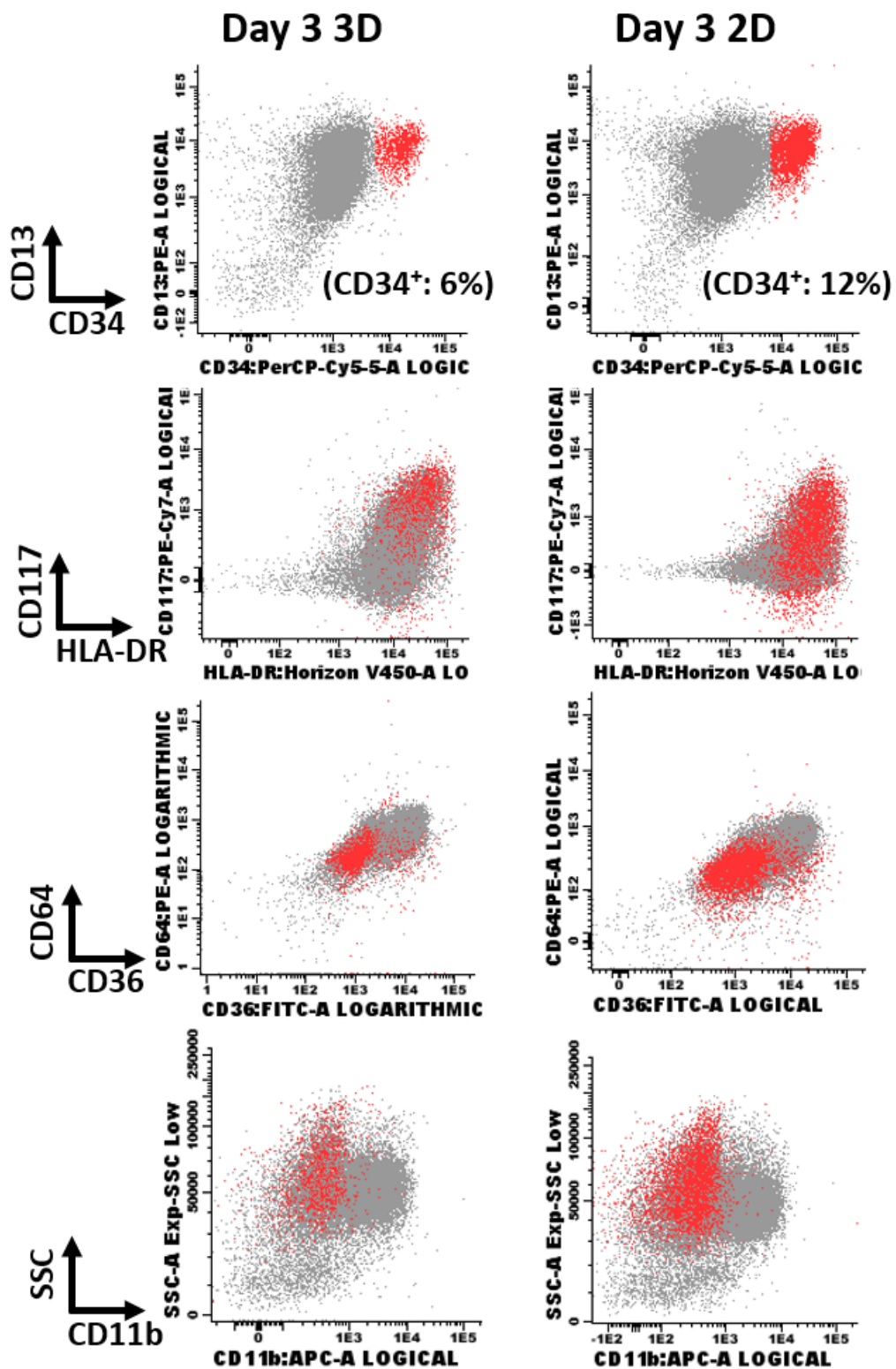


**Figure 72: Reduced level of CD34 markers during differentiation in 3D compare to 2D in AML cells (patient 3).**

*The myeloblasts were further depleted (down to 50%) in CD34<sup>+</sup> marker (red dots) after three days of culture in 3D compared to 2D.*

## **5.8 Resistance of the CML and AML cells to inhibitory effect of the drugs**

To investigate the potential drug resistance mediated by the foam-based scaffold, K562 and HL60 cells were treated with imatinib and doxorubicin, respectively. Treatment of K562 or HL60 cells in foam-based 3D culture reduced their sensitivity to imatinib or doxorubicin, respectively (Figure 73 a, b). As stroma is an important component of the BM microenvironment, to assess the sensitivity of leukaemia cells to antileukaemia agents in the context of stromal cells, BM-derived HS-5 stromal cells were seeded to the foam-based scaffold.

Addition of HS-5 cells to the scaffold is expected to influence the leukaemia cells in culture through direct contact and also via secretion of cytokine. It was shown earlier that HL60 cells were sensitive to even 0.1  $\mu\text{M}$  doxorubicin while HS5 cells were not affected to doxorubicin at this dose. This made it possible to investigate the impact of HS-5 on the viability of HL60 to doxorubicin at this dose. For HL60 cells, the addition of HS-5 cells further reduced the sensitivity of HL60 to 0.1  $\mu\text{M}$  doxorubicin (Figure 73b).

The addition of HS-5 cells to foam scaffolds increased the trend towards resistance. However, this trend did not become significant for K562 cells treated with 0.5 or 1  $\mu\text{M}$  imatinib (Figure 73a).

The lack of any trend towards resistance in the co-culture of HL60 and HS-5 in foam-based scaffold, compared to no HS-5 condition, might be due to the inhibitory dose of doxorubicin on HS-5 at doses higher than 0.1  $\mu\text{M}$

doxorubicin (Figure 73b). To show whether primary leukaemia cells behave similarly, primary myeloblasts from an AML patient were cultured in the presence or absence of foam-based scaffolds and treated with or without doxorubicin (0.1, 0.2 and 0.4  $\mu\text{M}$ ), followed by cell proliferation and viability using MTS assay at 72 hours. Foam scaffolds reduced the sensitivity of AML cells to doxorubicin at 0.2 and 0.4  $\mu\text{M}$  (Figure 73c). The lack of difference at 0.1  $\mu\text{M}$  seems to be due to the lower sensitivity of primary AML cells to doxorubicin compared to HL60 cells.

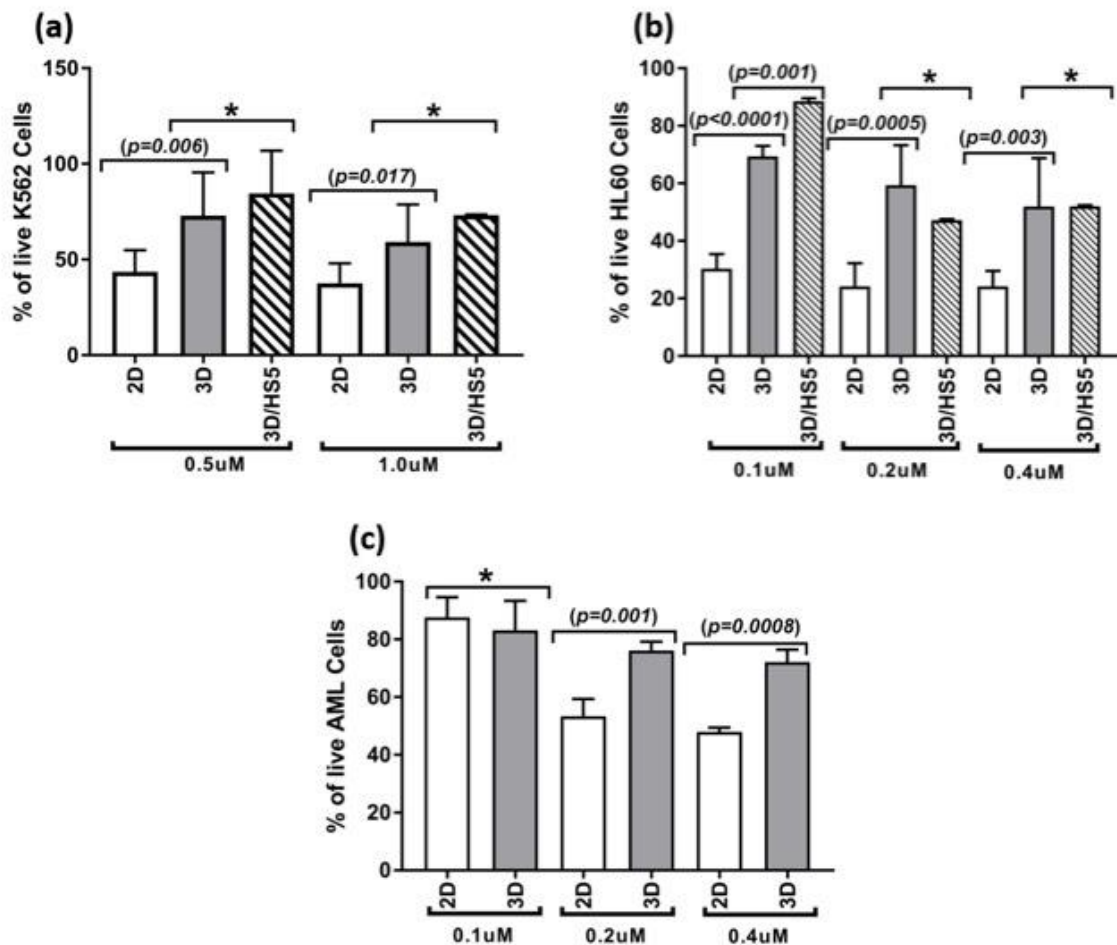


**Figure 73: The inhibitory effect of imatinib and doxorubicin on leukaemia cell line and primary cells in the presence or absence of foam scaffold.**

The inhibitory effect of imatinib and doxorubicin on leukaemia cell line and primary cells in the presence or absence of foam scaffold (with or without HS-5) is shown here. (a) Shows the percentage of live K562 cells compared to untreated control for each condition 72 hours after adding 0.5 or 1 μM imatinib. (b) Shows the percentage of live HL60 cells compared to untreated control for each condition 72 hours after adding 0.1, 0.2 or 0.4 μM doxorubicin. (c) Shows the influence of foam-based scaffold on the inhibition of primary AML cells from a patient. The X-axis represents various doses of imatinib (a) or doxorubicin (b, c).

## 5.9 Discussion

Tissue engineering scaffolds play an important role in biomedical applications by acting as a temporary tissue construct or building block for cell accommodation, proliferation and differential function (Weigelt & Bissell, 2008). In the current study foam scaffolds were prepared by using a microfluidic bubbling technique. To overcome the poor stability of the microbubbles, which is a limitation of this technique, cross-linking by calcium chloride was practised (Ekemen et al., 2011). To improve biocompatibility of the scaffold, porous foam was fabricated from natural polymer alginate. Many attempts have recently been made to improve cell seeding and growth, such as by coating the scaffolds with different proteins like collagen and FBS (Park et al., 2005; Nair et al., 2010; Phipps et al., 2011). Here we used HA nanoparticles to make the scaffold more similar to a BM microenvironment for biological investigations.

To develop a BM-like environment with niche-like structures we formed foam-based scaffolds derived from microbubbles. Application of this technology has the advantage of controlling the size of the microbubbles and as a result controlling the size of the microcavities in the foam. This enables production of scaffold with pores of about 200  $\mu\text{m}$  in diameter, which is close in size to the microcavities in the bone (Lai et al., 2015; Nelson & Roy, 2016). The challenge in using this technology to produce foamed scaffolds is the instability of the produced bubbles, which results in the destruction of bubbles before forming solid foam during drying. To overcome this problem, we

collected microbubbles in calcium chloride solution, which caused cross-links in the microbubble shell and the formation of solid foam following drying. The images from these scaffolds showed the production of desired microcavities and validates the use of this approach for the production of foam-based scaffold.

One of the main reasons for developing artificial BM-like structures for culturing leukaemia cells is drug sensitivities (Rödling et al., 2017). Foam-based 3D culture similar to fibre scaffolds (Karimpoor et al., 2017) increases the resistance of the leukaemia cell lines to the inhibitory effects of imatinib and doxorubicin. Different applied materials in the structure of the fibre and foam-based scaffolds, and the observation of similar phenotypes in K562 and HL60 cells in response to imatinib and doxorubicin, suggest that the 3D environment and interaction of the leukaemia cells at different spatial positions have an important influence on the cells' survival and activated signalling pathways, and as a result the response to antileukaemia drugs (Hutchinson & Kirk, 2011). It has been shown before that 3D cultures influence the cell phenotype and their gene expression compared to a 2D environment (Luca et al., 2013). This altered phenotype might be due to the activation of another signalling pathway which is targeted by the inhibitor. The other possibility is that of altered oxygen concentration in 3D compared to 2D culture. Hypoxia is an important component of the BM niche, contributes to the maintenance of AML cells (Forristal et al., 2015; Irigoyen, García-Ruiz, & Berra, 2017) and also selects bortezomib-resistant CML stem cells (Tanturli et al., 2011). It has been shown that 3D-cultures are better than 2D-cultures

in simulating important tumour characteristics *in vivo*, such as hypoxia and the resulting drug resistant phenotype (Imamura et al., 2015). The mechanism of resistance might also be due to poor access of drugs to the cells hidden in the niche-like spaces in the scaffold. These provide more evidence for the application of 3D culture for drug sensitivity studies. Conventional 2D cultures have been proven to be an unreliable drug development model for prediction of *in vivo* drug efficacy and toxicity (Hutchinson & Kirk, 2011). Creating a third dimension for cell culture is clearly more relevant and has to be considered as a practical alternative (Saleh & Genever, 2011).

Our data showed enhanced myeloid differentiation in both normal progenitor and AML myeloblasts in 3D foam-based culture. 3D cultures have also been reported in other studies to be capable of inducing differentiation of the haematopoietic stem cells compared to 2D cultures (Liu & Roy, 2005; Pietrzyk-Nivau et al., 2015). 3D cultures (Edmondson et al., 2014) mimic an environment similar to BM niches at inducing cell differentiation (Sharma, Limaye, & Kale, 2012). Although this observation does not address directly how this can influence resistance to therapeutic agents, it might suggest that 3D culture causes higher resistance to antileukaemia agents compared to 2D cultures by inducing higher differentiation rate, and the production of the more mature cells, which are less sensitive to the inhibitory effect of antileukaemia agents. As resistance or relapse in AML is considered to be mainly due to the role of LSCs, future investigations should aim at measuring the impact of 3D cultures on LSCs and determining if induced differentiation is along with

enhanced self-renewal activity of the LSCs. In summary, the conventional 2D culture is not a highly reliable system for drug sensitivity investigations as the drug sensitivity of leukaemia cells obtained from 2D culture is different from what is observed *in vivo* (Edmondson et al., 2014). Our foam-based 3D culture reduced the sensitivity of leukaemia cells to antileukaemia agents and further induced the differentiation of the normal and leukaemia cells compared to that in 2D culture. These differences might be attributed to microcavities mimicking BM niches in foam-based 3D culture. We propose to apply this foam-based 3D culture for drug sensitivity investigations and therapeutic target discoveries.

# Chapter 6

## Conclusions and future work

### 6.1 Conclusion

The first section of this thesis focused on the design of a floatable and low-density method in order to improve oral drug delivery to the gastrointestinal system using microbubbles.

- Alginate microbubbles with the liquid suspension of gold nanoparticles in the shell were prepared by microfluidic V-junction. They were found with the present of gold particles to have significantly enhanced stability compared with bubbles coated with only surfactant.
- The results of the experiments in this work show that alginate microbubbles collected in calcium chloride through a cross-linking process and suspended in glycerol can make the alginate microbubble stable by reducing surface tension and consequently increasing the lifetime of the bubbles. Enhanced stability of the microbubbles increases the efficiency of the administered drug; this is beneficial in targeted drug delivery since increasing the stability of microbubbles can improve the efficiency of the treatment.
- In order to assess the stability of the alginate microbubbles in gastric condition, bubbles were tested as a function of heating temperature in the range of 20 °C to 37 °C and collected in acidic condition to better control the stability of the bubbles. It was found that by increasing the

temperature, the lifetime of the bubbles will be reduced, and therefore the body temperature will have a significant effect on the microbubbles' stability.

- The proposed method in this study, using microbubbles for oesophageal drug delivery, can take advantages from both mucoadhesive and floating systems. The hypothesis is that some of the alginate bubbles after administration will attach to the oesophageal surface, and the remains of the alginate bubbles entering the stomach will remain floatable and will not sink to the bottom of the gastric system. Gastric waves make the floatable bubbles hit the gastroesophageal junction region, which in turn increases the contact of the deliver drugs to the mucosal surface.
- In the second part of chapter 4, the feasibility of the oesophageal adhesive alginate microbubbles drug delivery system was investigated, with a particular view of establishing the potential of alginate microbubbles solutions as liquid bioadhesive systems to increase absorption of model drug. Experiment results indicate that alginate microbubbles prepared by microfluidic V-junction with fluorescent dye in the shell can adhere to oesophageal tissue. Microbubble adhesion helps to increase absorption of fluorescent dye to the targeted region. This study demonstrates that alginate microbubbles suspension can have an application as a bioadhesive agent.

In the second section of this thesis, the application of microfluidic microbubble technology to produce scaffold for development of 3D culture as a platform for *in vitro* antileukaemia drug sensitivities was investigated. Recent developments in understanding the role of BM microenvironment in the formation and progress of various myeloid leukaemia has provided a new opportunity for developing novel therapeutic approaches. Targeting the interaction between the leukaemia cells and the microenvironment is expected to eradicate leukaemia cells residing in the BM niches. Mesenchymal stromal cells, osteoblasts and extracellular matrix are amongst the main components of the BM microenvironment, whereby their special 3D organisation contributes to the formation of the niches. This is a very different structure compared to conventional 2D cultures, which have been used extensively for measuring the sensitivity of the leukaemia cells to various antileukaemia agents.

- The experiments in this thesis showed that a higher level of resistance to antileukaemia agents is induced by 3D culture mimicking BM, compared to 2D culture, and supported the application of 3D culture as the *in vitro* model to investigate the sensitivity to various antileukaemia agents. This was achieved by using an alginate foam-based scaffold, prepared using microbubbles generated by a microfluidic device. The scaffold produced from the alginate microbubbles, using the methodology described in this thesis, simulated BM structure regarding the holes and lacuna, and also provided the space for the leukaemia cells to reside and interact with the mesenchymal stromal cells.

- This model is shown to have the potential of being used for drug sensitivity screens in the leukaemia research lab, as the preparation of 3D using this type of scaffold is easy and can be used by any biological lab. The nature of the alginate makes it cell-friendly, which is an advantage over some of the artificial polymers that are not cell-friendly. Also, the important role of calcium in forming cross-links between the alginate molecules makes it possible to retrieve the cultured cells in these scaffolds by removing the calcium using chelating agents, such as EDTA, for downstream investigations. The result of this study concludes that alginate-based microbubble scaffolds have the potential of being an informative tool for routine screening of drug sensitivities for various types of leukaemia.

## **6.2 Future work**

The future work can be divided into three categories. The first part is to further improve the microbubbles as a method of drug delivery. The second part of future work focuses on improving foam-based scaffold through further modifications which make it more similar to bone marrow, and the third part will be the investigation of how this 3D culture reduces the sensitivity of leukaemia cells to antileukaemia agents.

### **6.2.1 Further improvement of microbubbles as a method of drug delivery**

To complete the mucoadhesive study using microbubbles it is essential to measure the life time of microbubbles after applying them on the animal tissue. For future studies it is important to find a method for assessing the bubbles on the tissue surface. Also, the microbubble time study can be extended by using various conditions where other factors and their influence on the bubbles' stability are investigated.

### **6.2.2 Further modification of the alginate scaffolds**

The alginate-based scaffold can be further developed by adding other components of the BM such as collagen or fibronectin. By adding other components of the BM such as endothelial cells, the scaffold can be further developed to mimic physiological condition. This is a potential diagnostic tool; however, the stability of the scaffold should be further developed prior to converting it into a routine diagnostic tool. This requires stability studies under various conditions such as various life-time, temperature and humidity.

### **6.2.3 Exploring the mechanisms through which the alginate scaffold exerts its biological impact on the cells**

Gene expression study of the cultured leukaemia cells in this type of scaffold and correlation of the data with the activity of the altered genes would be an important aspect of the proposed work for future. The future research in this

direction would compare the gene expression profile of the cultured cells in this type of scaffold against the cells in conventional 2D cultures. The differential gene expression would provide informative data on which signalling pathways have been activated by this type of scaffold. The next experiment will investigate whether the activated pathways are the same for a specific leukaemia cell when it is grown in 3D cultures with different types of scaffold. Different signalling pathways activation when a particular cell is cultured in various scaffolds would indicate the significance of material type on the biological activity of the cells. Whereas, the activation of the same signalling pathways in various scaffolds in a particular cell type would suggest the third dimension, rather than the materials of the scaffold, as having the major role on leukaemia cells' response to therapy.

Hypoxia is a mechanism of resistance to antileukaemia in BM through changing the metabolism of LSCs. I propose for future work that the concentration of oxygen in different sections of the scaffolds be investigated. Demonstrating the heterogeneous concentration of oxygen in different sections of the scaffold and correlating these regions with the cell density would be of significant value as it would provide additional evidence for the similarity of this 3D culture to bone marrow niches. The concentration of the oxygen is very low in certain regions of the bone marrow, and these regions are the main sites for the residence of the quiescent stem cells which are highly resistant to anticancer therapy.

Induction of resistance to antileukaemia agents might be due to physical contact of the cells with scaffolds. The leukaemia cells which bind to the

scaffold might have a different metabolism or cell cycle compared to the floating ones. Investigation of these differences can be another topic for investigation in future.

Finally, the higher resistance of the leukaemia cells to antileukaemia agents in the presence of the scaffolds might be due to unequal distribution of the drug in various parts of the scaffold. This might be due to various absorptions of the drug to the various components of the scaffold. Measurement of intracellular concentration of an antileukaemia agent in the cells retrieved from the different parts of the scaffold is expected to provide useful information. Biomedical studies investigating the interaction between the applied antileukaemia drugs and the scaffold structure are also required, along with measuring the half-life of the applied drug in the presence of the scaffold.

## References

- Abou-Taleb, M. H. (2014). Characterization of Polymer Blends Using UV-Visible Spectroscopy. *Characterization of Polymer Blends: Miscibility, Morphology and Interfaces*, 789–820.
- Adan, A., Alizada, G., Kiraz, Y., Baran, Y., & Nalbant, A. (2017). Flow cytometry: Basic principles and applications. *Critical Reviews in Biotechnology*, 37(2), 163–176. doi: 10.3109/07388551.2015.1128876
- Ahmed, N., & Jameson, G. J. (1985). The effect of bubble size on the rate of flotation of fine particles. *International Journal of Mineral Processing*, 14(3), 195–215. doi: 10.1016/0301-7516(85)90003-1
- Ahmad, Z., Nangrejo, M. E. E. S., Edirisinghe, M., Stride, E., Colombo, P., & Zhang, H. B. (2009). Engineering a material for biomedical applications with electric field assisted processing. *Applied Physics A: Materials Science and Processing*, 97(1), 31–37. doi: 10.1007/s00339-009-5359-z
- Ahmad, B., Stride, E., & Edirisinghe, M. (2012). Calcium alginate foams prepared by a microfluidic T-Junction system: Stability and food applications. *Food and Bioprocess Technology*, 5(7), 2848–2857. doi: 10.1007/s11947-011-0650-3
- Aljittawi, O. S., Li, D., Xiao, Y., Zhang, D., Ramachandran, K., Stehno-Bittel, L., ... & Garimella, R. (2014). A novel three-dimensional stromal-based model for in vitro chemotherapy sensitivity testing of leukemia cells. *Leukemia and Lymphoma*, 55(2), 378–391. doi: 10.3109/10428194.2013.793323
- Allegra, J. C., & Lippman, M. E. (1978). Growth of a human breast cancer cell line in serum-free hormone-supplemented medium. *Cancer Research*, 38(11 Pt 1), 3823–3829.
- Andrews, G. P., Lavery, T. P., & Jones, D. S. (2009). Mucoadhesive polymeric platforms for controlled drug delivery. *European Journal of Pharmaceutics and Biopharmaceutics*, 71(3), 505–518. doi: 10.1016/j.ejpb.2008.09.028
- Atta, K. R., Gavril, D., Loukopoulos, V., & Karaiskakis, G. (2004). Study of the influence of surfactants on the transfer of gases into liquids by inverse gas chromatography. *Journal of Chromatography A*, 1023(2), 287–296. doi: 10.1016/j.chroma.2003.10.013
- Azmin, M., Mohamedi, G., Edirisinghe, M., & Stride, E. P. (2012). Dissolution of coated microbubbles: The effect of nanoparticles and surfactant concentration.

*Materials Science and Engineering C. Elsevier B.V.*, 32(8), 2654–2658. doi: 10.1016/j.msec.2012.06.019

Baccarani, M., Saglio, G., Goldman, J., Hochhaus, A., Simonsson, B., Appelbaum, F., ... & Gratwohl, A. (2006). Evolving concepts in the management of chronic myeloid leukemia: Recommendations from an expert panel on behalf of the European LeukemiaNet. *Blood*, 108(6), 1809–1820. doi: 10.1182/blood-2006-02-005686

Baker, B. M., & Chen, C. S. (2012). Deconstructing the third dimension – How 3D culture microenvironments alter cellular cues. *Journal of Cell Science*, 125(13), 3015–3024. doi: 10.1242/jcs.079509

Balabanov, S., Braig, M., & Brümmendorf, T. H. (2014). Current aspects in resistance against tyrosine kinase inhibitors in chronic myelogenous leukemia. *Drug Discovery Today: Technologies*, 11(1), 89–99. doi: 10.1016/j.ddtec.2014.03.003

Barnes, D., & Sato, G. (1979). Growth of a human mammary tumour cell line in a serum-free medium. *Nature*, 281(5730), 388–389. doi: 10.1038/281388a0

Baumgartner, S., Kristl, J., Vrečer, F., Vodopivec, P., & Zorko, B. (2000). Optimisation of floating matrix tablets and evaluation of their gastric residence time. *International Journal of Pharmaceutics*, 195(1–2), 125–135. doi: 10.1016/S0378-5173(99)00378-6

Bendall, L. J., Daniel, A., Kortlepel, K., & Gottlieb, D. J. (1994). Bone marrow adherent layers inhibit apoptosis of acute myeloid leukemia cells. *Experimental Hematology*, 22(13), 1252–1260.

Bettger, W. J., & Ham, R. G. (1982). The nutrients requirements of cultured mammalian cells. In *Advances in Nutritional Research*, 249–286.

Bhatia, R., Holtz, M., Niu, N., Gray, R., Snyder, D. S., Sawyers, C. L., ... & Forman, S. J. (2003). Persistence of malignant hematopoietic progenitors in chronic myelogenous leukemia patients in complete cytogenetic remission following imatinib mesylate treatment. *Blood*, 101(12), 4701–4707. doi: 10.1182/blood-2002-09-2780

Boehm, D., & Bell, A. (2014). Simply red: A novel spectrophotometric erythroid proliferation assay as a tool for erythropoiesis and erythrototoxicity studies. *Biotechnology Reports*, 4(1), 34–41. doi: 10.1016/j.btre.2014.07.005

Borden, M. A., & Longo, M. L. (2002). Dissolution behavior of lipid monolayer-coated, air-filled microbubbles: Effect of lipid hydrophobic chain length. *Langmuir*,

18(24), 9225–9233. doi: 10.1021/la026082h

Bottenstein, J. E., & Sato, G. H. (1979). Growth of a rat neuroblastoma cell line in serum-free supplemented medium. *Proceedings of the National Academy of Sciences*, 76(1), 514–517. doi: 10.1073/pnas.76.1.514

Braccini, A., Wendt, D., Jaquiere, C., Jakob, M., Heberer, M., Kenins, L., ... & Martin, I. (2005). Three-dimensional perfusion culture of human bone marrow cells and generation of osteoinductive grafts. *Stem Cells*, 23(8), 1066–1072. doi: 10.1634/stemcells.2005-0002

Bratt-Leal, A. M., Carpenedo, R. L., & McDevitt, T. C. (2009). Engineering the embryoid body microenvironment to direct embryonic stem cell differentiation. *Biotechnology Progress*, 25(1), 43–51. doi: 10.1002/btpr.139

Butt, H.J., Graf, K., & Kappl, M. (2006). *Physics and chemistry of interfaces*. John Wiley & Sons. doi: 10.1632/074069503X85526.

Campbell, J. J., Davidenko, N., Caffarel, M. M., Cameron, R. E., & Watson, C. J. (2011). A multifunctional 3D co-culture system for studies of mammary tissue morphogenesis and stem cell biology. *PLoS ONE*, 6(9). doi: 10.1371/journal.pone.0025661

Campbell, G. M., & Mougeot, E. (1999). Creation and characterisation of aerated food products. *Trends in Food Science and Technology*, 283–296. doi: 10.1016/S0924-2244(00)00008-X

Carletti, E., Endogan, T., Hasirci, N., Hasirci, V., Maniglio, D., Motta, A., & Migliaresi, C. (2011). Microfabrication of PDLLA scaffolds. *Journal of Tissue Engineering and Regenerative Medicine*, 5(7), 569–577. doi: 10.1002/term.349

Carugo, D., Owen, J., Crake, C., Lee, J. Y., & Stride, E. (2015). Biologically and acoustically compatible chamber for studying ultrasound-mediated delivery of therapeutic compounds. *Ultrasound in Medicine & Biology*, 41(7), 1927–1937. doi: 10.1016/j.ultrasmedbio.2015.03.020

Cassell, E. A., Kaufman, K. M., & Matuevic, E. (1975). The effects of bubble size on microflotation. *Water Research*, 9(12), 1017–1024. doi: 10.1016/0043-1354(75)90095-0

Chan, B. P., & Leong, K. W. (2008). Scaffolding in tissue engineering: General approaches and tissue-specific considerations. *European Spine Journal*, 17(4), 467–479. doi: 10.1007/s00586-008-0745-3

Chen, G. (2004). Electrochemical technologies in wastewater treatment. *Separation and Purification Technology*, 38(1), 11–41. doi: 10.1016/j.seppur.2003.10.006

- Chickering, D. E., & Mathiowitz, E. (1995). Bioadhesive microspheres: I. A novel electrobalance-based method to study adhesive interactions between individual microspheres and intestinal mucosa. *Journal of Controlled Release*, 34(3), 251–262. doi: 10.1016/0168-3659(95)00011-V
- Chu, L. B., Xing, X. H., Yu, A. F., Zhou, Y. N., Sun, X. L., & Jurcik, B. (2007). Enhanced ozonation of simulated dyestuff wastewater by microbubbles. *Chemosphere*, 68(10), 1854–1860. doi: 10.1016/j.chemosphere.2007.03.014
- Clift, R., Grace, J. R., & Weber, M. E. (2005). *Bubbles, drops, and particles*. Dover Publications.
- Cortes, J., Hochhaus, A., Hughes, T., & Kantarjian, H. (2011). Front-line and salvage therapies with tyrosine kinase inhibitors and other treatments in chronic myeloid leukemia. *Journal of Clinical Oncology: Official Journal of the American Society of Clinical Oncology*, 29(5), 524–531. doi: 10.1200/JCO.2010.31.3619
- Cox, T. R., & Erler, J. T. (2011). Remodeling and homeostasis of the extracellular matrix: Implications for fibrotic diseases and cancer. *Disease Models & Mechanisms*, 4(2), 165–178. doi: 10.1242/dmm.004077
- Cui, W., Bei, J., Wang, S., Zhi, G., Zhao, Y., Zhou, X., ... & Xu, Y. (2005). Preparation and evaluation of poly(L-lactide-co-glycolide) (PLGA) microbubbles as a contrast agent for myocardial contrast echocardiography. *Journal of Biomedical Materials Research - Part B Applied Biomaterials*, 73(1), 171–178. doi: 10.1002/jbm.b.30189
- Cutroneo, K. R. (2003). Gene therapy for tissue regeneration. *Journal of Cellular Biochemistry*, 88(2), 418–425. doi: 10.1002/jcb.10357
- Dang, J. M., & Leong, K. W. (2006). Natural polymers for gene delivery and tissue engineering. *Advanced Drug Delivery Reviews*, 58(4), 487–499. doi: 10.1016/j.addr.2006.03.001
- Darido, E. 12 August 2016. Weight Loss Surgery website. [online]. [Accessed 05 August 2018]. Available from: <https://houstonsleevesurgeon.com/the-gastric-fundus-and-lap-band-removal/>
- Defenderauto, 26 Feb 2017. Defenderauto website. [online]. [Accessed 03 August 2018]. Available from: <http://defenderauto.info/pyloric-sphincter/>
- Dhami, S. P. S., Kappala, S. S., Thompson, A., & Szegezdi, E. (2016). Three-dimensional ex vivo co-culture models of the leukaemic bone marrow niche for functional drug testing. *Drug Discovery Today*, 21(9), 1464–1471. doi: 10.1016/j.drudis.2016.04.019

- Dhandayuthapani, B., Yoshida, Y., Maekawa, T., & Kumar, D. S. (2011). Polymeric scaffolds in tissue engineering application: A review. *International Journal of Polymer Science*, 2011. doi: 10.1155/2011/290602
- Dick, J. E. (2005). Acute myeloid leukemia stem cells. *Annals of the New York Academy of Sciences*, 1044(1), 1–5. doi: 10.1196/annals.1349.001
- Druker, B. J., Guilhot, F., O'Brien, S. G., Gathmann, I., Kantarjian, H., Gattermann, N., ... & Cervantes, F. (2006). Five-year follow-up of patients receiving imatinib for chronic myeloid leukemia. *N Engl J Med*, 355(23), 2408–2417. doi: 10.1056/NEJMoa062867
- Edmondson, R., Broglie, J. J., Adcock, A. F., & Yang, L. (2014). Three-dimensional cell culture systems and their applications in drug discovery and cell-based biosensors. *ASSAY and Drug Development Technologies*, 12(4), 207–218. doi: 10.1089/adt.2014.573
- Ekemen, Z., Chang, H., Ahmad, Z., Bayram, C., Rong, Z., Denkbaz, E. B., ... & Edirisinghe, M. (2011). Fabrication of biomaterials via controlled protein bubble generation and manipulation. *Biomacromolecules*, 12(12), 4291–4300. doi: 10.1021/bm201202y
- El-Sherbiny, I. M. I. M. I., & Yacoub, M. H. M. M. H. M. (2013). Hydrogel scaffolds for tissue engineering: Progress and challenges. *Global Cardiology Science and Practice*, 2013(3), 38. doi: 10.5339/gcsp.2013.38
- Elsayed, M., Huang, J., & Edirisinghe, M. (2015). Bioinspired preparation of alginate nanoparticles using microbubble bursting. *Materials Science and Engineering: C. Elsevier B.V.*, 46, 132–139. doi: 10.1016/j.msec.2014.09.036
- Essers, M. A. G., & Trumpp, A. (2010). Targeting leukemic stem cells by breaking their dormancy. *Molecular Oncology*, 4(5), 443–450. doi: 10.1016/j.molonc.2010.06.001
- Fang, Y., & Eglen, R. M. (2017). Three-dimensional cell cultures in drug discovery and development. *SLAS DISCOVERY: Advancing Life Sciences R&D*, 22(5), 456–472. doi: 10.1177/2472555217696795
- Farook, U., Stride, E., & Edirisinghe, M. J. (2009). Stability of microbubbles prepared by co-axial electrohydrodynamic atomisation. *European Biophysics Journal*, 38(5), 713–718.
- Farook, U., Stride, E., Edirisinghe, M. J., & Moaleji, R. (2007). Microbubbling by co-axial electrohydrodynamic atomization. *Medical & Biological Engineering & Computing*, 45(8), 781–789. doi: 10.1007/s11517-007-0210-1

Fava, C., & Saglio, G. (2010). Can we and should we improve on frontline imatinib therapy for chronic myeloid leukemia? *Seminars in Hematology*, *47*(4), 319–326. doi: 10.1053/j.seminhematol.2010.06.001

Forristal, C. E., Brown, A. L., Helwani, F. M., Winkler, I. G., Nowlan, B., Barbier, V., ... & Martin, S. (2015). Hypoxia inducible factor (HIF)-2 $\alpha$  accelerates disease progression in mouse models of leukemia and lymphoma but is not a poor prognosis factor in human AML. *Leukemia*, *29*(10), 2075–2085. doi: 10.1038/leu.2015.102

Frantz, C., Stewart, K. M., & Weaver, V. M. (2010). The extracellular matrix at a glance. *Journal of Cell Science*, *123*(24), 4195–4200. doi: 10.1242/jcs.023820

Fraser, C. C., Eaves, C. J., Szilvassy, S. J., & Humphries, R. K. (1990). Expansion in vitro of retrovirally marked totipotent hematopoietic stem cells. *Blood*, *76*(6), 1071–1076.

Friedl, P., Sahai, E., Weiss, S., & Yamada, K. M. (2012). New dimensions in cell migration. *Nature Reviews Molecular Cell Biology*, *13*(11), 743–747. doi: 10.1038/nrm3459

Garg, S., Thomas, A. A., & Borden, M. A. (2013). The effect of lipid monolayer in-plane rigidity on in vivo microbubble circulation persistence. *Biomaterials*, *34*(28), 6862–6870. doi: 10.1016/j.biomaterials.2013.05.053

Garstecki, P., Fuerstman, M. J., Stone, H. A., & Whitesides, G. M. (2006). Formation of droplets and bubbles in a microfluidic T-junction—Scaling and mechanism of break-up. *Lab on a Chip*, *6*(3), 437. doi: 10.1039/b510841a

Garstecki, P., Gañán-Calvo, A. M., & Whitesides, G. M. (2005). Formation of bubbles and droplets in microfluidic systems. *Bulletin of the Polish Academy of Sciences*, *53*(4), 361–372. doi: 10.1007/978-90-481-9029-4

Gienger, J. Gross, H. Neukammer, J. c2016. Physikalisch Technische Bundesanstalt website. [online]. [Accessed 01 August 2018]. Available from: <https://www.ptb.de/cms/en/ptb/fachabteilungen/abt8/fb-84/ag-841/flowzytometrie-841.html>

Gilkes, D. M., Semenza, G. L., & Wirtz, D. (2014). Hypoxia and the extracellular matrix: Drivers of tumour metastasis. *Nature Reviews Cancer*, *14*(6), 430–439. doi: 10.1038/nrc3726

Glaysher, S., & Cree, I. A. (2011). Cancer cell culture. *Methods in Molecular Biology (Clifton, N.J.)*, *731*(5), 135–140. doi: 10.1007/978-1-61779-080-5

Goldman, J. M., & Melo, J. V. (2003). Chronic myeloid leukemia--Advances in

biology and new approaches to treatment. *The New England Journal of Medicine*, 349(15),1451–1464. doi: 10.1056/NEJMra020777

Gombotz, W. R., & Pettit, D. K. (1995). Biodegradable polymers for protein and peptide drug delivery. *Bioconjugate Chemistry*, 6(4), 332–351. doi: 10.1021/bc00034a002

Gombotz, W. R., & Wee, S. (1998). Protein release from alginate matrices. *Advanced Drug Delivery Reviews*, 31(3), 267–285. doi: 10.1016/S0169-409X(97)00124-5

Gombotz, W. R., & Wee, S. F. (2012). Protein release from alginate matrices. *Advanced Drug Delivery Reviews*, 194–205. doi: 10.1016/j.addr.2012.09.007

Gomes, M. E., & Reis, R. L. (2004). Biodegradable polymers and composites in biomedical applications: From catgut to tissue engineering. *International Materials Reviews*, 49(5), 261–273.

Gorre, M. E., Mohammed, M., Ellwood, K., Hsu, N., Paquette, R., Rao, P. N., & Sawyers, C. L. (2001). Clinical resistance to STI-571 cancer therapy caused by BCR-ABL gene mutation or amplification. *Science*, 293(5531), 876–880. doi: 10.1126/science.1062538

Goycoolea, F. M., Lollo, G., Remunán-López, C., Quaglia, F., & Alonso, M. J. (2009). Chitosan-alginate blended nanoparticles as carriers for the transmucosal delivery of macromolecules. *Biomacromolecules*, 10(7), 1736–1743. doi: 10.1021/bm9001377

Van Der Graaf, S., Nisisako, T., Schroen, C. G. P. H., Van Der Sman, R. G. M., & Boom, R. M. (2006). Lattice Boltzmann simulations of droplet formation in a T-shaped microchannel. *Langmuir*, 22(9), 4144–4152. doi: 10.1021/la052682f

Griessinger, E., Anjos-Afonso, F., Pizzitola, I., Rouault-Pierre, K., Vargaftig, J., Taussig, D., ... & Bonnet, D. (2014). A niche-like culture system allowing the maintenance of primary human acute myeloid leukemia-initiating cells: A new tool to decipher their chemoresistance and self-renewal mechanisms. *Stem Cells Translational Medicine*, 3(4), 520–529. doi: 10.5966/sctm.2013-0166

Ham, R. G. (1963). An improved nutrient solution for diploid Chinese hamster and human cell lines. *Experimental Cell Research*, 29(3), 515–526. doi: 10.1016/S0014-4827(63)80014-2

Hayflick, L. (1965). The limited in vitro lifetime of human diploid cell strains. *Experimental Cell Research*, 37(3), 614–636. doi: 10.1016/0014-4827(65)90211-9

Haylock, D. N., To, L. B., Dowse, T. L., Juttner, C. A., & Simmons, P. J. (1992).

Ex vivo expansion and maturation of peripheral blood CD34+ cells into the myeloid lineage. *Blood*, 80(6), 1405–1412.

Haynesworth, S. E., Reuben, D., & Caplan, A. I. (1998). Cell-based tissue engineering therapies: The influence of whole body physiology. *Advanced Drug Delivery Reviews*, 33(1–2), 3–14. doi: 10.1016/S0169-409X(98)00016-7

Hochhaus, A., O'Brien, S. G., Guilhot, F., Druker, B. J., Branford, S., Foroni, L., ... & Mone, M. (2009). Six-year follow-up of patients receiving imatinib for the first-line treatment of chronic myeloid leukemia. *Leukemia : Official journal of the Leukemia Society of America, Leukemia Research Fund, U.K*, 23(6), 1054–1061. doi: 10.1038/leu.2009.38

Hollister, S. J. (2005). Porous scaffold design for tissue engineering. *Nature Materials*, 4(7), 518–524. doi: 10.1038/nmat1421

Hu, X., Liu, S., Zhou, G., Huang, Y., Xie, Z., & Jing, X. (2014). Electrospinning of polymeric nanofibers for drug delivery applications. *Journal of Controlled Release*, 185, 12–21. doi: 10.1016/j.jconrel.2014.04.018

Huang, Z. M., Zhang, Y. Z., Kotaki, M., & Ramakrishna, S. (2003). A review on polymer nanofibers by electrospinning and their applications in nanocomposites. *Composites Science and Technology*, 63(15), 2223–2253. doi: 10.1016/S0266-3538(03)00178-7

Hutchinson, L., & Kirk, R. (2011). High drug attrition rates – Where are we going wrong? *Nature Reviews Clinical Oncology*, 189–190. doi: 10.1038/nrclinonc.2011.34

Imamura, Y., Mukohara, T., Shimono, Y., Funakoshi, Y., Chayahara, N., Toyoda, M., ... & Minami, H. (2015). Comparison of 2D- and 3D-culture models as drug-testing platforms in breast cancer. *Oncology Reports*, 33(4), 1837–1843. doi: 10.3892/or.2015.3767

Irigoyen, M., García-Ruiz, J.C., & Berra, E. (2017). The hypoxia signalling pathway in haematological malignancies. *Oncotarget*, 8(22), 36832–36844.

Ishikawa, F., Yoshida, S., Saito, Y., Hijikata, A., Kitamura, H., Tanaka, S., ... & Fukata, M. (2007). Chemotherapy-resistant human AML stem cells home to and engraft within the bone-marrow endosteal region. *Nature Biotechnology*, 25(11), 1315–1321. doi: 10.1038/nbt1350

James, H. P., John, R., Alex, A., & Anoop, K. R. (2014). Smart polymers for the controlled delivery of drugs – A concise overview. *Acta Pharmaceutica Sinica B*, 4(2), 120–127. doi: 10.1016/j.apsb.2014.02.005

- Jana, S., Gandhi, A., Sen, K. K., & Basu, S. K. (2011). Natural polymers and their application in drug delivery and biomedical field. *Journal of PharmaSciTech*, 1(1), 16–27.
- Jeitziner, M. (2014). Spectroscopic reagents for UV/Vis by Sigma Aldrich. *AnalytiX*, 7(Article 3).
- Jiang, X. S., Chai, C., Zhang, Y., Zhuo, R. X., Mao, H. Q., & Leong, K. W. (2006). Surface-immobilization of adhesion peptides on substrate for ex vivo expansion of cryopreserved umbilical cord blood CD34+ cells. *Biomaterials*, 27(13), 2723–2732. doi: 10.1016/j.biomaterials.2005.12.001
- Jiménez, C., Talavera, B., Saez, C., Cañizares, P., & Rodrigo, M. A. (2010). Study of the production of hydrogen bubbles at low current densities for electroflotation processes. *Journal of Chemical Technology and Biotechnology*, 85(10), 1368–1373. doi: 10.1002/jctb.2442
- Johnson, J. I., Decker, S., Zaharevitz, D., Rubinstein, L. V., Venditti, J. M., Schepartz, S., ... & Sausville, E. A. (2001). Relationships between drug activity in NCI preclinical in vitro and in vivo models and early clinical trials. *British Journal of Cancer*, 84(10), 1424–1431. doi: 10.1054/bjoc.2001.1796
- Kang, S.-T., & Yeh, C.-K. (2012). Ultrasound microbubble contrast agents for diagnostic and therapeutic applications: Current status and future design. *Chang Gung Medical Journal*, 35(2), 125–139.
- Kantarjian, H., O'Brien, S., Jabbour, E., Garcia-Manero, G., Quintas-Cardama, A., Shan, J., ... & Borthakur, G. (2012). Improved survival in chronic myeloid leukemia since the introduction of imatinib therapy: A single-institution historical experience. *Blood*, 119(9), 1981–1987. doi: 10.1182/blood-2011-08-358135
- Kappelle, W. F. W., & Vleggaar, F. P. (2016). Palliative treatment of malignant dysphagia: Stent by and await further instructions. *Gastrointestinal Endoscopy*, 83(4), 753–755. doi: 10.1016/j.gie.2015.10.012
- Karimpoor, M., Illangakoon, E., Reid, A. G., Claudiani, S., Edirisinghe, M., & Khorashad, J. S. (2017). Development of artificial bone marrow fibre scaffolds to study resistance to anti-leukaemia agents. *British Journal of Haematology*. doi: 10.1111/bjh.14883
- Ketkar, D. R., Mallikarjunan, R., & Venkatachalam, S. (1991). Electroflotation of quartz fines. *International Journal of Mineral Processing*, 31(1–2), 127–138. doi: 10.1016/0301-7516(91)90009-8
- Khorashad, J. S., de Lavallade, H., Apperley, J. F., Milojkovic, D., Reid, A. G.,

- Bua, M., ... & Marin, D. (2008). Finding of kinase domain mutations in patients with chronic phase chronic myeloid leukemia responding to imatinib may identify those at high risk of disease progression. *Journal of Clinical Oncology : Official Journal of the American Society of Clinical Oncology*, 26(29), 4806–4813. doi: 10.1200/JCO.2008.16.9953
- Kikendall, J. W., Friedman, A. C., Oyewole, M. A., Fleischer, D., & Johnson, L. F. (1983). Pill-induced esophageal injury. Case reports and review of the medical literature. *Digestive Diseases and Sciences*, 28(2), 174–182. doi: 10.1007/BF01315148
- Kim, J. W., Ho, W. J., & Wu, B. M. (2011). The role of the 3D environment in hypoxia-induced drug and apoptosis resistance. *Anticancer Research*, 31(10), 3237–3245.
- Lee, S., Shin, S., Kim, H., Han, S., Kim, K., Kwon, J., ... & Kim, K. (2011). Anti-inflammatory function of arctiin by inhibiting COX-2 expression via NF- $\kappa$ B pathways. *Journal of Inflammation*, 8(1), 16. doi: 10.1186/1476-9255-8-16
- Klibanov, A. L. (1999). Targeted delivery of gas-filled microspheres, contrast agents for ultrasound imaging. *Advanced Drug Delivery Reviews*, 37(1–3), 139–157. doi: 10.1016/S0169-409X(98)00104-5
- Krivtsov, A. V., Twomey, D., Feng, Z., Stubbs, M. C., Wang, Y., Faber, J., ... & Golub, T. R. (2006). Transformation from committed progenitor to leukaemia stem cell initiated by MLL-AF9. *Nature*, 442(7104), 818–822. doi: 10.1038/nature04980
- Kučerka, N., Nieh, M. P., & Katsaras, J. (2011). Fluid phase lipid areas and bilayer thicknesses of commonly used phosphatidylcholines as a function of temperature. *Biochimica et Biophysica Acta (BBA)-Biomembranes*, 1808(11), 2761–2771.
- Kulkarni, V., Butte, K., & Rathod, S. (2012). Natural polymers – A comprehensive review. *International Journal of Research in Pharmaceutical and Biomedical Sciences*, 3(4), 1597–1613.
- Kumar, A., & Starly, B. (2015). Large scale industrialized cell expansion: Producing the critical raw material for biofabrication processes. *Biofabrication*, 7(4), 044103. doi: 10.1088/1758-5090/7/4/044103
- Kunz-Schughart, L. A., Freyer, J. P., Hofstaedter, F., & Ebner, R. (2004). The use of 3-D cultures for high-throughput screening: The multicellular spheroid model. *Journal of Biomolecular Screening*, 9(4), 273–285. doi: 10.1177/1087057104265040
- Lai, X., Price, C., Modla, S., Thompson, W. R., Caplan, J., Kirn-Safran, C. B., &

- Wang, L. (2015). The dependences of osteocyte network on bone compartment, age, and disease. *Bone Research*, 3, 15009. doi: 10.1038/boneres.2015.9
- de Lavallade, H., Apperley, J. F., Khorashad, J. S., Milojkovic, D., Reid, A. G., Bua, M., ... & Marin, D. (2008). Imatinib for newly diagnosed patients with chronic myeloid leukemia: Incidence of sustained responses in an intention-to-treat analysis. *Journal of Clinical Oncology*, 26(20), 3358–3363. doi: 10.1200/JCO.2007.15.8154
- Lawrence, B. J., & Madihally, S. V. (2008). Cell colonization in degradable 3D porous matrices. *Cell Adhesion & Migration*, 2(1), 9–16. doi: 10.4161/cam.2.1.5884
- Le, T. S., McCann, M., Azarin, S. M., & Hu, W. S. (2016). An introduction to mammalian cell culture. *Chemical Engineering Progress*, 112(4), 34–40.
- Lee, K. Y., & Mooney, D. J. (2012). Alginate: Properties and biomedical applications. *Progress in Polymer Science*, 37(1), 106–126. doi: 10.1016/j.progpolymsci.2011.06.003
- Lee, K., Silva, E. A., & Mooney, D. J. (2011). Growth factor delivery-based tissue engineering: General approaches and a review of recent developments. *Journal of The Royal Society Interface*, 8(55), 153–170. doi: 10.1098/rsif.2010.0223
- Levitzki, A., & Gazit, A. (1995). Tyrosine kinase inhibition: An approach to drug development. *Science (New York, N.Y.)*, 267(5205), 1782–1788. doi: 10.1126/SCIENCE.7892601
- Li, M., Mondrinos, M. J., Gandhi, M. R., Ko, F. K., Weiss, A. S., & Lelkes, P. I. (2005). Electrospun protein fibers as matrices for tissue engineering. *Biomaterials*, 26(30), 5999–6008. doi: 10.1016/j.biomaterials.2005.03.030
- Liechty, W. B., Kryscio, D. R., Slaughter, B. V., & Peppas, N. (2010). Polymers for drug delivery systems. *Annual Review of Chemical and Biomolecular Engineering*, 1(1), 149–173. doi: 10.1146/annurev-chembioeng-073009-100847
- Liu, J., Morykwas, M. J., Argenta, L. C., & Wagner, W. D. (2011). Development of a biodegradable foam for use in negative pressure wound therapy. *Journal of Biomedical Materials Research – Part B Applied Biomaterials*, 98B(2), 316–322. doi: 10.1002/jbm.b.31854
- Liu, H., & Roy, K. (2005). Biomimetic three-dimensional cultures significantly increase hematopoietic differentiation efficacy of embryonic stem cells. *Tissue Engineering*, 11(1–2), 319–330. doi: 10.1089/ten.2005.11.319
- Longo, D. L. (Ed.). (2015). Acute myeloid leukemia. *New England Journal of Medicine*, 373(12), 1136–1152. doi: 10.1056/NEJMra1406184

- Loscertales, I. G., Barrero, A., Guerrero, I., Cortijo, R., Marquez, M., & Ganan-Calvo, A. M. (2002). Micro/nano encapsulation via electrified coaxial liquid jets. *Science*, 295(5560), 1695–1698. doi: 10.1126/science.1067595
- Luca, A. C., Mersch, S., Deenen, R., Schmidt, S., Messner, I., Schäfer, K. L., ... & Krieg, A. (2013). Impact of the 3D microenvironment on phenotype, gene expression, and EGFR inhibition of colorectal cancer cell lines. *PLoS ONE*, 8(3). doi: 10.1371/journal.pone.0059689
- Lucas, C. M., Wang, L., Austin, G. M., Knight, K., Watmough, S. J., Shwe, K. H., ... & Seale, J. R. C. (2008). A population study of imatinib in chronic myeloid leukaemia demonstrates lower efficacy than in clinical trials. *Leukemia*, 22(10), 1963–1966. doi: 10.1038/leu.2008.225
- Ma, P. X., & Zhang, R. (1999). Synthetic nano-scale fibrous extracellular matrix. *Journal of Biomedical Materials Research*, 46(1), 60–72. doi: 10.1002/(SICI)1097-4636(199907)46:1<60::AID-JBM7>3.0.CO;2-H
- Di Maggio, N., Piccinini, E., Jaworski, M., Trumpp, A., Wendt, D. J., & Martin, I. (2011). Toward modeling the bone marrow niche using scaffold-based 3D culture systems. *Biomaterials*, 32(2), 321–329. doi: 10.1016/j.biomaterials.2010.09.041
- Mahadevan, V. (2017). Anatomy of the oesophagus. *Surgery (United Kingdom)*, 35(11), 603–607. doi: 10.1016/j.mpsur.2017.08.003
- Mahalingam, S., Meinders, M. B. and Edirisinghe, M. (2014) ‘Formation, stability, and mechanical properties of bovine serum albumin stabilized air bubbles produced using coaxial electrohydrodynamic atomization’, *Langmuir*, 30(23), pp. 6694–6703. doi: 10.1021/la5011715.
- Malafaya, P. B., Silva, G. A., & Reis, R. L. (2007). Natural-origin polymers as carriers and scaffolds for biomolecules and cell delivery in tissue engineering applications. *Advanced Drug Delivery Reviews*, 59(4–5), 207–233. doi: 10.1016/j.addr.2007.03.012
- Malik, R., Garg, T., Goyal, A. K., & Rath, G. (2015). Polymeric nanofibers: Targeted gastro-retentive drug delivery systems. *Journal of Drug Targeting*, 109–124. doi: 10.3109/1061186X.2014.965715
- Mano, J. F., Silva, G. A., Azevedo, H. S., Malafaya, P. B., Sousa, R. A., Silva, S. S., ... & Neves, N. M. (2007). Natural origin biodegradable systems in tissue engineering and regenerative medicine: Present status and some moving trends. *Journal of The Royal Society Interface*, 4(17), 999–1030. doi: 10.1098/rsif.2007.0220

- Mansuri, S., Kesharwani, P., Jain, K., Tekade, R. K., & Jain, N. K. (2016). Mucoadhesion: A promising approach in drug delivery system. *Reactive and Functional Polymers*, 151–172. doi: 10.1016/j.reactfunctpolym.2016.01.011
- Martinez, C. J. (2009). Bubble generation in microfluidic devices. *Bubble Science, Engineering & Technology*, 1(1), 40–52. doi: 10.1179/175889709X446561
- Medyouf, H. (2017). The microenvironment in human myeloid malignancies: Emerging concepts and therapeutic implications. *Blood*, 129(12), 1617–1626. doi: 10.1182/blood-2016-11-696070
- Meng, X., Leslie, P., Zhang, Y., & Dong, J. (2014). Stem cells in a three-dimensional scaffold environment. *SpringerPlus*, 3(1), 1–8. doi: 10.1186/2193-1801-3-80.
- Mikos, A. G., Thorsen, A. J., Czerwonka, L. A., Bao, Y., Langer, R., Winslow, D. N., & Vacanti, J. P. (1994). Preparation and characterization of poly(l-lactic acid) foams, *Polymer*, 35(5), 1068–1077. doi: 10.1016/0032-3861(94)90953-9
- Mittal, R. K., & Goyal, R. K. (2006). Sphincter mechanisms at the lower end of the esophagus. *GI Motility online*, pp. 1–34. doi: 10.1038/gimo14.
- Mohamed Abdulkadir Hassan Kadle, O. M. D. (2015). Oesophageal carcinoma in a young adult somali patient: A case report with brief literature review. *Case Reports in Clinical Medicine*, 4.
- Mohamedi, G., Azmin, M., Pastoriza-Santos, I., Huang, V., Pérez-Juste, J., Liz-Marzán, L. M., ... & Stride, E. (2012). Effects of gold nanoparticles on the stability of microbubbles. *Langmuir*, 28(39), 13808–13815.
- Moore, G. E., & Glick, J. L. (1967). Perspective of human cell culture. *The Surgical Clinics of North America*, 47(6), 1315–1324. doi: 10.1016/S0039-6109(16)38380-3
- Moore, G. E., & Pickren, J. W. (1967). Study of a virus-containing hematopoietic cell line and a melanoma cell line derived from a patient with a leukemoid reaction. *Lab Invest*, 16(6), 882–891.
- Morrison, S. J., & Spradling, A. C. (2008). Stem cells and niches: Mechanisms that promote stem cell maintenance throughout life. *Cell*, 132(4), 598–611. doi: 10.1016/j.cell.2008.01.038
- Murakami, H., & Masui, H. (1980). Hormonal control of human colon carcinoma cell growth in serum-free medium. *Proceedings of the National Academy of Sciences of the United States of America*, 77(6), 3464–3468.
- Mustin, B., & Stoeber, B. (2008). Design considerations for robust suspension-

- based microfluidic systems for biomedical applications. In *2008 IEEE 14th International Mixed-Signals, Sensors, and Systems Test Workshop, IMS3TW*. doi: 10.1109/IMS3TW.2008.4581610
- Nair, L. S., & Laurencin, C. T. (2007). Silver nanoparticles: Synthesis and therapeutic applications. *Journal of Biomedical Nanotechnology*, 3(4), 301–316. doi: 10.1166/jbn.2007.041
- Nair, A., Thevenot, P., Dey, J., Shen, J., Sun, M. W., Yang, J., & Tang, L. (2010). Novel polymeric scaffolds using protein microbubbles as porogen and growth factor carriers. *Tissue Engineering. Part C, Methods*, 16(1), 23–32. doi: 10.1089/ten.TEC.2009.0094
- Napper, D. H. (1977). Steric stabilization. *Journal of Colloid and Interface Science*, 58(2), 390–407. doi: 10.1016/0021-9797(77)90150-3
- Nayak, A. K., Maji, R., & Das, B. (2010). Gastroretentive drug delivery systems: A review. *Asian Journal of Pharmaceutical and Clinical Research*, 3(1), 2–10.
- Nelson, M. R., & Roy, K. (2016). Bone-marrow mimicking biomaterial niches for studying hematopoietic stem and progenitor cells. *J. Mater. Chem. B*, 4(20), 3490–3503. doi: 10.1039/C5TB02644J
- O'Hare, T., Walters, D. K., Stoffregen, E. P., Jia, T., Manley, P. W., Mestan, J., ... & Druker, B. J. (2005). In vitro activity of Bcr-Abl inhibitors AMN107 and BMS-354825 against clinically relevant imatinib-resistant Abl kinase domain mutants. *Cancer Research*, 65(11), 4500–4505. doi: 10.1158/0008-5472.CAN-05-0259
- Østberg, T., Vesterhus, L., & Graffner, C. (1993). Calcium alginate matrices for oral multiple unit administration: II. Effect of process and formulation factors on matrix properties. *International Journal of Pharmaceutics*, 97(1–3), 183–193. doi: 10.1016/0378-5173(93)90138-6
- Owen, J., Crake, C., Lee, J. Y., Carugo, D., Beguin, E., Khrapitchev, A. A., ... & Stride, E. (2017). A versatile method for the preparation of particle-loaded microbubbles for multimodality imaging and targeted drug delivery. *Drug Delivery and Translational Research*, 1–15. doi: 10.1007/s13346-017-0366-7
- Owen, J., Grove, P., Rademeyer, P., & Stride, E. (2014). The influence of blood on targeted microbubbles. *Journal of the Royal Society, Interface / The Royal Society*, 11(100), 20140622. doi: 10.1098/rsif.2014.0622
- Parhizkar, M., Edirisinghe, M., & Stride, E. (2013). Effect of operating conditions and liquid physical properties on the size of monodisperse microbubbles produced in a capillary embedded T-junction device. *Microfluidics and Nanofluidics. Royal*

*Society of Chemistry*, 14(5), 797–808. doi: 10.1007/s10404-012-1098-0

Parhizkar, M., Edirisinghe, M., & Stride, E. (2015). The effect of surfactant type and concentration on the size and stability of microbubbles produced in a capillary embedded T-junction device. *RSC Adv.*, 5(14), 10751–10762. doi: 10.1039/C4RA15167D

Parhizkar, M., Sofokleous, P., Stride, E., & Edirisinghe, M. (2014). Novel preparation of controlled porosity particle/fibre loaded scaffolds using a hybrid micro-fluidic and electrohydrodynamic technique. *Biofabrication*, 6(4), 45010. doi: 10.1088/1758-5082/6/4/045010

Parhizkar, M., Stride, E., & Edirisinghe, M. (2014). Preparation of monodisperse microbubbles using an integrated embedded capillary T-junction with electrohydrodynamic focusing. *Lab on a Chip*, 14(14), 2437–2446. doi: 10.1039/c4lc00328d

Park, H., Radisic, M., Lim, J. O., Chang, B. H., & Vunjak-Novakovic, G. (2005). A novel composite scaffold for cardiac tissue engineering. *In Vitro Cellular & Developmental Biology-Animal*, 41(7), 188–196. doi: 10.1290/0411071.1

Parmar, A., Marz, S., Rushton, S., Holzwarth, C., Lind, K., Kayser, S., ... & Götze, K. S. (2011). Stromal niche cells protect early leukemic FLT3-ITD+progenitor cells against first-generation FLT3 tyrosine kinase inhibitors. *Cancer Research*, 71(13), 4696–4706. doi: 10.1158/0008-5472.CAN-10-4136

Patel, N., & Gohil, P. (2012). A review on biomaterials: Scope, applications & human anatomy significance. *International Journal of Emerging Technology and Advanced Engineering*, 2(4), 91–101.

Pawar, V. K., Kansal, S., Garg, G., Awasthi, R., Singodia, D., & Kulkarni, G. T. (2011). Gastroretentive dosage forms: A review with special emphasis on floating drug delivery systems. *Drug Delivery*, 97–110. doi: 10.3109/10717544.2010.520354

Pereira, R. F., Barrias, C. C., Granja, P. L., & Bartolo, P. J. (2013). Advanced biofabrication strategies for skin regeneration and repair. *Nanomedicine*, 8(4), 603–621. doi: 10.2217/nnm.13.50

Phipps, M. C., Clem, W. C., Catledge, S. A., Xu, Y., Hennessy, K. M., Thomas, V., ... & Bellis, S. L. (2011). Mesenchymal stem cell responses to bone-mimetic electrospun matrices composed of polycaprolactone, collagen I and nanoparticulate hydroxyapatite. *PLoS ONE*, 6(2), e16813. doi: 10.1371/journal.pone.0016813

Pietrzyk-Nivau, A., Poirault-Chassac, S., Gandrille, S., Derkaoui, S. M., Kauskot,

- A., Letourneur, D., ... & Baruch, D. (2015). Three-dimensional environment sustains hematopoietic stem cell differentiation into platelet-producing megakaryocytes. *PLoS ONE*, *10*(8), e0136652. doi: 10.1371/journal.pone.0136652
- Pillai, O., & Panchagnula, R. (2001). Insulin therapies – Past, present and future. *Drug Discovery Today*, *6*(20), 1056–1061. doi: 10.1016/S1359-6446(01)01962-6
- Plaks, V., Kong, N., & Werb, Z. (2015). The cancer stem cell niche: How essential is the niche in regulating stemness of tumor cells? *Cell Stem Cell*, *16*(3), 225–238. doi: 10.1016/j.stem.2015.02.015
- Pollyea, D. A., & Jordan, C. T. (2017). Therapeutic targeting of acute myeloid leukemia stem cells. *Blood*, *129*(12), 1627–1635. doi: 10.1182/blood-2016-10-696039.
- Pooja Mathur, Kamal Saroha, Navneet Syan \*, S. V. and V. K. (2010). Floating drug delivery system: An innovative acceptable approach in gastroretentive drug delivery, Scholars Research Library. Kurukshetra, Haryana, India.
- Prajapati, J., & Agrawal, Y. (2012). Synthesis, characterization and application of microbubbles: A review. *International Journal*, *3*(06), 1532–1543.
- Prasad, K. N., & Kumar, S. (1975). Role of cyclic AMP in differentiation of human neuroblastoma cells in culture. *Cancer*, *36*(4), 1338–1343.
- Redaelli, S., Piazza, R., Rostagno, R., Magistroni, V., Perini, P., Marega, M., ... & Boschelli, F. (2009). Activity of bosutinib, dasatinib, and nilotinib against 18 imatinib-resistant BCR/ABL mutants. *Journal of Clinical Oncology*, *27*(3), 469–471. doi: 10.1200/JCO.2008.19.8853
- Rinaudo, M. (2008). Polyelectrolytes derived from natural polysaccharides. In *Monomers, Polymers and Composites from Renewable Resources*, pp. 495–516. doi: 10.1016/B978-0-08-045316-3.00024-7
- Rödling, L., Schwedhelm, I., Kraus, S., Bieback, K., Hansmann, J., & Lee-Thedieck, C. (2017). 3D models of the hematopoietic stem cell niche under steady-state and active conditions. *Scientific Reports*, *7*(1). doi: 10.1038/s41598-017-04808-0
- Rodrigues, R. T., & Rubio, J. (2007). DAF–dissolved air flotation: Potential applications in the mining and mineral processing industry. *International Journal of Mineral Processing*, *82*(1), 1–13. doi: 10.1016/j.minpro.2006.07.019
- Rosa, A. L., de Oliveira, P. T., & Beloti, M. M. (2008). Macroporous scaffolds associated with cells to construct a hybrid biomaterial for bone tissue engineering. *Expert Review of Medical Devices*, *5*(6), 719–728. doi: 10.1586/17434440.5.6.719

- Rossi, D. J., Jamieson, C. H. M., & Weissman, I. L. (2008). Stems cells and the pathways to aging and cancer. *Cell*, *132*(4), 681–696. doi: 10.1016/j.cell.2008.01.036
- Ryan, S. L., Baird, A. M., Vaz, G., Urquhart, A. J., Senge, H., Richard, D. J., ... & Davies, A. M. (2016). Drug discovery approaches utilizing three-dimensional cell culture. *ASSAY and Drug Development Technologies*, *14*(1), 19–28. doi: 10.1089/adt.2015.670
- Sagdic, E., Bolukcu, E., & Kilic, S. (2015). Effect of temperature on lipid-based microbubbles. 2015-01564. doi: 10.2514/3.2192
- Saleh, F. A., & Genever, P. G. (2011). Turning round: Multipotent stromal cells, a three-dimensional revolution? *Cytotherapy*, *13*(8), 903–912. doi: 10.3109/14653249.2011.586998
- Sato, J. D., Gao, H. T., Kayada, Y., Cabot, M. C., Sato, G. H., Okamoto, T., & Welsh, C. J. (1988). Effects of proximate cholesterol precursors and steroid hormones on mouse myeloma growth in serum-free medium. *In Vitro Cellular & Developmental Biology*, *24*(12), 1223–1228. doi: 10.1007/BF02624194
- Schofield, R. (1978). The relationship between the spleen colony-forming cell and the haemopoietic stem cell. *Blood Cells*, *4*(1–2), 7–25.
- Shah, N. P., Nicoll, J. M., Nagar, B., Gorre, M. E., Paquette, R. L., Kuriyan, J., & Sawyers, C. L. (2002). Multiple BCR-ABL kinase domain mutations confer polyclonal resistance to the tyrosine kinase inhibitor imatinib (STI571) in chronic phase and blast crisis chronic myeloid leukemia. *Cancer Cell*, *2*(2), 117–125. doi: 10.1016/S1535-6108(02)00096-X
- Sharma, M. B., Limaye, L. S., & Kale, V. P. (2012). Mimicking the functional hematopoietic stem cell niche in vitro: Recapitulation of marrow physiology by hydrogel-based three-dimensional cultures of mesenchymal stromal cells. *Haematologica*, *97*(5), 651–660. doi: 10.3324/haematol.2011.050500
- Shay, J. W., & Wright, W. E. (2000). Hayflick, his limit, and cellular ageing. Nature reviews. *Molecular Cell Biology*, *1*(1), 72–76. doi: 10.1038/35036093
- Shen, Y., Longo, M. L., & Powell, R. L. (2008). Stability and rheological behavior of concentrated monodisperse food emulsifier coated microbubble suspensions. *Journal of Colloid and Interface Science*, *327*(1), 204–210. doi: 10.1016/j.jcis.2008.07.047
- Sirsi, S. R., & Borden, M. A. (2009). Microbubble compositions, properties and biomedical applications. *Bubble Science, Engineering & Technology*, *1*(1–2), 3–17.

doi: 10.1179/175889709X446507

Smart, J. D. (2005). The basics and underlying mechanisms of mucoadhesion. *Advanced Drug Delivery Reviews*, 57(11), 1556–1568. doi: 10.1016/j.addr.2005.07.001

Smith, C. C., Wang, Q., Chin, C. S., Salerno, S., Damon, L. E., Levis, M. J., ... & Zarrinkar, P. P. (2012). Validation of ITD mutations in FLT3 as a therapeutic target in human acute myeloid leukaemia. *Nature*, 485(7397), 260–263. doi: 10.1038/nature11016

Stepniewski, M., Pasenkiewicz-Gierula, M., Róg, T., Danne, R., Orłowski, A., Karttunen, M., ... & Bunker, A. (2011). Study of PEGylated lipid layers as a model for PEGylated liposome surfaces: Molecular dynamics simulation and langmuir monolayer studies. *Langmuir*, 27(12), 7788–7798. doi: 10.1021/la200003n

Stolze, B., Emmendorffer, A., Corbacioglu, S., König, A., Welte, K., & Ebell, W. (1995). Effects of bone marrow fibroblasts on the proliferation and differentiation of myeloid leukemic cell lines. *Experimental Hematology*, 23(13), 1378–1387.

Stops, F., Fell, J. T., Collett, J. H., & Martini, L. G. (2008). Floating dosage forms to prolong gastro-retention—The characterisation of calcium alginate beads', *International Journal of Pharmaceutics*, 350(1–2), 301–311. doi: 10.1016/j.ijpharm.2007.09.009

Stride, E. (2009). Physical principles of microbubbles for ultrasound imaging and therapy, *Cerebrovascular Diseases*, 27(SUPPL. 2), 1–13. doi: 10.1159/000203122

Stride, E., & Edirisinghe, M. (2008). Novel microbubble preparation technologies. *Soft Matter*, 4(12), 2350–2359. doi: 10.1039/b809517p

Stride, E., & Edirisinghe, M. (2009). Novel preparation techniques for controlling microbubble uniformity: A comparison. *Medical and Biological Engineering and Computing*, 47(8), 883–892. doi: 10.1007/s11517-009-0490-8

Stride, E., & Saffari, N. (2003a). Investigating the potential for thermal damage posed by microbubble ultrasound contrast agents.

Stride, E., & Saffari, N. (2003b). Microbubble ultrasound contrast agents: A review. *Proceedings of the Institution of Mechanical Engineers, Part H: Journal of Engineering in Medicine*, 217(6), 429–447. doi: 10.1243/09544110360729072

Sullivan, A. C. and Jayasinghe, S. N. (2007). Development of a direct three-dimensional biomicrofabrication concept based on electro spraying a custom made siloxane sol. *Biomicrofluidics*, 1(3), 034103. doi: 10.1063/1.2766761

- Suslick, K. S., Didenko, Y., Fang, M. M., Hyeon, T., Kolbeck, K. J., McNamara, W. B., ... & Wong, M. (1999). Acoustic cavitation and its chemical consequences. *Philosophical Transactions of the Royal Society A: Mathematical, Physical and Engineering Sciences*, 357(1751), 335–353. doi: 10.1098/rsta.1999.0330
- Szekely, P., Dvir, T., Asor, R., Resh, R., Steiner, A., Szekely, O., ... & Wolf, T. (2011). Effect of temperature on the structure of charged membranes. *J Phys Chem B*, 115(49), 14501–14506.
- Szűjjártó, C., Rossi, S., Waton, G., & Krafft, M. P. (2012). Effects of perfluorocarbon gases on the size and stability characteristics of phospholipid-coated microbubbles: Osmotic effect versus interfacial film stabilization. *Langmuir*, 28(2), 1182–1189. doi: 10.1021/la2043944
- Tabe, Y., & Konopleva, M. (2015). Role of microenvironment in resistance to therapy in AML. *Current Hematologic Malignancy Reports*, 10(2), 96–103. doi: 10.1007/s11899-015-0253-6
- Talukder, R., & Fassihi, R. (2004). Gastroretentive delivery systems: A mini review. *Drug Development and Industrial Pharmacy*, 30(10), 1019–1028. doi: 10.1081/DDC-200040239
- Tan, J., Liu, T., Hou, L., Meng, W., Wang, Y., Zhi, W., & Deng, L. (2010). Maintenance and expansion of hematopoietic stem/progenitor cells in biomimetic osteoblast niche. *Cytotechnology*, 62(5), 439–448. doi: 10.1007/s10616-010-9297-6
- Tang, K., & Gomez, A. (1994). On the structure of an electrostatic spray of monodisperse droplets. *Physics of Fluids*, 6(7), 2317–2332. doi: 10.1063/1.868182
- Tanturli, M., Giuntoli, S., Barbetti, V., Rovida, E., & Sbarba, P. D. (2011). Hypoxia selects Bortezomib-resistant stem cells of chronic myeloid leukemia. *PLoS ONE*, 6(2), e17008. doi: 10.1371/journal.pone.0017008
- Terstappen, L. W., & Loken, M. R. (1990). Myeloid cell differentiation in normal bone marrow and acute myeloid leukemia assessed by multi-dimensional flow cytometry. *Analytical Cellular Pathology: The Journal of the European Society for Analytical Cellular Pathology*, 2(4), 229–240.
- TFOT, c2017. The Future of Things website. [online]. [Accessed 01 August 2018]. Available from: <https://thefutureofthings.com/3805-ultrasound-activated-microbubbles-fight-cancer/>
- Todaro, G. J., & Green, H. (1963). Quantitative studies of the growth of mouse embryo cells in culture and their development into established lines. *The Journal of Cell Biology*, 17(2), pp. 299–313. doi: 10.1083/jcb.17.2.299

- Toussaint, J., Gossuin, A., Deruyttere, M., Huble, F., & Devis, G. (1991). Healing and prevention of relapse of reflux oesophagitis by cisapride. *Gut*, *32*(11), 1280–1285. doi: 10.1136/gut.32.11.1280
- Tseng, L. F., Mather, P. T., & Henderson, J. H. (2013). Shape-memory-actuated change in scaffold fiber alignment directs stem cell morphology. *Acta Biomaterialia*, *9*(11), 8790–8801. doi: 10.1016/j.actbio.2013.06.043.
- Vakarelski, I. U., Manica, R., Tang, X., O'Shea, S. J., Stevens, G. W., Grieser, F., ... & Chan, D. Y. (2010). Dynamic interactions between microbubbles in water. *Proceedings of the National Academy of Sciences*, *107*(25), 11177–11182. doi: 10.1073/pnas.1005937107
- Vats, A., Tolley, N. S., Polak, J. M., & Gough, J. E. (2003). Scaffolds and biomaterials for tissue engineering: A review of clinical applications. *Clinical Otolaryngology and Allied Sciences*, *28*(3), 165–172. doi: 10.1046/j.1365-2273.2003.00686.x
- Venugopalan, G., Camarillo, D. B., Webster, K. D., Reber, C. D., Sethian, J. A., Weaver, V. M., ... & Rycroft, C. H. (2014). Multicellular architecture of malignant breast epithelia influences mechanics. *PLoS ONE*, *9*(8), e101955. doi: 10.1371/journal.pone.0101955
- Wang, H. J., Di, L., Ren, Q. S., & Wang, J. Y. (2009). Applications and degradation of proteins used as tissue engineering materials. *Materials*, *2*(2), 613–635. doi: 10.3390/ma2020613.
- Wang, J. C., & Dick, J. E. (2005). Cancer stem cells: Lessons from leukemia. *Trends in Cell Biology*, *15*(9), 494–501. doi: 10.1016/j.tcb.2005.07.004
- Wang, W., Moser, C. C., & Wheatley, M. A. (1996). Langmuir trough study of surfactant mixtures used in the production of a new ultrasound contrast agent consisting of stabilized microbubbles. *Journal of Physical Chemistry*, *100*(32), 13815–13821. doi: 10.1021/jp9613549
- Wang, T. Y., Wilson, K. E., Machtaler, S., & Willmann, J. K. (2013). Ultrasound and microbubble guided drug delivery: Mechanistic understanding and clinical implications. *Current Pharmaceutical Biotechnology*, *14*(8), 743–752. doi: 10.1016/j.biotechadv.2011.08.021.Secreted
- Weaver, V. M., Lelièvre, S., Lakins, J. N., Chrenek, M. A., Jones, J. C., Giancotti, F., ... & Bissell, M. J. (2002). Beta4 integrin-dependent formation of polarized three-dimensional architecture confers resistance to apoptosis in normal and malignant mammary epithelium. *Cancer Cell*, *2*(3), 205–216. doi: S1535610802001253 [pii]

- Weigelt, B., & Bissell, M. J. (2008). Unraveling the microenvironmental influences on the normal mammary gland and breast cancer. *Seminars in Cancer Biology*, 18(5), 311–321. doi: 10.1016/j.semcancer.2008.03.013
- Welge, L. S., & Berardi, R. R. (2000). Evaluation of omeprazole, lansoprazole, pantoprazole, and rabeprazole in the treatment of acid-related diseases. *Journal of the American Pharmaceutical Association (1996)*, 40(1), 52–62. doi: 10.1016/S1086-5802(16)31036-1
- Wells, W. A. (2005). A cell line that is under control. *Journal of Cell Biology*, 168(7), 988. doi: 10.1083/jcb1687fta1
- Wongsasulak, S., Puttipaiboon, N., & Yoovidhya, T. (2013). Fabrication, gastromucoadhesivity, swelling, and degradation of zein-chitosan composite ultrafine fibers. *Journal of Food Science*, 78(6). doi: 10.1111/1750-3841.12126
- Xiong, R., Bai, M., & Chung, J. N. (2007). Formation of bubbles in a simple co-flowing micro-channel. *Journal of Micromechanics and Microengineering*, 17(5), 1002–1011. doi: 10.1088/0960-1317/17/5/021
- Xu, N., Papagiannakopoulos, T., Pan, G., Thomson, J. A., & Kosik, K. S. (2009). MicroRNA-145 Regulates OCT4, SOX2, and KLF4 and represses pluripotency in human embryonic stem cells. *Cell*, 137(4), 647–658. doi: 10.1016/j.cell.2009.02.038
- Yin, Q., Shen, J., Zhang, Z., Yu, H., & Li, Y. (2013). Reversal of multidrug resistance by stimuli-responsive drug delivery systems for therapy of tumor. *Advanced Drug Delivery Reviews*, 65(13–14), 1699–1715. doi: 10.1016/j.addr.2013.04.011
- Yobas, L., Martens, S., Ong, W. L., & Ranganathan, N. (2006). High-performance flow-focusing geometry for spontaneous generation of monodispersed droplets. *Lab on a Chip*, 6(8), 1073. doi: 10.1039/b602240e
- Zhang, C., Xu, M., Tao, X., Tang, J., Liu, Z., Zhang, Y., ... & Tang, X. (2012). A floating multiparticulate system for ofloxacin based on a multilayer structure: In vitro and in vivo evaluation. *International Journal of Pharmaceutics. Elsevier B.V.*, 430(1–2), 141–150. doi: 10.1016/j.ijpharm.2012.04.013
- Zhang, Y., & Wang, L. (2009). Experimental investigation of bubble formation in a microfluidic T-shaped junction. *Nanoscale and Microscale Thermophysical Engineering*, 13(4), 228–242. doi: 10.1080/15567260903276999
- Zhang, J., Yan, S., Yuan, D., Alici, G., Nguyen, N. T., Warkiani, M. E., & Li, W. (2016). Fundamentals and applications of inertial microfluidics: A review. *Lab on a Chip*, 16(1), 10–34. doi: 10.1039/C5LC01159K

Zhao, C. X., & Middelberg, A. P. J. (2011). Two-phase microfluidic flows.  
*Chemical Engineering Science*, 66(7), 1394–1411. doi: 10.1016/j.ces.2010.08.038

## Appendix

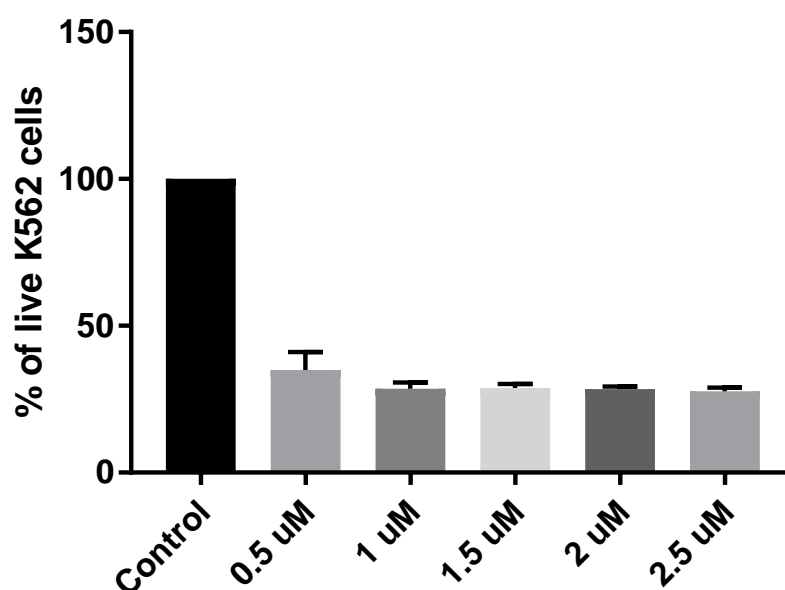
Name(s)c	Manufacturer	Stabilising coating	Filling gas
SonoVue®	Bracco Diagnostics, Inc.	Phospholipid	Sulphur hexafluoride
Definity®	Bristol-Myers Squibb	Phospholipid	Octafluoropropane
Optison™	Amersham Health PLC	Human serum albumin	Octafluoropropane
Filmix™	Cav-Con Inc.	Phospholipid	Air
Imavist™	Schering A.G.	Surfactant	Perfluorocarbon & air
Albunex®	Molecular Biosystems	Human serum albumin	Air
Sonazoid™	Amersham Health PLC	Phospholipid	Perfluorocarbon
BiSphere™	Point Biomedical Corp.	Polymer/protein bilayer	Air
Quantison™	Quadrant Healthcare PLC.	Spray dried serum albumin	Air
Echovist®	Schering AG.	None	Air
Levovist®	Schering AG.	Palmitic acid	Air
Sonavist™	Schering AG.	Cyanoacrylate	Air
Echogen®	Sonus Pharmaceuticals	Surfactant	Dodecafluoropentane

### Different types of commercial surfactant

Polymer	Drug incorporated	Feature
Polyacrylic acid with PEG	Botulinum toxin	Mucoadhesion from polymers prolong gastric retention of this formulation when administered
Sodium alginate	Captopril	This polymer confers substantial mucoadhesion capabilities to captopril microcapsules for prolonged release in stomach
Carboxymethyl cellulose	Famotidine	Increasing amounts of carboxymethyl cellulose in this formulation improved mucoadhesion of famotidine microspheres
Chitosan	Amoxicillin	Chitosan improves in situ gelation nanoparticle formulation of amoxicillin
Positively charged gelatine	Amoxicillin	Improved mucoadhesive properties of modified gelatine microspheres of amoxicillin
polyglycerol esters of fatty acids	Furosemide	Improved mucoadhesive properties of microspheres for better bioavailability
Polyethylene oxide	Famotidine	Confers mucoadhesive properties to nanosuspensions of famotidine

**Mucoadhesive polymers:** Some mucoadhesive polymers used to improve performance of various pharmaceutical preparations

	Control	0.5 $\mu$ M	1 $\mu$ M	1.5 $\mu$ M	2 $\mu$ M	2.5 $\mu$ M	
1	0.488	0.161	0.166	0.156	0.160	0.165	
2	0.596	0.178	0.150	0.168	0.166	0.170	
3	0.558	0.179	0.156	0.171	0.156	0.155	
4	0.585	0.239	0.160	0.169	0.165	0.154	
5	0.650	0.209	0.180	0.158	0.172	0.163	
6	0.587	0.245	0.178	0.177	0.165	0.153	



### Calculation of imatinib sensitivity in K562 cell line

*Calculation of K562 cells' sensitivity to various doses of imatinib. The table shows the recorded absorbance by spectrophotometry from the MTS assay plates in which six conditions were measured. They included untreated (control) and treated cells with 0.5, 1, 1.5, 2 and 2.5  $\mu$ M imatinib. For each condition there were five replicates. The results of the replicate for each condition was normalised against the untreated control and presented as a percentage. The figure shows the normalised data and the error bars represent the variations among the replicates for each condition.*